UC Santa Cruz
UC Santa Cruz Previously Published Works

Title

Protein bioelectronics: a review of what we do and do not know

Permalink

https://escholarship.org/uc/item/64n3k4pf

Journal

Reports on Progress in Physics, 81(2)

ISSN

0034-4885

Authors

Bostick, Christopher D
Mukhopadhyay, Sabyasachi
Pecht, Israel
et al.

Publication Date

2018-02-01

DOI

10.1088/1361-6633/aa85f2

Copyright Information

Peer reviewed

REVIEW

Protein bioelectronics: a review of what we do and do not know

To cite this article: Christopher D Bostick *et al* 2018 *Rep. Prog. Phys.* **81** 026601

View the article online for updates and enhancements.

Review

Protein bioelectronics: a review of what we do and do not know

Christopher D Bostick[1,2,5]**, Sabyasachi Mukhopadhyay**[3,5,6]**, Israel Pecht**[3]**, Mordechai Sheves**[3]**, David Cahen**[3] **and David Lederman**[4]

[1] Department of Pharmaceutical Sciences, West Virginia University, Morgantown, WV 26506, United States of America
[2] Institute for Genomic Medicine, Columbia University Medical Center, New York, NY 10032, United States of America
[3] Weizmann Institute of Science, Rehovot, 76100, Israel
[4] Department of Physics, University of California, Santa Cruz, CA 95060, United States of America

E-mail: david.cahen@weizmann.ac.il, dlederma@ucsc.edu, mudi.sheves@weizmann.ac.il and israel.pecht@weizmann.ac.il

Corresponding Editor Professor Masud Mansuripur

Abstract

We review the status of protein-based molecular electronics. First, we define and discuss fundamental concepts of electron transfer and transport in and across proteins and proposed mechanisms for these processes. We then describe the immobilization of proteins to solid-state surfaces in both nanoscale and macroscopic approaches, and highlight how different methodologies can alter protein electronic properties. Because immobilizing proteins while retaining biological activity is crucial to the successful development of bioelectronic devices, we discuss this process at length. We briefly discuss computational predictions and their connection to experimental results. We then summarize how the biological activity of immobilized proteins is beneficial for bioelectronic devices, and how conductance measurements can shed light on protein properties. Finally, we consider how the research to date could influence the development of future bioelectronic devices.

Keywords: bioelectronic, electron transport, immobilization, electron transfer, monolayer, protein

(Some figures may appear in colour only in the online journal)

Contents

[5] These authors contributed equally to the work.
[6] Current affiliation: Department of Physics, School of Engineering and Applied Sciences, SRM University-AP, Amaravati, Andhra Pradesh 522502, India.

Glossary

AFM	Atomic force microscopy
apo	Protein without cofactor
CP-AFM	Conductive probe atomic force microscopy
CD	Circular dichroism
Cofactor	Non-peptide organic or inorganic group or ion in protein, necessary for protein's biological activity; can have/be aromatic rings, conjugated chains, or metal ions
CPR	Cytochrome P450 reductase
CV	Cyclic voltammetry
CYP2C9	Cytochrome P450 2C9
CYT C	Cytochrome c
EC-STM	Electrochemical scanning tunneling microscopy
EDC	1-ethyl-3-[3-dimethylaminopropyl]carbodiimide hydrochloride
ET	Electron transfer
ETp	Electron transport
FAD	Flavine adenine dinucleotide
FMN	Flavin mononucleotide
FR	Flickering resonance
GCE	Glassy carbon electrodes

H_{ab}	Interaction hamiltonian
Holo	Fully intact protein, including cofactor
HSA	Human serum albumin
K_a	Binding association rate
K_D	Binding dissociation constant
K_d	Binding dissociation rate
k_{ET}	Electron transfer rate
LbL	Layer-by-layer
LOFO	Lift-off float-on
Mb	Myoglobin protein
MUA	11-mercaptoundecanoic acid
NADPH	Nicotinamide adenine dinucleotide phosphate
NHE	Normal hydrogen electrode
NHS	N-hydroxysuccinimide
OT	8-octanethiol (OT)
P450	Cytochrome P450
PDMS	Polydimethylsiloxane
PFV	Protein film voltammetry
PG	Pyrolytic graphite
Prosthetic group	Tightly bound cofactor
PSI	Photosystem I (protein)
QCM	Quartz crystal microbalance
RCI	Photosystem I reaction center
SAM	Self assembled monolayer
SCE	Saturated calomel electrode
SE	Superexchange
SERRS	Surface-enhanced resonance Raman spectroscopy
SPM	Scanning probe microscopy
SPR	Surface plasmon resonance
STM	Scanning tunneling microscopy
STS	Scanning tunneling spectroscopy
Turnover rate	Rate of protein biological activity for small molecule transformation (exp. oxidation or reduction)
UV–vis	Ultraviolet–visible spectroscopy
YCC	Yeast cytochrome c
WT	Wild type, i.e. natural form of the protein
β	Distance decay factor in tunneling transport $\left[\ln\left(\frac{I}{I_0}\right) \propto -\beta L;\ L \text{ is distance}\right]$
γCPR	Yeast cytochrome P450 reductase protein
ϵ	Optical extinction coefficient

1. Introduction

Recent advances in the development of biocompatible electronics have been motivated by applications where interfacing with sensory function in humans (e.g. artificial retinas) is desired, some of which can have direct applications for improving human health (e.g. *in situ*, real time monitoring of glucose or drug concentration in the blood). A fundamental understanding of the properties of biomaterials at the nanoscale is essential for progress towards interfacing with sub-cellular organelles or other nanoscale structures present in living systems. Moreover, because many biologically relevant reactions occur at substrate surfaces and interfaces, exploring

interactions between individual biomolecules and various substrate surfaces is of fundamental importance.

Proteins have evolved over billions of years into structures capable of precise reactions, including highly specific substrate recognition, analyte binding, and facile and directional electron tunneling [1]. In addition, proteins are essential to many chemical processes essential to life, such as photosynthesis, respiration, water oxidation, molecular oxygen reduction, and nitrogen fixation [2–7]. Due to their ability to catalyze a vast number of reactions, there has been much interest in harnessing their abilities. One application is in bio-catalysis in synthetic organic chemistry. The high chemo-, regio-, and stereo-selectivity of enzymes negates the need for protecting groups, and thus reduces synthetic steps and simplifies work flow [8]. As such, the pharmaceutical industry is interested in proteins in bioreactors (vessels in which chemical reactions are carried out by biological components) for production of fine chemicals [9–13] and to filter out toxic or hazardous substances by naturally occurring organisms [14]. The high specificity of proteins also makes them ideal candidates for use as sensors. In many sensor applications, proteins are immobilized onto a solid support and act as transducers of optical [15, 16] or electronic [17] signals that correlate with specific protein-ligand interactions. Interfacing with solid state electronics has demonstrated that this approach allows biosensing at low voltages with high sensitivities and low detection limits, and offers long-term stability for measurements [18–20]. Protein-based biosensors are currently being developed for use in drug monitoring [21], environmental toxin detection [22, 23], and early disease detection [24, 25].

Using single organic molecules as electronic components [26] has been suggested as a possible solution to the physical limitations of micro- and nano-scale electronic development. Proteins could provide a way to realize this, because they are small (nm-scale) and capable of undergoing chemo-mechanical, electromechanical, opto-mechanical, and opto-electronic processes [27]. Proteins have been studied for use in the design of bio-electronic devices, including field effect transistors for sensing [28–32], bio-molecular transistors for data storage [33], bio-molecular circuits [34], bio-hybrid solar cells [35], bio-computers [36], and enzymatic biofuel cells [37–39]. Biomedical applications exist in devices such as implantable sensors for monitoring chemicals [40, 41] and diagnostics [42], as well as the creation of artificial retinas [43] and noses [44]. There has been extensive research done on electron transfer in proteins [45–47] especially in well-characterized model systems such as cytochrome c [48], plastocyanin [49], and azurin [50–53]. Other studies have explored the solid state electronic transport properties of proteins whose mechanisms of action rely on electron transfer, ET [54, 55].

Several books [28, 54–59], recent special issues of journals (from which we cite results published therein [51, 60]), and reviews [1, 47, 51, 61–63] have appeared over the years, going back to the early [64] and late 1990s (1st edn. of [55]). All deal with various aspects of the topics considered here and, taken together, they reflect to some extent the evolution of the idea of protein bioelectronics. Recent interest in possible applications

of new protein electronics have laid bare practical problems and stimulated interest in their fundamental scientific issues.

In parallel, the research of ET has remained very active, and we rely heavily in this review on our present understanding of ET to discuss what can be learned from protein bioelectronics devices. We therefore start with a presentation of fundamental concepts related to the electronic properties of proteins as they relate to ET and electron transport, ETp, (see next section for an explanation of the difference between ET and ETp) and compare the two processes. Because until now all ETp measurements involve immobilizing proteins on an electronically conducting solid surface used as an electrode, we review the current state of the field regarding protein immobilization techniques, including characterization of the resulting biomolecular films. Subsequently, we discuss the results of measurements on immobilized proteins and their impact on our fundamental understanding of protein electronics. Finally, the implications of the research to date and their possible implications for future protein bioelectronic devices are noted and reviewed.

2. Electron transfer (ET) and electron transport (ETp) in proteins

Electron flow through a protein molecule involves intramolecular charge transport and electron exchange with the surroundings [65]. These two distinct, and widely studied processes cannot be unambiguously separated since the interface of a molecule with an adjacent electrode or ionic solution can have a profound influence on the molecular properties, and hence on the molecule's electrical conductance [66]. The process of directed electron motion, or electron flow, through molecular structures is termed electron transport or electron transfer, depending on the environment in which it occurs. In the discussion below, we denote as electron transfer (ET) the electron flow process with all or part of the protein in direct contact with an electrolyte, which is ionically conducting and which can function as an electron sink or source via a redox process (figure 2). The electrolyte also provides charges, which screen the change in electrical potential due to the electron flow. Electron flow in which an electrolyte is absent, or does not participate in the electron flow process, with electrodes that are not ion conductors, is termed electron transport (ETp) (figure 2). ETp is usually measured in a solid state configuration[7]. In ETp normally there is no possibility for charge balance via ions from an electrolyte, while ET involves a surrounding medium with mobile ions which can provide such charge balance.

ET consists of electrons moving from specific electronically localized donors to acceptors, which can be domains in the protein, redox agents, or one electrode (in an electrochemical cell) in contact with the protein. ET is driven by a difference in redox potential between donor and acceptor [48, 68–70]. ET *within* proteins occurs between donor and acceptor sites. In model systems, one of these is chemically

---

[7] We note that systems can be thought of where the distinction does not hold, such as solid-molecule-solid measurements in an electrolyte or use of an ionic liquid to gate a solid state junction.
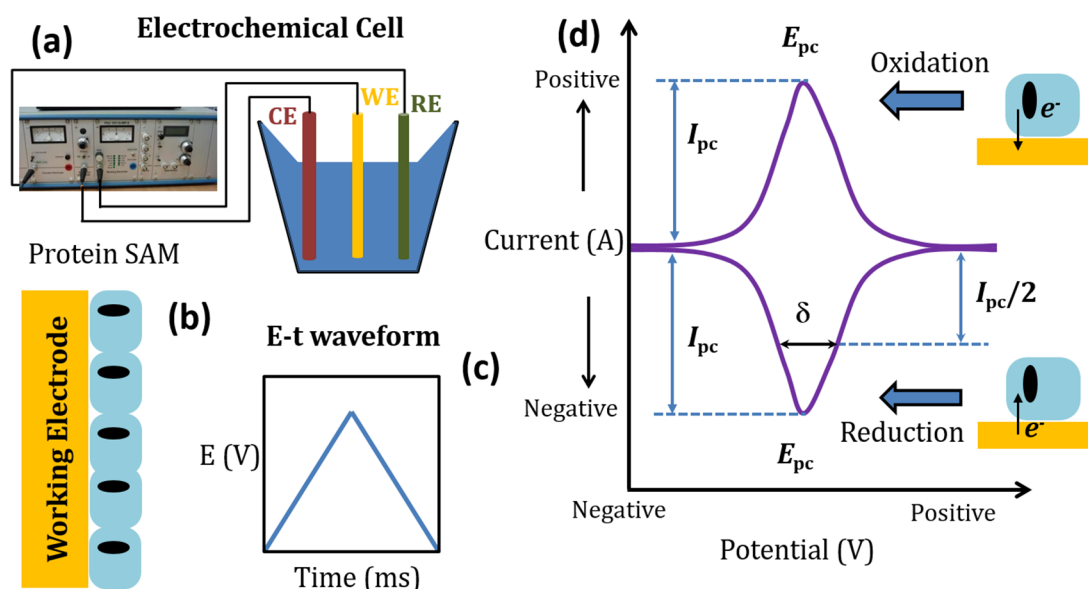
Figure 1. (a) Schematic experimental setup for electrochemical charge transfer studies across self-assembled monolayers of redox-active proteins on conducting electrodes as shown in (b). (c) Time varying electric field applied between counter (CE) and working (WE) electrode with respect to reference electrode (RE). (d) Electrochemical current profile during oxidation and reduction process at the surface of working electrode (details in [45, 50, 60, 67]).

conjugated to the protein, located at a known position, which therefore allows studying ET between specific positions of the protein (figure 2).

If the proteins are immobilized on an electrode, ET occurs between the electrode and a redox-active protein cofactor, and between the cofactor and the protein surface exposed to the redox electrolyte used for the experiment (figure 1). Thus, in this case, there is a transition from electronic to ionic charge transport, as is also the case in nature. Within the protein, charge is transferred by electrons, even if a redox center is involved, as that redox-active species does not itself move within the protein. However, charge transfer out of the protein requires reduction/oxidation of a redox-active species in the electrolyte that contacts the protein. This means that the redox-active species is now ionized differently than before, and thus the charge will flow with this ionic species until the next step in the overall process, as is the case in electron transport chains (discussed further below). The change of charge state of the redox-active species in the electrolyte is accompanied by a change in the protein's electrical charge state. This change induces electrical screening to reduce the electrostatic energy barrier for the subsequent steps. In nature and in an electrochemical experiment, this can occur because of the surrounding electrolyte. Naturally, the polarizability of the protein itself also affects the ET process.

Multiple ET processes occur in proteins, such as in respiration or photosynthetic complexes, that involve *electron transport chains* [61, 71, 89, 94]. Proton-coupled electron transport (PCET) can also occur, which is especially prevalent at metal cofactors that activate carbon, oxygen, nitrogen, and sulphur atoms of enzyme substrate molecules [72]. Protein cofactors are organic or inorganic components, with conjugated chains, or metal ions that assist the protein's biological activity. As noted above, redox reactions with biomolecules such as proteins can be studied with electrochemical experiments

as shown in figure 1, i.e. with one electronically conducting, ionically blocking contact (the electrode) and one ionically conducting, electronically blocking contact (the redox electrolyte). ETp, however, requires electronic conduction across proteins set between two electronically conducting, ionically blocking electrodes; it is defined as the flow of electrons across/through the protein that is contacted by these electrodes (figure 2)[8].

Electric charges in biological systems are generally transported by ions, and thus in nature ET is always coupled to ionic transport where the redox processes serve as donor (Red → Ox) and acceptor (Ox → Red) electrical 'contacts'. Thus, from a device perspective, there is no *a priori* reason for electrons involved in (solid-state) ETp to use the same conduction mechanism as those involved in ET processes. Nevertheless, there is experimental evidence that a protein's ETp characteristics are correlated with its ET and redox potential [73, 74], and therefore it is likely that there is a fundamental connection between the ET and ETp processes and mechanisms.

From an experimental point of view (figure 2), measuring ETp across bio-molecules in dry, solid state condition is fundamentally different from measuring ET. In ETp, the absence of a liquid electrolyte (with its above-noted ability for electrical screening) will normally drive electrons from source to drain electrode, without intra-protein redox process, via some electron transport mechanism (to be discussed later in this review).

ETp is measured on a single protein or on ensembles of proteins (such as monolayers) between the two electronically conducting electrodes (see [75] for a discussion of the differences between molecular junctions with single and many molecules). While this type of junction can be thought of as a

---

[8] We note that ET and ETp are generally described in terms of holes and electrons. We define a hole as is commonly described now days as a missing electron, instead of the traditional solid state physics definition of the behavior of electrons of a nearly full band.
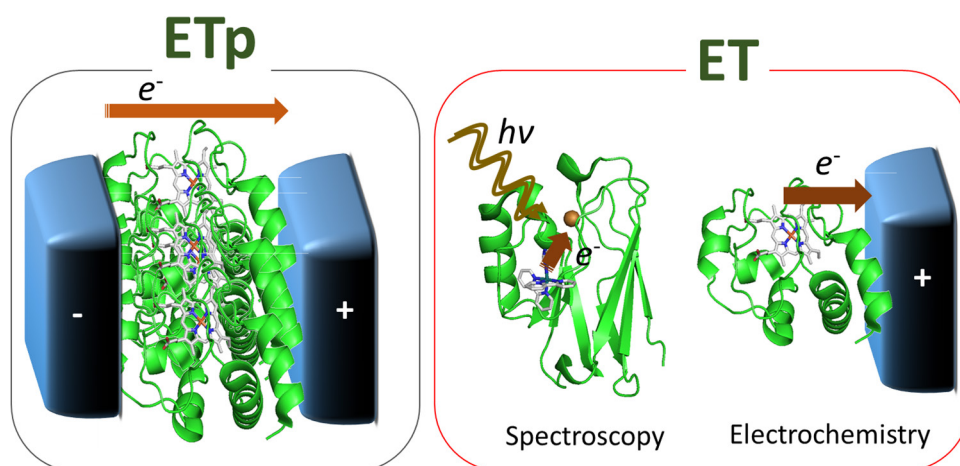
Figure 2. Diagram representing solid state electron transport (ETp) and electron transfer (ET) measurements using spectroscopy and electrochemistry (see introduction to section 2 for more complete distinction between ET and ETp). The very important counter charges around the protein are not shown in the ET configurations.

donor-bridge-acceptor junction, the driving force of the transport is the electrical potential difference between the electrodes (if the electrodes are made of the same material [76]) rather than a difference in chemical potential of the electrons between two regions. In solution experiments, the chemical potential differences of the redox-active ions need to be included [47].

For practical purposes, the redox potential can be identified with the electrochemical potential of the electron, $\tilde{\mu}_e$ ($\simeq E_F$, Fermi level) [77–81], where $\tilde{\mu}_e = \mu_e + q\phi$, the sum of the contribution of the electrical potential, ϕ, (q is the electron charge) and that of the electron's chemical potential, $\mu_e = \mu_{0,e} + kT \ln n_e$. Here $\mu_{0,e}$ is the standard chemical potential of the electron, kT is the thermal energy, and n_e is the electron concentration, defined by the difference in activities of the reduced and the oxidized form of the redox species. The latter can be identified as the difference in chemical potential of the (mostly ionic) reduced and oxidized species, and it can drive ET, but not ETp (with electrodes of the same materials, i.e. with the same electron chemical potential).

An additional important difference between ET and ETp is the fact that ET occurs in an electrolyte solution, which allows for electrostatic screening around (parts of) the protein. This is what makes the change in charge of the protein, which otherwise would carry a very high electrostatic energy price, possible. Except for rare cases, no such change in charge state occurs in ETp and electroneutrality is preserved. These differences allow the characterization of ETp distances not considered possible in biological ET. Gray, Winkler, Dutton, and coworkers have estimated the upper limit of D–A separation distances in biological ET (pure quantum mechanical tunneling) to be $\leqslant 20$ Å and $\leqslant 14$ Å, respectively [61, 82]. However, recent ETp measurements across proteins yield measurable currents over electrode separations of up to ~100 Å [83].

Cofactors are responsible for the functional properties of proteins because they enable redox activity, including the metal center of metalloproteins, such as Cu^{2+} in the blue copper proteins, Fe^{3+} in the iron-sulfur proteins and cytochromes, or flavins found in flavoproteins [64]. Some redox-inactive proteins, such as the light-driven transmembrane proteins bacteriorhodopsin and halorhodopsin, which contain a retinal

cofactor, also support ETp, which, remarkably, is at least as efficient as that of redox-active proteins.

In measurements of the differences in ETp observed between the holo- and apo- forms of proteins, their electrical conduction properties were shown to depend strongly on having the cofactors. Such experiments have been performed with the Cu redox protein azurin [1, 53], the heme-redox protein cytochrome c [84], the O_2-binding protein myoglobin [32, 85], and ferritin [86]. Similarly, changes in transport mechanisms have been deduced from temperature-dependent ETp studies on the proton or Cl^- pumping photoactive membrane proteins, bacteriorhodopsin, bR [87], or halorhodopsin, phR [88], and their derivatives lacking retinal, for bR, or retinal and/or carotenoid for phR.

As noted above, multiple ET processes, often involving several proteins and other redox molecules, carry electron transfer over relatively large distances. In the respiratory [89, 90] and photosynthetic chains (>50 Å) [91–94], ET occurs sequentially across several proteins (inter-protein, or protein–protein ET [95, 96]); in hydrogenases (FeS clusters, ~52 Å) [97], carbon monoxide-dehydrogenases [98, 99] and other enzymes [100], the processes are within one protein complex. This complicated and diverse behavior has made it clear that it is important to develop a theoretical understanding of biological ET and its possible implications to solid-state ETp.

In the following sub-sections, we review the mechanisms that have been developed to explain ET essentially in terms of the Marcus model and various mechanisms that rely on it. Then we briefly discuss ETp in terms of the Landauer one-dimensional conduction model, which has been applied to molecular electronics, while keeping in mind that once electrons enter the protein, ET-like mechanisms may play an important role. ETp is discussed in more detail in terms of specific experiments in section 4. We end this section by discussing the effects of protein structure and protein immobilization on ET and ETp.

2.1. Electron transfer

In 1956, Marcus presented a model describing ET reactions from a donor to an acceptor that is close to it [101, 102].
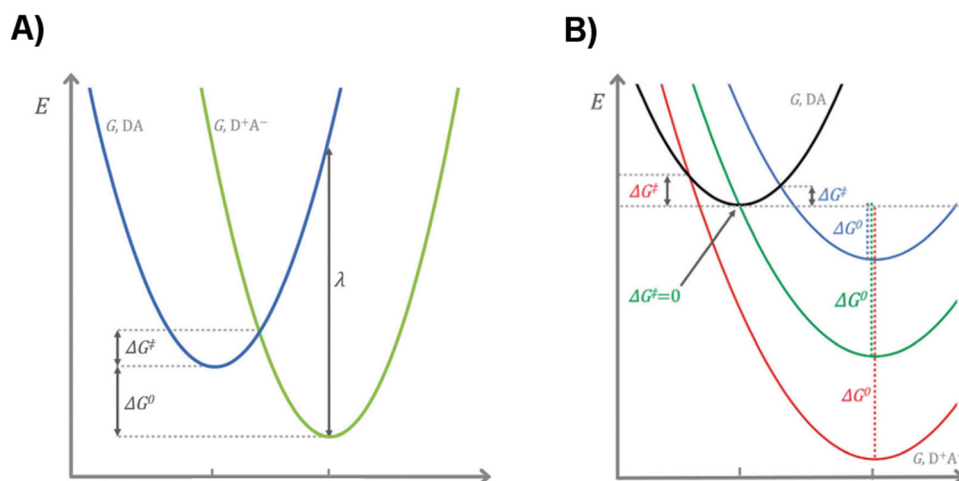
A)

B)

Figure 3. (A) Schematic diagram of the Marcus model for electron transfer, showing the Gibbs free energy (*Y*-axis) surface for the nuclear motion along a reaction coordinate (*X*-axis) of the donor and acceptor in the initial state, prior to ET (G, DA in blue), and post-ET from the donor to the acceptor (G, D$^+$A$^-$, green). $\Delta G^{\ddagger}$, ΔG^0, and λ are the activation energy, the free energy driving force, and the outer shell reorganization energy of the ET event, respectively. (B) A diagram of the Gibbs free energy surface as in (A) showing the effect of increasing ΔG^0 on the $\Delta G^{\ddagger}$. As ΔG^0 increases, a decrease in $\Delta G^{\ddagger}$ is seen until $\Delta G^{\ddagger} = 0$ (green curve). After this point increases in ΔG^0 (from the green to red curve) lead to decreases in $\Delta G^{\ddagger}$ as energy must be dissipated for an ET event, which is known as the inverted region. Note that λ does not change for the different scenarios in B), because the nuclear coordinate (*X*-axis) of the post-ET state does not change. Adapted from [104] with permission of The Royal Society of Chemistry.

Table 1. Summary of experimentally obtained ET rate constant for different metalloproteins (see text for discussion)[a].

Protein	Electrochemical rate constant (ET) k_{ET} (s^{-1})	References	Spectroscopy rate constant (ET) k_{ET}(s^{-1})	References
Cyt C	0.2[b]	[110]	9.4×10^{5}[b]	[61]
	0.63[c]	[110]	2.7×10^{6}[c]	[61]
Myoglobin	60	[111, 112]	2.3×10^{6}	[61]

[a] The difference between the two entries for Cyt C result from experiments with different donor–acceptor separations (different mutations).

[b] ~14 Å.

[c] ~17 Å.

The Marcus theory was originally developed to explain outer sphere ET, where participating redox centers are not linked by any bridge, and electrons 'hop' from the reducing center to the acceptor. It has since been extended to cover inner sphere ET, where two redox centers are linked covalently during transfer, and heterogeneous ET, where an electron moves between a biomolecule (protein, small molecule, cofactor, etc) and an electrical contact. In the Marcus description, nuclear motions of the reactant and the surrounding environment are approximated by a simple harmonic oscillator potential along a reaction coordinate (figure 3) [103, 104]. The left parabola in figure 3(A) represents the Gibbs free energy surfaces for the nuclear motion of the reactants prior to ET, and the right parabola represents this free energy for the nuclear motion of the products after ET. The two driving parameters for the ET reaction to overcome the activation free-energy barrier ($-\Delta G^{\ddagger}$) are the driving force, characterized by the Gibbs free energy of activation ($-\Delta G^0$), determined from the difference in oxidation potentials of the donor and acceptor, and the reorganization energy (λ) needed for the nuclear rearrangements that accompany ET [105]. The rate of electron transfer, k_{ET}, depends on $-\Delta G^0$ relative to λ. The basic expression for k_{ET} in the Marcus theory is

$$k_{ET} = \frac{2\pi}{\hbar}H_{AD}^2 \frac{1}{\sqrt{4\pi\lambda k_B T}}\exp\left(\frac{-(\lambda + \Delta G^o)^2}{4\lambda k_B T}\right) \quad (1)$$

where H_{AD} is the quantum mechanical electronic coupling between the initial and final (donor and acceptor) states, k_B is the Boltzmann constant, and T is the temperature. A maximum, or optimal ET rate occurs for activation-less ET ($-\Delta G^0 = \lambda$) that decreases with decreasing driving force. The Marcus theory also predicts an inverted region ($-\Delta G^0 > \lambda$) where energy must be dissipated to allow ET and where the rate decreases with increasing driving force. According to the semi-classical Marcus' theory, electron transfer takes place when a thermal fluctuation of the solvent or of the nuclear coordinate of the donor and acceptor shifts the donor and acceptor electronic states into resonance. The quantity H_{AD} in equation (1) originates from Fermi's Golden Rule. H_{AD} contains the interaction overlap integral (matrix element) between the donor (reactant) and acceptor (product) electronic states
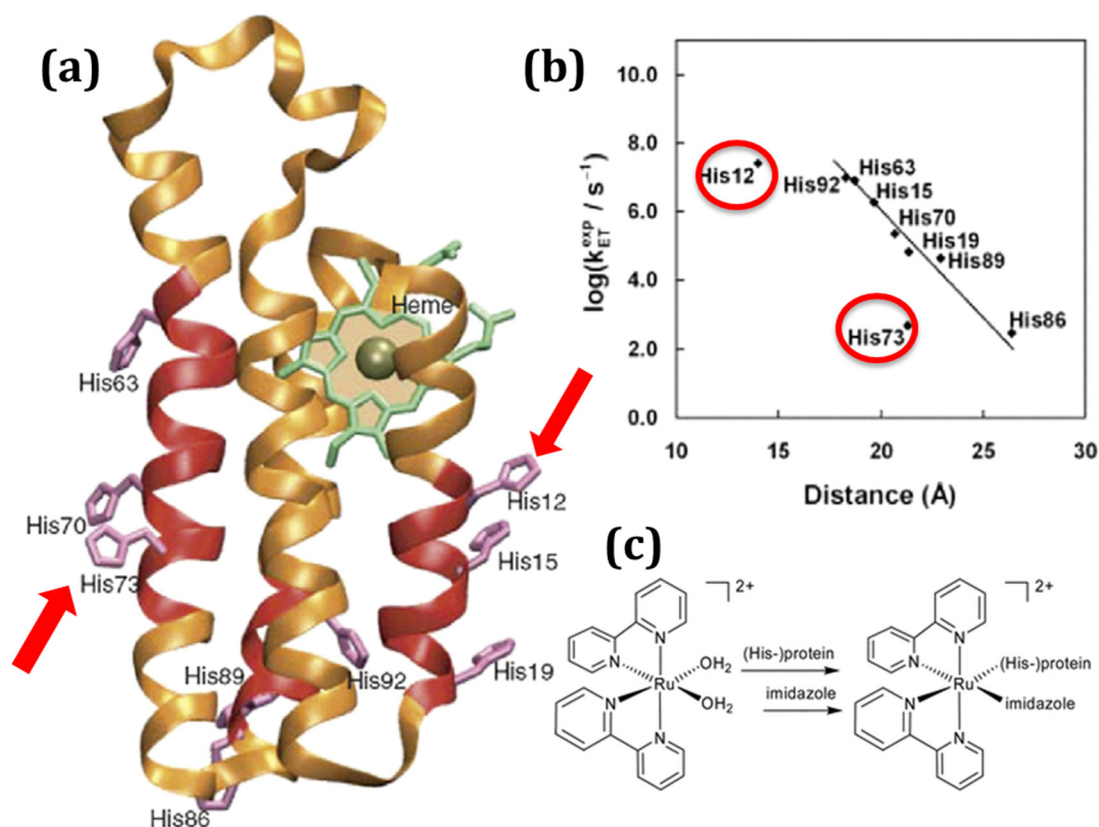
Figure 4. (a) Ribbon diagram indicating the positions of the nine histidine sites on cyt b562, where a Ru complex was connected to different histidine groups in different mutants, to measure variations in electrochemical electron transfer rates between each of these sites and the heme group. (b) Seven ET rates follow the exponential distance dependency of equation (1), whereas in two cases slower rates than predicted by equation (1) were measured. (c) Chemical reaction to connect the Ru complex with different histidines in different mutants. From [129]. Reprinted with permission from AAAS.

and the density of states, and thus depends on the distance between the states (see also equation (2) below) [72, 106]. The interaction between the donor and acceptor in a polarizable solvent is known as the outer-sphere interaction. When electron transfer occurs within molecules where it causes changes in bond lengths and local symmetries, a similar result is obtained, although the origin of the interaction energy is more complicated. This result related to the so-called inner-sphere interactions was developed by Hush [107], and the joint theory of the inner- and outer-sphere interactions is sometimes called the Marcus–Hush theory (section 4).

Over the years, several theoretical frameworks and computational tools have been developed to explain the biological electron transfer process [108]. In particular, there has been much interest in understanding how the protein structure determines the protein redox function, the implication being that enhanced comprehension could allow for control and tailored biological electron transfer by targeted mutants. The field has evolved significantly since the early ideas of bridge-mediated electron tunneling, first proposed by Halpern *et al* in the early 1960s, and the square barrier-tunneling model that Hopfield proposed in the 1970s [106, 109].

Many experimental studies have been carried out to understand how long-range biological ET (over, at least, several direct bond distances) is accomplished [45, 46, 61, 82, 101, 113]. ET rate has been determined in cytochromes from line broadening, magnetization transfer, or relaxation measurements in NMR

[114, 115]. In addition, k_{ET} has been extracted from electrochemistry of a monolayer of a protein (azurin, cytochrome c, myoglobin and other metalloproteins) attached to a working electrode (figure 1(d)) [116]. Until now, most conclusive and systematic ET rate (k_{ET}) data have been obtained via electrochemical [110–112, 117] or spectroscopic flash quench studies [45, 61, 65, 95, 117–119]. Table 1 gives some experimental data for two well-studied proteins, obtained by using mutated proteins to vary the donor–acceptor separations.

Gray, Winkler and co-workers have used modified metalloproteins to understand distance-dependent ET between a dye molecule and a metal ion that acts as quencher in azurin and cytochrome b562 proteins (figure 4) using flash-quenching, where a foreign dye is introduced on a protein surface and ET processes between redox centers of the protein and dye molecules are monitored [65, 100, 120]. By introducing ruthenium and rhenium complexes as donors which are known to attach to certain histidine residues at known distances from Cu (azurin), Fe (in the heme group in cytochrome) or Zn (modified cytochrome) cofactors, they were able to show experimentally (figure 4) that

$$k_{ET} \propto e^{-\beta L}, \qquad (2)$$

where L represents the donor–acceptor distance and $1/\beta$ is a characteristic decay distance. Studies by Gray and Winkler [121] demonstrated that out of nine k_{ET} values for histidine-modified cyt b$_{562}$ derivatives, seven were accurately fit by the
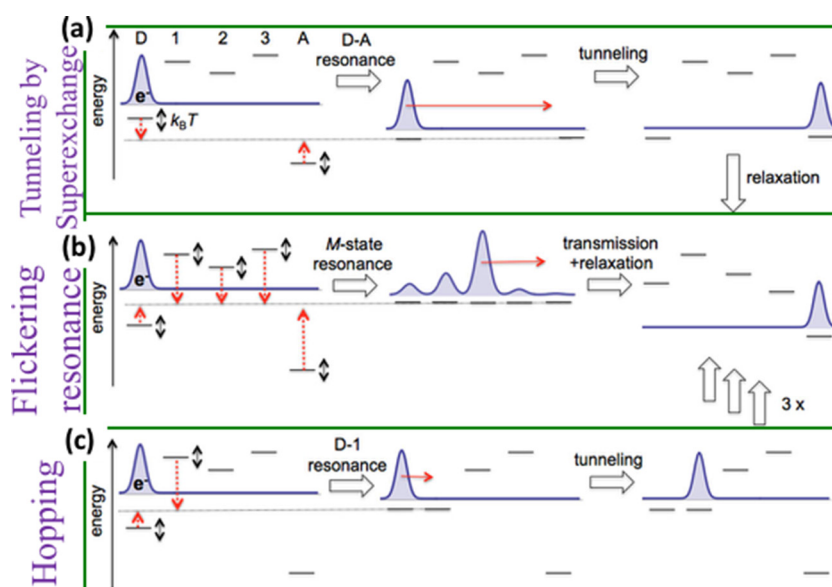
Figure 5. (a) Illustration of protein-mediated electron transfer models, tunneling (via super-exchange), flickering resonance and hopping, along a chain of 5 redox active sites (as could be the case in a multi-heme or multi-copper protein), where D is the electron donor and A is the acceptor (A), leaving three sites (1, 2, 3) between D and A. One-electron energy levels are drawn as black lines for each site. The electron that is transferring from D to A is shown as a Gaussian. In (a) thermal fluctuations bring D and A levels into resonance (middle scheme), which allows tunneling from D to A. Also during these process sites 1,2, 3 are non-resonant; they enhance tunneling but are not significantly occupied by the tunneling electron at any time, i.e. there is no nuclear relaxation as a result of electron occupation. In (b) ET occurs only when all levels are in resonance and the tunneling electron transfers ballistically (with tunneling probability of 1). In (c) [131] D and nearest neighbor site 1 become resonant, allowing efficient electron tunneling from D to 1, and so forth till A. Reprinted with permission from [108]. Copyright (2015) American Chemical Society.

tunneling model, but two showed k_{ET} slower than predicted by equation (2), as shown in figure 4(b). This implies that a different transfer mechanism is at work for those residues. Surprisingly, protein electron transfer rates deduced from electrochemical and spectroscopic methods were significantly different (table 1). This difference may indicate that protein immobilization on solid surfaces used in the electrochemical methods constrains some of the electron transfer pathways, while in spectroscopic methods performed in solution, more protein conformations and transfer pathways are available. Alternatively, or additionally, the switch from electronic to ionic conduction (assuming the redox center to solution step is the rate-determining one) may affect the measured rate.

Another useful approach to investigate ET in proteins has been pulse radiolysis, primarily those containing transition metal ions in the active sites. There were two main, complementary objectives guiding these studies. One was attaining an understanding of the electron-transfer process within the polypeptide matrix separating the redox centers and defining the parameters controlling their rates. The second was resolving the detailed mechanism of the function(s) performed by the protein, notably enzymes [120]. Azurin has been a model system for pursuing the first objective and was extensively investigated using pulse radiolysis. Triggering an intramolecular ET from the residual radical ion to the Cu(II) site over a 2.7 nm separation turned out to be useful for examining the impact of specific structural differences introduced by mutations on ET rates. Parameters examined ranged from changes in the medium separating the redox sites to those in the actual coordination of copper site, which drastically affected its reorganization energy [122–125].

Over the years, more sophisticated theoretical models have been developed to understand ET in proteins, including bridge-mediated electron tunneling [109] and square barrier tunneling [106]. These models establish the theory of ET between fixed sites within the proteins through electron tunneling. In the case of redox proteins, multiple electron transfer pathways often exist, and pathways can be highly dependent on protein structure and the surrounding environment. Refinements by Beratan *et al* [126, 127] of these early models show that electrons can tunnel across proteins through favorable pathway(s), which include mostly bonded groups, with less favorable non-bonded interactions being important when the through-bond pathway is prohibitively long and a shorter through-space path exists [128].

A square-barrier tunneling model, combined with a suitable decay constant, has given a surprisingly good description for experimentally obtained biological ET (figure 2) [130]. This model was subsequently refined by Beratan and coworkers, who proposed that electrons tunnel along specific pathways, connecting electron donating and accepting cofactors [130]. The theory of ET in biochemical systems with several intermediary tunneling (bridge) states was recently reviewed by Blumberger [108], who summarized several models that are currently considered viable for explaining electron transfer in biomolecules, all based on the Marcus theory. These are the super-exchange (multi-step tunneling), flickering resonance (proposed by Beratan, Skourtis, and coworkers [131]; *vide infra*), and hopping models, based on consecutive, incoherent tunneling steps, as mechanisms of electron transfer (figure 5).
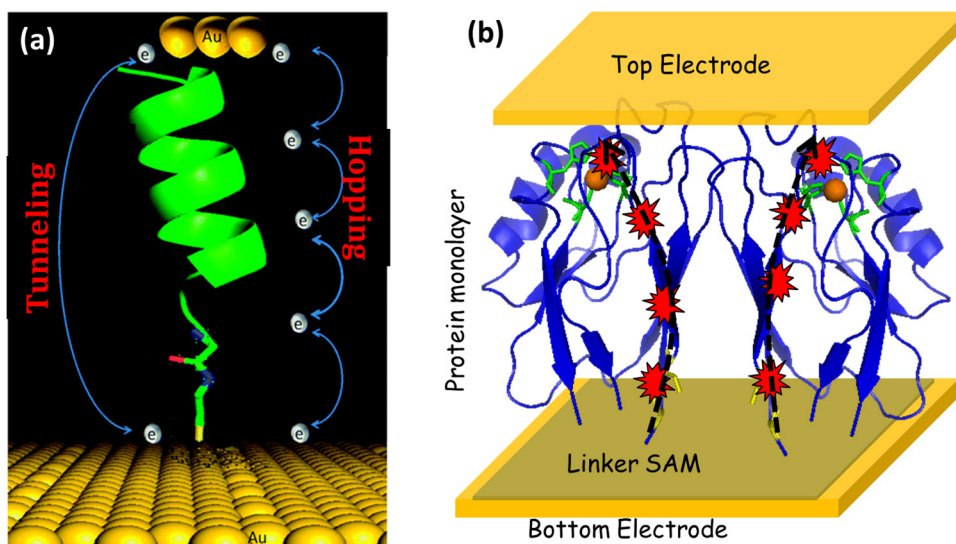
Figure 6. Diagram comparing electron transport by superexchange and hopping across single α-helical peptide at nanoscopic configuration. Reproduced from [135] with permission of The Royal Society of Chemistry. (b) Diagram of electron transport process across dehydrated protein monolayer sandwiched between two macroscopic metal electrodes. SAM: self-assembled monolayer; linker: small molecule with terminal groups to bind to the protein and to the substrate. The protein shown is azurin.

In the *superexchange model* for ET the donor and acceptor energy levels are brought into resonance via bridge energy states, and then direct tunneling occurs, bypassing the intermediate energy levels completely. Superexchange therefore provides a model for direct tunneling, with a dependence of the electron transfer rate on distance between donor and acceptor, R, given by

$$k_{ET} = A e^{-\beta(R-\Delta R)} \qquad (3)$$

where ΔR is the distance between intermediate states, and $1/\beta$ is a characteristic decay length. The proportionality constant A depends on temperature as $A \propto T^{-1/2}\exp(-b/k_B T)$, where b is a constant that has units of energy, but is independent of R and ΔR, while $\beta \propto 1/\Delta R$ and is temperature-independent.

The *flickering resonance (FR)* model, proposed by Beratan, Skourtis, and coworkers, considers the dynamical nature of the system (see also discussion in section 4.1) [131]. For flickering resonance to occur, the energies of the donor, acceptor, *and* intermediate energy levels need all to be brought into resonance by thermal fluctuations to allow coherent tunneling ($\neq$hopping) between the donor and acceptor sites. In this case, the transfer rate has the same distance dependence as in equation (3), with the same $\beta \propto 1/\Delta R$ dependence. The proportionality constant A has essentially the same temperature dependence as for the superexchange mechanism, but with a $A \propto (R/\Delta R)^{-1}$ dependence for its upper bound value. Although it has not been possible so far to unequivocally identify flickering resonance in experimental data, this model might in principle be applicable to ETp in biomolecules if it is sufficiently efficient over long distances (10 s of nm to μm). Moreover, biological ET often involves multiple groups and redox cofactors in van der Waals contact with each other, and coupling rates are highly sensitive to conformational fluctuations. Thus, the flickering resonance model may be relevant to understand the electrical

conductance in bacterial nanowires and multiheme proteins, with strongly coupled porphyrin arrays with closely packed ($\lesssim$15 Å) redox groups [132, 133].

For larger distances, ET is assumed to occur primarily via *hopping*. In this mechanism, the electron *incoherently* hops from site to site in a sequential fashion, with a certain probability of hopping backwards and forwards. The transfer rate for this model is expected to depend on R as

$$k_{Hop} = A/(c + R/\Delta R), \qquad (4)$$

where c is independent of temperature and $A \propto \exp(-\Delta A_{DB}/k_B T)$, where ΔA_{DB} is the free energy difference between the electron on the donor (D) and the bridge (B) sites. The hopping mechanism is thought to be especially relevant for longer biomolecules, such as membrane proteins (figure 6) [51, 61], where the electron transfer distance between donor and acceptor is more than ~2 nm. The rate of hopping can also be described by the relation

$$k_{ET} \propto N^x, \qquad (5)$$

where $N \sim R/\Delta R$ is the total number of steps and x depends on whether the steps are reversible or irreversible, and has a value between 1 and 2 [7, 105][9]. It has been proposed that in ribonucleotide reductases, responsible for catalyzing the conversion of nucleotides to deoxynucleotides in all organisms, the long ET distance of 35 Å is covered via short electron hopping steps between conserved aromatic amino acids, rather than a single superexchange step (as illustrated in figure 7) [134].

2.2. Electron transport

The fundamental mechanisms of ETp via proteins are less understood than those of ET processes. One important reason

---

[9] $x = 2$ for unbiased diffusive hopping, $1 < x < 2$—for acceptor direction-biased random walk, $x > 2$ for donor direction biased random walk.
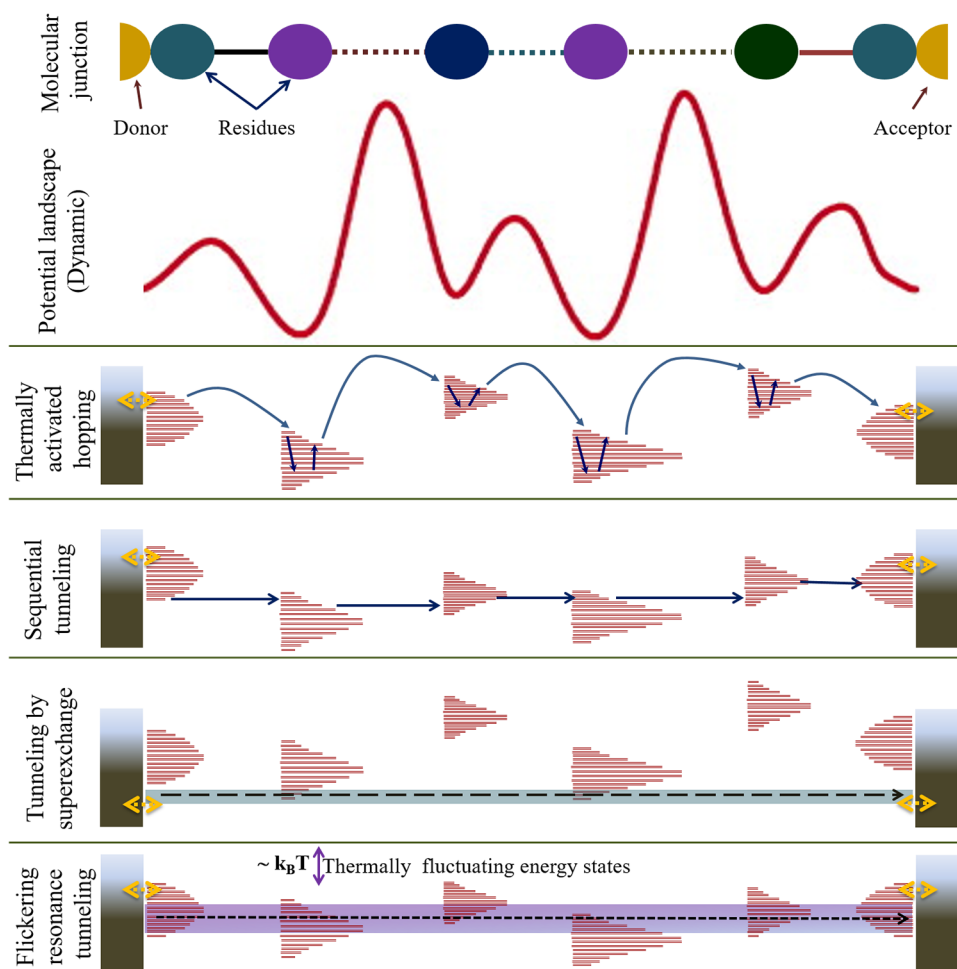
Figure 7. Illustration of how ideas and models from ET can be used as bases for ETp models, using figure 5(a) as starting point. The top panel describes a scheme with donor and acceptor states (as in ET) that can be the two electrodes of a molecular junction (as in ETp). Different amino acid residues, which may include also possible cofactors, are indicated. Below the top panel a possible 1D snapshot of the dynamic, varying electric potential profile in the protein, is shown between the electrodes of a molecular junction. The lower four panels are highly schematic illustrations of one-dimensional transport modes under an applied electrical potential between the right and left electrodes, with the y-axis being an energy scale. The Fermi energy distribution of the metallic contacts (dark-gray rectangles) and the broadening of the intervening electronic states within the protein (in red) are indicated with Gaussian(-like) distributions.

is that, as discussed above, ETp measurements are not done in solution, and therefore there are no ionic charges in the medium surrounding the protein to screen charging as the electron moves across the protein. Another reason is that the interaction between the metal electrodes, which effectively act as initial and final donor and acceptor states, are defined by the Fermi level (electrochemical potential) of the electrons of the metals used, rather than by discrete molecular orbitals. Nevertheless, some of the ET ideas and models discussed above (figure 5) have been used as starting points to describe ETp from a microscopic point of view. Some of the most widely accepted ETp models based on ET ideas are illustrated in figure 7. The top panel describes a scheme with donor and acceptor states (as in ET) that can be the two electrodes of a molecular junction in ETp. Different amino acid residues, which may also include a cofactor, affect the potential that the electron encounters as it is transported through the protein. The lower four panels in figure 7 are highly schematic illustrations of one-dimensional modes of ETp under an applied electrical potential between the right and left electrodes, according to the different proposed models.

In the **hopping** model, transport between electrodes occurs via intermediate sites that are potential wells for the electron, requiring activation energy to escape, i.e. this process is always incoherent and dissipative. We note that this model is not the same as the Hubbard model for the hopping mechanism in solid state physics, which relies on an effective repulsive potential between sites. For the hopping model, the conductance temperature dependence in ETp should be similar to that in ET, $\propto \exp(-b/k_{\mathrm{B}}T)$, because the intermediate hopping sites exist within the protein.

In the **tunneling via superexchange** model, transport is coherent in a similar fashion to the superexchange model used in ET, but because the Fermi levels of the electrodes are tuned by the externally applied electric potential, it does not rely on a spontaneous thermal alignment of D–A levels. As a result, the temperature dependence related to the D–A energies is different in ETp, and the tunneling barrier is influenced by the energy levels of the intervening medium.

The term **sequential tunneling** has been and is used in different publications for different processes and, as a

result, its use is ambiguous. It has been stated that sequential tunneling refers to hopping (see e.g. [71]) or that it is equivalent to resonant tunneling [136]. Büttiker considered the issue, and concluded that tunneling probability through a barrier can in general consist of coherent and incoherent parts [137]. The incoherent part, where inelastic processes occur, destroys phase coherence. In a completely incoherent tunneling process, the electron can scatter backwards or forwards. According to Büttiker, purely sequential (incoherent) tunneling occurs if tunneling occurs solely through an inelastic channel; on the other hand, if tunneling occurs through the coherent channel, *coherent resonant tunneling* occurs. In general, a tunneling process with intervening energy states is composed of both incoherent (sequential) and coherent tunneling channels. In this situation, Büttiker has demonstrated that if the two channels are connected in series, they are not independent of each other. In other words, increasing the sequential tunneling probability affects the coherent channel probability.

Whether the transport process is coherent or incoherent depends mainly on the residence time of the electron at the intermediate electronic states available for transport in the medium between the electrodes. For example, if the electron spends enough time in the resonant state so that a nuclear relaxation accompanies this process (a time $t \sim 1/f$, where f is the characteristic frequency of the vibrational energy associated with state), inelastic tunneling will occur. It is also important to note that while inelastic transport is always incoherent, elastic transport can in general be coherent or incoherent. Randomization of the phase of the electron during elastic, incoherent tunneling can occur, for example, because of elastic scattering that randomizes the electron's momentum direction without changing its magnitude, as in a diffusive process. Another example is when the resonant energy level is sufficiently narrow that the electron is effectively localized for a significant amount of time during which memory of the phase is lost. Thus, depending on what is meant by sequential tunneling, the process can be temperature dependent (hopping) or not. Therefore, whenever the term 'sequential tunneling' is encountered, *caveat lector*!

The *flickering resonance* model was described in the ET discussion above and is further discussed in section 4.1. The main difference between the FR and sequential tunneling models is that flickering resonance is a coherent tunneling process involving several intermediate resonant energy states, where the electron does not spend much time within each intermediate energy state, and the entire process is elastic and is described by a single wave function within the barrier.

In all four cases, the energy levels of the intervening states inside the protein are generally considered to be thermally broadened, instead of the sharp resonance states used for the ET models shown in figure 5.

Proteins in molecular electronic devices have also been modeled as one-dimensional solid-state conductors (such as carbon nanotubes), in which case the Landauer formalism has been used to describe their ETp characteristics. This model ignores inelastic interactions and only takes into account elastic scattering at interfaces. If the molecule is considered a

tunneling barrier, and the temperature is low, the conductance is described by the Landauer formula

$$G = G_0 T(E_F), \qquad (6)$$

where $G_0 = \frac{2e^2}{h} \approx (12.9 \ \text{k}\Omega)^{-1}$ is the quantum unit of conductance (taking into account spin degeneracy) and $T(E_F)$ is the transmission coefficient of the barrier evaluated at the Fermi energy of the metallic contacts [56, 138]. The Landauer model can be extended to include molecular energy levels by taking into account resonant tunneling, in which case the transmission coefficient can be modeled by an effective Lorentzian width of the molecular energy level given by

$$T(E) = \frac{4\Gamma_L \Gamma_R}{(E - \varepsilon_0)^2 + (\Gamma_L + \Gamma_R)^2}. \qquad (7)$$

In equation (7), known as the Breit–Wigner formula, Γ_L and Γ_R are the coupling energies of the molecular orbitals to the left and right electrodes, respectively, E is the energy of the tunneling electron, and ε_0 is the energy of the molecular orbital (which in general can depend on the coupling of the orbital to the electrodes). This approximation is valid when $E \approx \varepsilon_0$ and the separation between molecular energy levels is greater than $\Gamma_L + \Gamma_R$. Note that if $E = \varepsilon_0$ and $\Gamma_L = \Gamma_R$, $T(E) = 1$, that is, perfect resonance occurs which results in ballistic transport.

We reiterate that in this review we focus on describing protein ETp (electron transport occurring in dry, solid state conditions) and on making further connections with ET (electron transfer that occurs in conditions where electrolytes play a role in the process) and protein biological function. To make real ETp measurements, it is necessary to immobilize the protein (unlike in measurements made in solution). This adds complexity to the problem because attachment of the protein to an electrode can itself change its electronic structure. This can occur as a result of hybridization with the metallic electrical contacts and/or the formation of Schottky barriers and image charges in the contacts. These interactions can change the electronic structure directly or by causing a configurational change that in many cases can render the protein biologically inactive. Therefore, understanding the effects of immobilization of proteins on their electronic structure is crucial to the interpretation of real experiments where ETp is measured. We discuss the effects of protein structure and immobilization of proteins in general on their ET and ETp properties below.

2.3. Protein structure, electron transfer (ET) and electron transport (ETp)

Biological functions of proteins are dependent on their structure in a fundamental way. As a result, preserving protein structure and chemical functionalities upon immobilization on a solid surface is key for studying both ET and ETp. In this section, we discuss some fundamental concepts related to protein structure that are relevant to ET and ETp.

Protein structure can be understood at several levels, the first being the primary structure, which is the linear sequence of amino acids, H_2N–(H)C(R)–CO(OH), held together by covalent, amide (or peptide) bonds, –(H)N–C(O)–, forming a polypeptide chain. The next level is the secondary structure,

where the polypeptide chains form higher order three-dimensional features (e.g. α-helices and β-sheets or turns) based on hydrogen bonding between amino acid peptide bonds. Lastly, a tertiary structure is formed by additional secondary structure elements that undergo the necessary folding by specific interactions, including formation of salt bridges, hydrogen bonds, and disulfide bonds, to achieve free energy optimization (lowest entropy) in the solvent, giving rise to a compact structure. Proteins are generally amphiphilic, i.e. they contain both hydrophobic and hydrophilic parts, with hydrophilic amino acids forming a protective shell via folding to minimize the exposure of hydrophobic amino acids to the solvent. In the case of multi-subunit proteins, where the sub-units are stabilized by the same interactions as the tertiary structure, a quaternary structure refers to the global structure of the connected subunits. Multi-subunit proteins are multi-protein complexes, with different complexes having different degrees of stability over time to achieve a specific set of functions. A well-known example is hemoglobin, which is a tetramer composed of four sub-units with a high degree of stability.

The oxidation-reduction potential of redox-active proteins is extremely sensitive to the structure of the polypeptides. For example, a single point mutation or minimal alteration of the secondary or tertiary structure of redox proteins can change the redox potential by 100 mV or more [139]. Conditions that break bonds or disrupt electrostatic interaction within proteins may result in a loss of the structural order of proteins, a process known as denaturation. Denatured proteins display some or complete loss of protein function.

Enzymes are proteins that act as macromolecular biological catalysts, and thus accelerate chemical reactions without themselves being altered by the reaction, often by binding to small molecules. An example of how enzymes work can be seen in the cytochrome family when discerning differences among members of the cytochrome P450s. Cytochrome P450 is denoted by 'CYP' followed by a number placing it in a gene family, a letter that denotes a sub family. An individual gene receives a second number. Thus, the name CYP2C9 represents a cytochrome P450 in the '2' family, the 'C' subfamily, and individual gene '9'. Both cytochrome c and cytochrome P450 are heme-containing metalloproteins (with Fe as the metal ion) that have comparable redox potentials for ET. P450s contain an active site that allows binding of small molecules, while cytochrome c does not. Different small molecules bind specifically to different P450s, coordinated to the heme group, and are known to alter the spin state of the heme Fe [140, 141]. Studies have shown that the presence of small molecules in the active site alters the rate of ET in multiple P450s [141] and our research has demonstrated that changes both in ET rate and ETp efficiencies of P450 from CYP2C9 occur when small molecules are bound inside the active site [142–144].

Electron transport across dry protein monolayers has been studied using solid-state protein-based molecular junctions, with macroscopic and nanoscopic current–voltage (*I–V*) methods [1, 47, 54, 145, 146]. Results have been reported for several protein types, such as those functioning as ET mediators, azurin (Az) and cytochrome c (CytC), or bacteriorhodopsin (bR), a light-driven H^+ pump protein, and proteins lacking any bound cofactor (bovine and human serum albumin, BSA and HSA). Despite some general similarities, these proteins differed in their ETp behavior. For instance, proteins with bound cofactors produce higher currents than those that lack it. These observations indicate not only that the primary sequence of the amino acid, which is mainly responsible for secondary structure is important, but also that the presence of a cofactor creates relatively efficient current transport paths and affects ETp in solid-state measurements.

The importance of the cofactor has also been demonstrated in studies of proteins for which the apo form (the protein without the cofactor) can be synthesized while retaining structural integrity. Specific examples are azurin, myoglobin and CytC, which have undergone rigorous studies in different forms. In the apo form, electrochemical redox properties are absent for all metalloproteins, and electron conduction efficiencies are reduced by only one to two orders of magnitude compared to the holo-protein, when both are measured in the dry solid state monolayer form [85]. For CytC, removing the heme group leads to denaturation, but it is possible to remove only the Fe (from the heme group), and this was found NOT to affect ETp at all, in contrast to its effect on ET, which showed loss of redox activity [147]. Cofactors often serve as the elements that facilitate superexchange-mediated tunneling for electronic charge carriers and protein-electrode electronic coupling, and alterations of these groups can affect ETp significantly [148]. Nanogap measurements of single myoglobin molecules in solid state demonstrated resonant tunneling through the heme group with a strong dependence on gate voltage only for the holo- but not the apo-protein [32]. In section 4.3.2 of the impact of cofactors on ETp is discussed further.

For electrochemical studies (figure 1), intramolecular electron transfer in redox proteins specifically relates to the binding sites of redox prosthetic groups and redox-active amino acids and their locations with respect to the working electrode, which influence the electronic coupling between the redox-active center and the electrode contact point [48, 50, 147, 149]. 'Doping' human serum albumin protein with hemin (porphyrin, protoporphyrin IX, with Fe^{3+}; in heme, the metal ion is Fe^{2+}) or retinoic acid enhances ETp efficiencies by more than an order of magnitude in solid state molecular junctions; with hemin, this protein also becomes redox-active in an electrochemical cell. The natural heme-containing protein, Cyt C, shows a symmetric cyclic voltammogram with an ET rate constant of $\sim 18\,s^{-1}$ (measured between the heme and the Au electrode), while the HSA–hemin complex exhibits an asymmetric curve with a somewhat lower ET rate constant of $\sim 5\,s^{-1}$ [147, 150]. In case of redox proteins we note that the cofactors carry out the redox reactions, which need not be so for solid-state ETp (details in section 4) [151].

In solid-state ETp across protein monolayers, electronic coupling (Γ, see equation (7)) to electrodes dramatically influences its efficiencies and the electron flow mechanisms [152, 153]. Experimentally, the thermal activation energy for ETp is found to be governed by Γ for all proteins that we have studied. This is illustrated by results on immobilized cytochrome c junctions, for which the thermal activation energy is reduced by approximately a factor of two, if it is covalently

rather than electrostatically bound to the electrode [153]. In the case of metalloproteins, electronic coupling is mainly controlled by the relative position of the redox cofactor w.r.t. the electrodes, and by its oxidation state [151, 153]. Covalent protein–electrode binding (hybridization) increases Γ, in the tunneling transport regime (30–150 K). Proteins that are covalently bound to the electrode via a cysteine thiolate yield ten times higher ETp efficiency than those that are electrostatically adsorbed on the surface [47, 84, 153]. Coordination changes of metal groups in different oxidation states also affect ETp. For example, the Fe in the heme group in myoglobin and cytochrome P450 (P450) undergoes a change in coordination upon ET that leads to a change between Fe^{3+} and Fe^{2+} oxidation states, which have different spin states. This type of coordination change is common in heme-containing proteins, and is known to have profound effects on both ET and ETp [51]. Another important consideration is how the cofactor is coupled in the ET pathway. Prytkova *et al* [129] proposed that the anomalously slow ET rates seen by Gray and Winkler in their histidine-modified cyt b_{562} derivatives (His 12 and His 73, see figure 4) could be explained by different coupling pathways to the heme group. In the case of these two slow ET rates, there is a pathway coupled to the ligand, axial (perpendicular to) the heme plane, as opposed to the other seven predicted rates with a pathway coupled to the heme edge.

An increase in transport efficiency was observed across a myoglobin monolayer on silicon if Mb was oriented by chemical binding of its hemin group to the substrate (via protein reconstitution) compared to a monolayer of Mb that was randomly oriented, i.e. its heme group was randomly oriented with respect to the substrate and, thus, with respect to the contacts [85]. This ability to change ET and ETp by binding and orientation could allow use of proteins with different properties in a precise way in bioelectronics.

One method for achieving desired characteristics is the design of metalloproteins *de novo* [154] or by utilizing native protein scaffolds [3]. *De novo* design has allowed the creation of metalloproteins with ET, redox-coupled proton exchange [155], hydroxylase [156], peroxidase [157], and oxygenase [158] activity. Metalloprotein design, using native protein scaffolds, has also been useful because the current incomplete understanding of protein folding mechanisms limits *de novo* design capabilities. Using techniques such as site-directed mutagenesis [159–161], it is possible to introduce new functions, metal specificity, and substrate specificity into existing metalloproteins [162–166]. A better understanding of protein function will allow greater control of protein design for use in bioelectronics.

2.4. General properties of immobilized proteins

The ability to immobilize proteins allows for a direct study of their electrical transport properties, including ETp (measured in solid state conditions) [47]. Protein immobilization is a powerful tool for controlling protein assembly and allows single molecule analysis. Immobilization entails physically localizing proteins in a region of space, usually on a solid-state substrate, while retaining their function for useful ETp

studies. Factors that determine protein function after immobilization include amino acid composition of their surface, physical and chemical properties of the solid substrate, and the type of interface between the protein and the substrate ('coupling') [167], all of which can affect the structure, orientation, and (average) conformation of the immobilized protein [131].

A variety of immobilization techniques have been used to link proteins to electronic components. For redox-active proteins immobilization should result in the part that is redox-active and the electronic component onto which the protein is immobilized appropriately positioned for efficient electronic coupling (but see discussion on [147], above). For photoactive proteins, immobilization should minimize fluorescence quenching by non-radiative energy transfer to the substrate.

Many proteins spontaneously adsorb on solid surfaces through hydrophobic or electrostatic interactions (physi-sorption), but uncontrolled and likely undesirable orientations of physisorbed proteins lead to multiple types of contacts and interactions with the surface, thus compromising the proteins' inherent functionality, which, for redox proteins often leads to a substantially slower electron transfer than in solution [47, 167–169]. For the creation of bioelectronic devices, achieving controlled immobilization via direct chemisorption of functional proteins on metal or semiconductor surfaces remains an important task. The challenge is to achieve direct ET between the protein and electrode.

Metalloproteins, such as azurin, plastocyanin and cytochrome c, adsorbed on the surface of solid substrates, have been extensively characterized by a combination of techniques, as assemblies or at the single molecule level. These techniques include measurements of their topography, as well as spectroscopic, and ET properties [28, 170–176].

Atomic force microscopy (see section 3.6.2) and scanning tunneling microscopy (STM) have been employed to investigate morphological properties, ETp, and redox activity of individual metalloproteins, chemisorbed on gold substrates [2, 32, 49, 83, 146, 177–183]. The arrangement and orientation of the proteins on a gold substrate, and their structural and dynamic properties, have been simulated using molecular dynamics [62, 178, 184, 185]. Conductive probe AFM (CP-AFM; see section 3.6.2) experiments and scanning tunneling spectroscopy (STS) have probed ETp across adsorbed proteins. Redox functionality of azurin, cytochrome c, and myoglobin, immobilized on gold, were found to be preserved by cyclic voltammetry measurements of ET [50, 111, 116, 186–190].

Electrochemical STM (EC-STM, see section 3.6.2) allows studying ET in solution with a variable electrochemical potential difference between sample and a reference electrode. In STM-based molecular junctions, redox-active cytochrome b_{562} was engineered by introducing a thiol group, allowing for controlled binding to gold electrodes [178, 191].

Various studies using a combination of spectroscopic and scanning probe techniques have found that immobilized proteins retain their structure at least partially over a range of electrochemical over-potential differences, as shown, for example, by the measurement of the ET properties of azurin immobilized on a gold substrate [174, 176, 192–195].
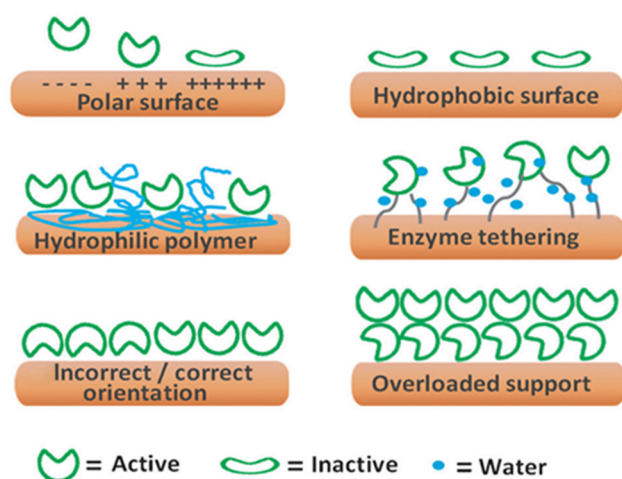
Figure 8. Enzyme immobilization on different interfaces and possible effects on the enzyme orientation/conformation. High charge density (above left) or hydrophobic surface (above right) are possible causes of enzyme conformational changes and inactivation. Enzyme co-immobilized with hydrophilic polymers (middle, left) or tethered (middle, right) can reduce unfolding and inactivating support–enzyme interactions. Incorrect orientation (below, left) and multilayer formation (below, right) may cause reduction of specific activity. Reproduced from [169] with permission of The Royal Society of Chemistry.

Proteins can be absorbed on surfaces through electrostatic interactions of charged surface amino acids and the solid surface [168], hydrophobic interactions if there are such exposed regions, or through tethering with a linker molecule [196–199]. Direct immobilization to the substrate not only gives poor control of the protein orientation, as noted above, but also often results in inactive protein conformations.

Proteins are classified into two groups in terms of rigidity, which is a measure of the protein's ability to resist conformational changes upon adsorption to a surface [169]. The terms 'hard' and 'soft' are used to characterize flexibility of a protein, as deduced from its molecular adiabatic compressibility [200]. Protein rigidity can affect the viability of the protein if attached to a solid-state surface. Hard proteins, such as horseradish peroxidase, lysozyme, and ribonuclease A, generally go through minimal conformational changes upon adsorption [201]. In contrast, soft proteins, such as bovine serum albumin, myoglobin, and hemoglobin, are usually more susceptible to interaction with the surface onto which they are adsorbed and can show marked changes in secondary and tertiary structure upon adsorption [202]. Strong interactions with a solid substrate can even denature soft proteins that lack a rigid structure [201]. The nominal surface coverage for maximum protein activity correlates with the rigidity of the protein [203]. Although adsorption on a solid surface can lower protein activity due to denaturation, in some instances it increases stability of proteins, and actually enhances activity. Several studies have demonstrated an enhancement of lipase activity if immobilized to hydrophobic supports [204, 205]. Enhancement of protein activity and increased stability were also demonstrated on nano-scale platforms, where a possible reason may be nano-structuring, i.e. binding between substrate and protein promotes more active and/or
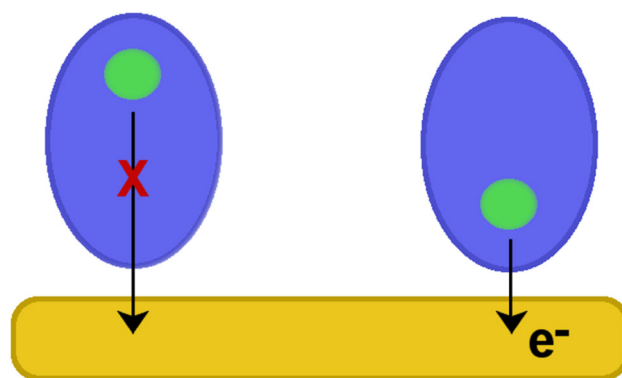

Figure 9. Effect of orientation of immobilized protein (blue) on direct electron transfer with electrode. On the left the redox group (green) is far away from the electrode (yellow), and electron transfer cannot be observed. On the right, the redox group is close to the electrode allowing for efficient electron transfer. Reproduced from [234]. CC BY 4.0.

stable conformations than is the case for the unbound protein [20, 206–209].

3. Methods of protein immobilization

Immobilizing proteins is critical for studying electron flow across proteins, especially those related to ETp, where electronically conducting contacts are required. For ETp studies to be biologically relevant, immobilized proteins must be in their native conformation with structural and biological activities preserved. For electrical conduction studies and other applications, historically the first strategy employed was protein immobilization on bare metal electrodes or metal electrodes modified with small molecules to promote protein adsorption. Direct absorption was found to be ineffective because of loss of biological function, and thus electrodes modified with organic overlayers were developed to address this problem. In this section, we review these attachment techniques and the ways in which the attached proteins can be characterized.

3.1. Direct adsorption

Polycrystalline metals, conducting polymers, semiconductors, especially silicon, or metal oxides, and carbon electrodes have all been used for direct immobilization (see [210] for a recent review of semiconductors as substrates/electrodes for molecular electronics) [211–216]). As mentioned previously, proteins are immobilized non-covalently by passive adsorption onto the surface through hydrophobic or electrostatic interactions (figure 8).

Redox-active proteins can be studied by protein film voltammetry (PFV), pioneered by Armstrong, where the protein is adsorbed directly on to the electrode surface and probed electrochemically with techniques such as cyclic voltammetry (figure 1) [217, 218]. In PFV it is important to choose an electrode surface that allows adsorption of the protein in an electroactive conformation, usually with the redox center near the electrode (figure 9). While electrodes
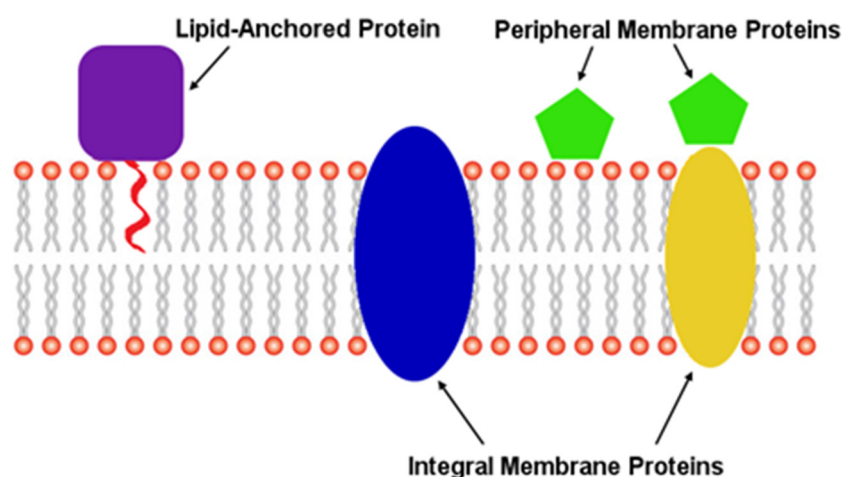
Figure 10. Example of protein interactions with lipid membranes in nature, which are dictated by the proteins' hydrophobic and hydrophilic surface groups. Membranes consist of amphiphilic phospholipids with hydrophilic phosphate heads and hydrophobic tails. Proteins can be embedded within the lipid environment as depicted for integral membrane proteins. They can be bound to lipid head groups or exterior surfaces of embedded proteins as seen for peripheral membrane proteins, or they can be linked to the membrane via a hydrophobic tail group that buries itself in the lipid membrane.

like pyrolytic graphite (PG), which can be polished to add oxide functionalities, making it hydrophilic, have a distinct advantage over metals in allowing multiple and varied interactions with protein surfaces, metal electrodes are better suited for chrono-amperometric and impedance measurements [69, 219, 220] due to the absence of slow charging issues with graphite [221].

Utilizing PFV, Hill, Kuwana, and co-workers demonstrated reversible diffusion-controlled voltammetry of adsorbed cytochrome c [222, 223]. This approach was further extended to other proteins, including azurin, to demonstrate electron-exchange studies [217, 221]. Direct adsorption of multi-heme proteins, such as cytochrome c nitrite reductase [224, 225], fumarate reductase [226–228], and flavocytochrome c₃ [229], reveal distinct redox peaks for each heme group. These studies enabled interrogation of ET in flavin adenine dinucleotide (FAD) cofactors, covalently attached to the redox enzyme fumarate reductase, and non-covalently attached to flavocytochrome c₃. FAD is particularly prominent in voltammetry because of its two-electron transfer center, which can be detected electrochemically easily, compared to other methods like UV–visible spectroscopy, where it is obscured by the intense bands from heme groups [230].

In situ vibrational (Raman and IR) spectroscopy measurements have been carried out to examine the retention of the structure and conformation of proteins after direct immobilization via adsorption or covalent attachment to electrode surfaces [231–233]. ET activity, as measured by electrochemistry, is often hindered by the large distance of redox-active groups (several nm) from the electrode surface upon adsorption (figure 9). The spectroscopy data, together with large changes in the electrochemical potentials, also have shown that direct immobilization can result in denaturation, such as a loosening of the helix packing, including partial dissociation of a histidine ligand in the ferrous state.

3.2. Modified electrodes

Indirect adsorption of proteins using a chemical linker or cross-linked reagent [235] on modified electrodes allows for better protein structure than direct adsorption. Thiol-containing molecules allow for the formation of self-assembled monolayers (SAMs) on metal surfaces, which provide a convenient and simple system with which to tailor the interfacial properties of electrodes [211, 236–237]. Proteins with a natural dipole moment (such as membrane proteins) are electrostatically adsorbed to a polar head (carboxylate, amine) group of a SAM, which in turn is attached to an electrode. Successful surface modifiers are often those that bind the protein in a fashion similar to that of known redox factors, i.e. small molecules or proteins, which mediate ET from a donor to an acceptor, and preferably at the same location [238]. Extensive characterization has revealed that binding of proteins to their redox partners often involves hydrophobic and electrostatic interactions [239–245], and thus tailoring the choice of surface modifier to mimic natural interaction can position and adjust the (average) protein conformation [131] for optimal electron transfer properties upon adsorption.

A number of surface modifiers have been evaluated for enhancement of heterogeneous ET of immobilized cytochrome c, and it has been proposed that successful modifiers allow a cytochrome c conformation with the prosthetic heme group close to the electrode [246, 247]. Later work demonstrated that electronic coupling greatly impacts ETp, with covalent attachment doubling the current density compared to electrostatic adsorption [153]. No correlation could be found between measured current and electrode-heme distances, although close electrode-heme distances generally displayed more efficient ETp [153]. Electron transfer of immobilized cytochrome c has been accomplished via various small organic linker molecules, especially those containing thiol groups [248–254].
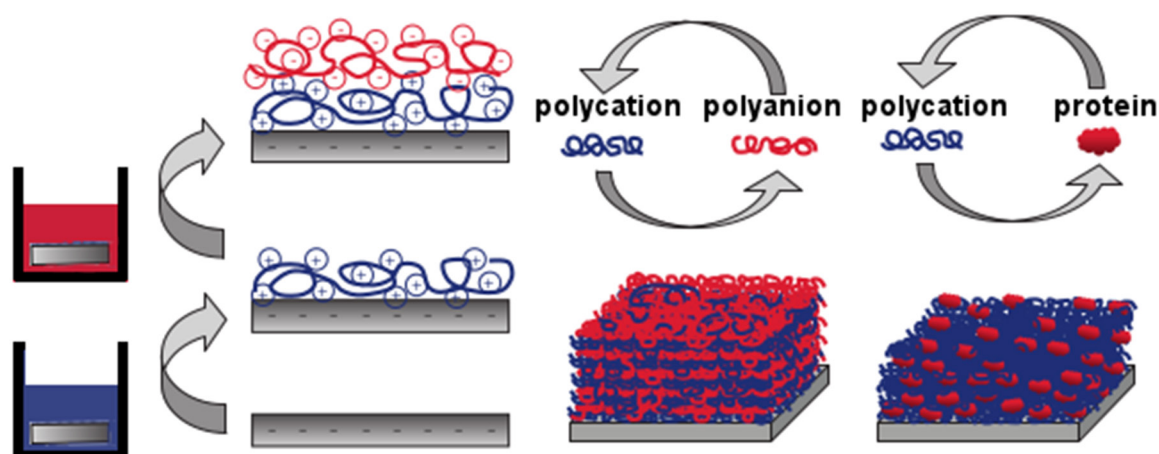
Figure 11. Representation of layer-by-layer (LbL) formation on a substrate using polyanions (negatively charged polymers, shown in red) and polycations (positively charged polymers, shown in blue). Layers are formed by immersion of the substrate in alternating solutions of polycations and polyanions. This allows the creation of a film to entrap a desired protein based on its surface charges, as shown on the right for the positively charged protein (in red). Reprinted by permission from Macmillan Publishers Ltd: Nature Materials [269], Copyright (2009).

Chemically functionalized long-chain molecules, such as silanes or thiols, can spontaneously assemble on metal, glass, and carbon surfaces to form stable covalent bonds between their terminal functional group and the activated metal, metal oxide, or silicate. Densely packed, organized molecular layers assemble approximately orthogonal to the surface via extended hydrocarbon chain linkers [236]. Early examples include monolayers of long chain alcohols on carbon glass [211, 255, 256], long chain amines on platinum [257], alkyl trichlorosilanes on silicon and mica [258], and long chain thiols, thioesters, thiones and alkyl disulfides [259–261] on gold.

Amphiphilic molecules, such as siloxanes, alkanethiols and carboxylic acids, form well-ordered mono-layers on metal and metal oxide surfaces [236, 262–264]. Long chain thiols such as the 11 carbon units long 11-mercapto-undecanoic acid (MUA; ~1.1. nm), shorter ones such as the 3 carbon unit long mercaptopropionic acid, and others have been used to immobilize proteins [265]. On metal electrodes, the long-chain thiols form a dense self-assembled layer that is effective as a promoter, i.e. an electro-inactive surface modifier that enhances ET of immobilized proteins [266, 267]. Linker length [47, 268] and composition [262] have been shown to affect the electron transfer rate.

The control of protein stability and orientation through surface modification has led to the development of many different techniques to enhance ET rates in, and ETp efficiency across proteins. In addition to the small molecules mentioned above, polymers [111, 198, 269–272], surfactants [185, 250, 273, 274], clay composites [275–279], and nanoparticles (NPs) [280–285] have been used to modify electrode surfaces to achieve effective coupling between the electrode surface and immobilized redox proteins. These compounds help to enhance protein immobilization through their entrapment in thin films. Thin films provide a favorable microenvironment for proteins, similar to biomembranes [286], allowing them to retain their native conformations while enhancing the electron transfer to/from the electrode with respect to systems where the proteins are closer/tighter bound to the substrate. As the adsorbed protein is strongly bound to the film, much lower protein concentrations are required for

SAM-modified surface methods than for direct immobilization, where the protein binds reversibly to the surface [287].

Electrodes modified with surfactants and/or lipids can mimic the membrane environment where proteins are found in nature. This is especially true for enzymes which function in nature while bound to, or embedded in bi-layer lipid membranes (figure 10) [288]. These surfactant/lipid films are generally water-insoluble, have polar head groups, and contain one or more relatively long hydrocarbon chains. Lipids and surfactants can form stable multilayers through electrostatic interactions with electrodes maintaining the native conformation [274, 286, 289]. Thus, the goal in this approach is to create an environment on the electrode that allows proteins to be immobilized in a manner that mimics their natural, membrane-bound environment and maintains their native conformation that facilitate electron transfer across protein-based junctions.

Work by Murray and co-workers is the first report of reversible ET of a protein incorporated in a polymer film on an electrode [290]. In their work, cyclic voltammograms for cytochrome c, incorporated in gel coatings of poly-acrylamide and polyethylene oxide, yielded reversible peaks, indistinguishable from cytochrome c in aqueous solution. The success of this study led to the investigation of different polymers and methodologies for direct electron transfer studies. Amphiphilic polymers, polymers containing both polar and non-polar groups, have been demonstrated to allow immobilization of myoglobin and hemoglobin, in their native conformations [291, 292]. In addition to amphiphilic polymers, there has also been increasing interest in using naturally created biopolymers as immobilization matrices for proteins because of their biocompatibility and non-toxicity, and a variety of natural supports have been used to immobilize proteins successfully [293]. Ultra-thin clay coatings, such as sodium montmorillonite, kaolinite, talc, goethite, and ochre, have also been demonstrated to promote the direct electrochemistry of heme-containing proteins [277–279, 294]. An example is sodium montmorillonite, which is used to immobilize redox proteins and enzymes onto glassy carbon electrodes (GCE) for sensitive chemical and gas sensor applications [295].
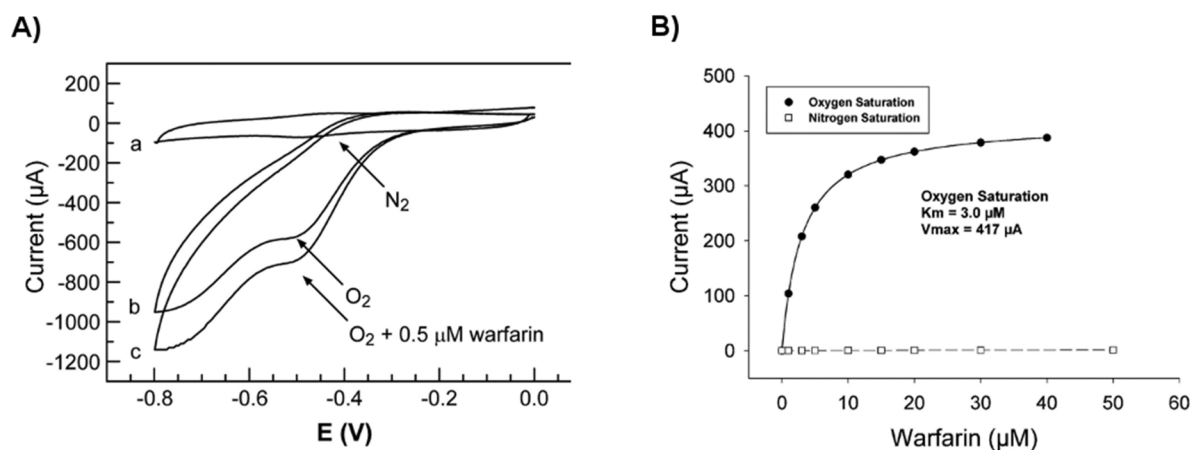
Figure 12. (a) Electrochemical Current–voltage curves, Cyclic Voltammograms, of CYP2C9, covalently immobilized to Au(111) via a linker SAM at a scan rate of 1.6 V s^{-1}. Curves were obtained in the absence (curves a, b) and presence of warfarin (curve c), a small molecule that binds CYP2C9 and coordinates with its heme group. In the absence of O_2 (curve a), the reaction stops at the conversion of Fe^{3+} to Fe^{2+} and there is no reduction. (b) Reduction (of P450) current dependence on the concentration of warfarin. The solid line is the non-linear regression fit of the oxygen-saturation data, and the dashed line is the linear regression line of the nitrogen-saturation data. Reproduced with permission from [144]. American Society for Pharmacology and Experimental Therapeutics (2009).

Polyelectrolytes, which are polymers with negative charges (polyanions) or positive charges (polycations), have also been used to immobilize proteins on a substrate surface, using layer-by-layer (LbL) deposition (figure 11). First proposed for the synthesis of charged colloidal particles and proteins [296], later work established that adsorption at every stage of poly-anion or polycation assembly leads to multilayer formation and a reversal in the terminal charge [297]. In LbL growth, multiple layers of oppositely charged films of proteins, which have natural surface charges, and polyelectrolytes of opposite charge, are built up on the electrode surface, providing several active layers of entrapped protein (figure 11). Layers can be formed by successive submersion/wash/submersion cycles of a substrate in solutions of the relevant polyelectrolytes, each at a pH suitable for the desired ionization; greater layer control and reproducibility can be achieved through electrochemical deposition [271]. The ability to incorporate multiple layers on an electrode increases the effective protein concentration on the surface, and could thus enhance downstream applications such as biosensing sensitivity. It, also enhances control over the film architecture when compared to solution-casting [289].

In addition to polyelectrolytes, NPs have also been investigated to generate ultrathin protein films [298–300]. Inorganic NPs have large surface areas, can have good biocompatibility, and provide a favorable microenvironment for electron transfer from electrodes to proteins. Using NPs in conjunction with polyelectrolytes leads to protein films on electrodes that are more electroactive than what is obtained by layer formation with polyelectrolytes alone. This is evidenced by an increase in how thick a protein layer remains electroactive, when formed with LbL immobilization: from ~1.4 electroactive layers for polyelectrolyte—myoglobin films on gold [111] to 7 electroactive layers of polyelectrolyte—myoglobin films on pyrolytic graphite [270], and up to 10 such layers with polycations and manganese oxide NPs [301]. He and Hu also demonstrated that LbL films of myoglobin, hemoglobin, and horseradish peroxidase with silicon dioxide nanoparticles

retained their electroactivity of samples up to 6 layers thick, and such immobilized proteins can electrochemically catalyze reactions with their respective bound ligands [283].

3.3. Protein tethering through linker

Proteins attached to substrate surfaces through an organized monomolecular layer with site-specific immobilization should provide better reproducibility and better control over electron transfer and transport measurements than randomly immobilized proteins, by eliminating unpredictable orientations and improving uniformity of protein conformation. Indeed, covalent attachment of proteins to an electrode via a tether has become a robust method to control protein adsorption [53, 192, 302]. This allows for a greater degree of control over protein orientation on the SAM surface, for an appropriate choice of linker and for controlled coupling chemistry [214].

To overcome the slow ET rates reported in studies of electrostatically adsorbed proteins on modified electrodes, researchers have immobilized unmodified proteins through *covalent* attachment to SAMs on an electrode. There are various techniques that have been used to covalently link proteins to SAMs [303]. One of these uses chemical activation with reagents ('EDC-NHS' method)[10] to bind a protein to a carboxylate (COO^-)-terminated SAM via a surface-exposed amine (NH_2) group of the protein. In this method, a covalent, amide bond (–(H)**N**–**C**(O)–) is formed [304] by activating the carboxyl group of the thiol linker molecule to allow bond formation with the amine (–NH_2) group of the protein [85]. If the substrate is reflective, then Fourier transform polarization-modulation infrared reflection-absorption spectroscopy, PM-IRRAS, can serve to confirm bond formation [305]. The EDC-NHS method has been used successfully to covalently

---

[10] 1-ethyl-3-(3-dimethylaminopropyl)carbodiimide. *1-Ethyl-3-(3-dimethyl-aminopropyl)carbodiimide* (https://en.wikipedia.org). Available at: https://en.wikipedia.org/wiki/1-Ethyl-3-(3-dimethylaminopropyl)carbodiimide.
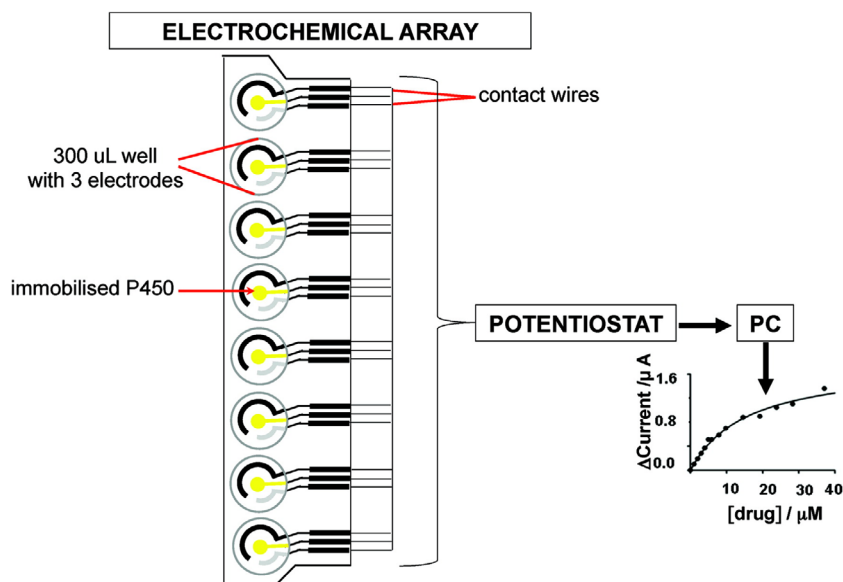
Figure 13. Schematic of a high-throughput drug screening plate with eight parallel cytochrome P450-electrode containing wells. The P450 was covalently immobilized through coupling between a sulfur atom of the linker molecules and the gold electrode (yellow). Each well also contains a Pt counter electrode (black) and carbon reference electrode (gray). Current was measured by a potentiostat as drug is added in increasing concentrations to determine current maxima. Reprinted with permission from [310]. Copyright (2011) American Chemical Society.
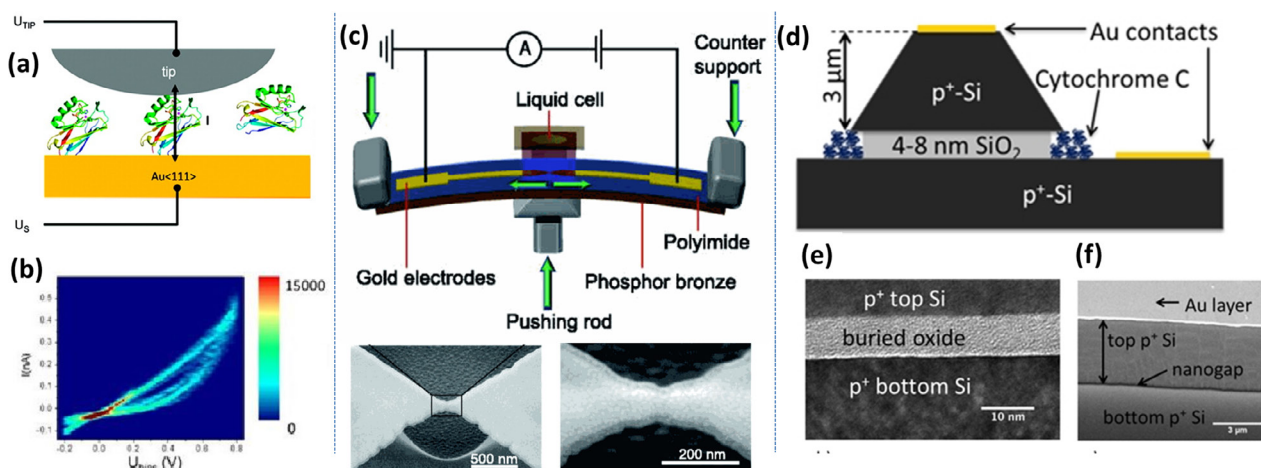

Figure 14. (a) Experimental electrochemical tunneling microscope, EC-STM, set-up for single protein junctions consisting of azurin-bridged between a gold substrate and the probe of an EC-STM and (b) 2D *I*–*V* histogram showing two populations of curves in azurin following its orientation in EC-STM junction configuration. (c) Schematic of the mechanically controlled break junction (MCBJ) with a liquid cell and scanning electron microscope images of electrodes in MCBJ devices. (d) Schematic of vertical nanogap device with protein molecules assembled in the gap (drawing is not to scale); (e) and (f) corresponding scanning electron microscope images. (a) Reprinted with permission from [31]. Copyright (2012) American Chemical Society. (b) Reprinted with permission from [316]. Copyright (2011) American Chemical Society. (c) Reprinted with permission from [317]. Copyright (2016), AIP Publishing LLC. (d–f) Reproduced from [318]. © IOP Publishing Ltd. All rights reserved.

attach different proteins to a gold surface [306]. For example, immobilized cytochrome P450(CYP2C9) was shown to retain its enzymatic activity in the presence of its redox partners cytochrome P450 reductase (CPR), and nicotinamide adenine dinucleotide phosphate (NADPH, a biological redox agent) [144]. A cyclic voltammetry scan of the Au/Linker/CYP2C9 electrode revealed quasi-reversible reduction and oxidation peaks in the range of known redox and oxidation potentials for P450s (figure 12(a)) [307]. CYP2C9-modified electrodes were also used to sense small molecules. This is possible as the current (*I*)–concentration (*C*) curves agree with the Michaelis–Menten equation [308],

$$I = \frac{i_{\max} C}{K_{\mathrm{M}}^{\mathrm{app}} \pm C}, \tag{8}$$

where $i_{\max}$ is the maximum current, C is the concentration of the drug, and $K_{\mathrm{M}}^{\mathrm{app}}$ is the Michaelis constant which describes how well a small molecule (ligand) binds to the enzyme (figure 12(a)). The work showed that concentration-dependent increases in current were observed only when the full P450 reaction cycle was completed, in the presence of both O_2 and Warfarin (ligand). More recently, Fantuzzi *et al* showed rapid determination of small molecule binding to various cytochrome P450s using a SAM linked P450-electrode integrated
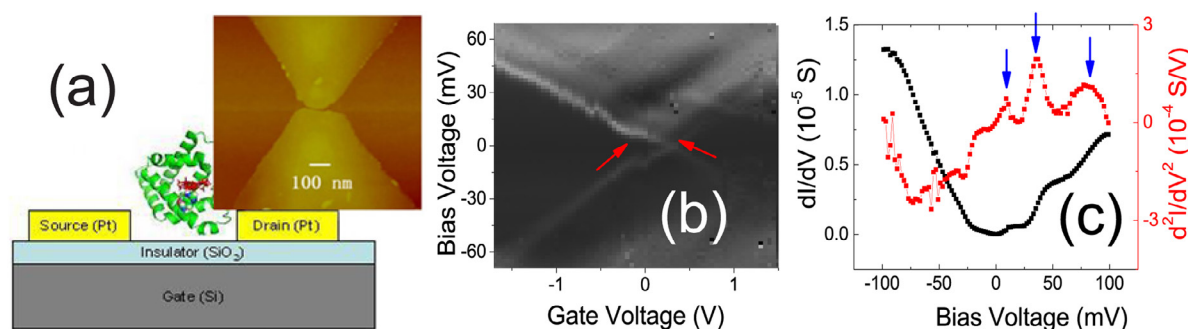
Figure 15. (a) Sketch of a three-terminal device and AFM image of a bare Pt junction broken by electromigration. The AFM image indicates that the gap is on the order of 5 nm wide. (b) Differential conductance (dI/dV) data from a Mb sample (gray scale from 0 (black) to 5.0×10^{-6} S (white)) at $T = 6$ K. The red arrows point to vibration-assisted (inelastic electron tunneling spectroscopy, IETS, see section 4.3.4. and figure 29) conduction lines. (**c**) dI/dV (black) and d^2I/dV^2 (red, the IETSpectrum) spectra at $V_G = 11$ V for another myoglobin sample at $T = 6$ K. The vertical arrows correspond to inelastic tunneling peaks (see section 4.3.4). Reproduced from [32]. © IOP Publishing Ltd. All rights reserved.

into a high-throughput plate format (figure 13) [309, 310]. Taken together, these results demonstrate successful use of a linker to preserve innate protein functionality, which allow for biologically-relevant ET(p) studies and suggest possible bio-sensing platforms.

Non-redox proteins were also successfully attached on Au(111) surface using carboxylic acid-terminated thiol (–SH) molecules, where the thiol group binds to the Au surface following the EDC-NHS reactions discussed above [85, 311, 312].

Protein immobilization by itself does not guarantee that individual proteins can be placed exclusively on specific sites on a device. To achieve placement, multifaceted approaches have been implemented that combine different techniques. For example, a regular array of Au bottom nanowells (100 nm diameter), fabricated using nanosphere lithography, was modified by covalent immobilization of biologically active cytochrome P450 (CYP2C9) via coupling to a SAM of octa-nethiol [313]. An array of 10 nm diameter Au nanopillars, functionalized with suitable SAMs, allowed reliable determination of β values (see equation (2)) for alkanethiols that agreed with previous studies [314]. With a similar approach, we used an indexed array of gold nanopillars as individual pixels for protein immobilization to which CYP2C9 could be linked using a SAM comprised of a mixed thiol layer [142, 143]. Indexing of the array allowed multiple studies on the same P450 enzyme exposed to different substrates.

3.4. Break-junction, nanoscopic techniques

To help understand protein structure–function relations, and explore the use of protein properties for bioelectronics, the ability to study single proteins is an important complement to the monolayer studies discussed above. Measurements of monolayers provide average values of a large ensemble of proteins in various conformations, and thus the data represent a statistical average over all proteins that may hide specific transport features. In single molecule break-junction studies, a conductance trace across a single protein captures a time-averaged statistical histogram of conductance distributions over many conformations (>~10 000 traces, depending on the temperature and how fast the data are acquired). Thus, the

method can provide information on conductance variations over protein conformation fluctuations.

There have been several investigations of ET and ETp properties of single proteins. One method involves the use of electrochemical scanning tunneling microscopy (EC-STM; see section 3.6.2) to investigate electron transport across a single azurin protein [176, 195, 315, 316]. An advantage of this method is the high spatial resolution of EC-STM that allows visualization of single proteins that are measured (figure 14(a)). Although EC-STM allows confirmation of the existence of single proteins, it does not provide a means of controlling aggregation. Another disadvantage of this method is that it does not allow multiple measurements to be conducted on the same protein after removing the sample, which prevents systematic studies to be performed under different conditions. The recently reported possibility to use mechanical controlled break junctions in aqueous environment [317] opens the possibility of forming such junctions with proteins, which may improve the control over the force applied to this floppy system, something that is a problem in other single molecule junction methods (figure 14(b)).

Another nanoscale technique for studying single proteins involves the creation of nano-gap electrodes through mechanical breaking [319, 320] or electromigration techniques [321]. Electromigration has been used to create electrodes with 5 nm gaps for protein entrapment between Pt source and drain electrodes deposited on Si oxide/Si substrates [32]. This narrow gap allowed isolation and interrogation of molecular energy levels of apo-myoglobin or myoglobin single proteins [29, 32].

The availability of apo-myoglobin (myoglobin without the heme group) allows performing controlled experiments to determine the relevance of the heme group to ETp. The role of the heme group was studied explicitly by Li *et al* using Pt break junctions deposited on a SiO$_2$/doped Si substrate. A drop of the protein solution was placed on the Pt junction, which was then cooled to 6 K and broken by applying a large voltage (electromigration) [32]. In a successful sample, a single protein would fall into the ~5 nm gap, and using the Pt contacts as source and drain electrodes, and a bottom contact on the Si substrate as a gate electrode, a transistor structure was formed (figure 15(a)). Coulomb blockade triangles were observed at

6 K in the drain-source versus gate voltage conductance maps for myoglobin samples, indicating the presence of single electron transistor (SET) behavior (figure 15(b)), but not in any apo-myoglobin samples. During the tunneling process in a SET, the Coulomb repulsion between a tunneling electron and electrons at the contacts precludes simultaneous tunneling of more than one electron at a time, and the transport is characterized by Coulomb blockade triangles in the differential conductance data. The presence of Coulomb triangles in the myoglobin data proved that ETp across the protein can proceed via energy levels that allow resonant tunneling within the protein. We note, however, that the conductivities measured were an order of magnitude larger than those observed in semiconductor quantum dot SETs [322–324]. Inelastic electron tunneling spectroscopy (IETS), where the second derivative of the conductance data is measured to determine if vibrational levels are involved in the tunneling process (IETS is discussed further in section 4.3.4), indicated that these resonant energy levels are associated with electronic energy levels of the heme group (figure 15(c)) [32]. The results of this work are consistent with ETp composed of an incoherent sequential tunneling process (see section 2.2) through the protein with resonant energy levels associated with the iron heme. The key role played by the heme group energy levels in the enhancement of the (ETp) conductivity in metalloproteins is consistent with the work of Raichlin *et al* [85] on myoglobin and apo-myoglobin, and with some of the theoretical models discussed in section 2 above, which rely on the alignment of internal energy levels for efficient ET and ETp.

In more recent work, ETp in cytochrome c was characterized with a vertical nanogap device [318]. The devices were comprised of all silicon contacts and represent the first approach towards nanometer-spaced silicon contacts to proteins. The work demonstrated the ability to conduct nanoscopic solid-state ETp measurements via a protein, revealing thermal activation only above 140 K.

The success of these studies on heme-containing myoglobin and cytochrome c is proof that nanogaps can be applied to study other (metallo) proteins. However, nanogap contact configurations have several drawbacks. Creation of working junctions is inefficient (low yields) and, if not performed correctly, can result in probing of the characteristics of non-molecular components of the junction. For example, if metal nanoscale islands remain in the gap during the electromigration process, they could dominate the measurements instead of the molecule of interest [32, 325]. In addition, to date it has been not possible to control the orientation nor to determine the conformation of the protein on the electrodes. More details about the nanoscopic techniques are discussed in section 3.6.2.

3.5. Macroscopic and permanent contact measurement

Studies on the single molecule level are of great scientific importance, but reaching conclusions is limited by the statistics and reproducibility that can be achieved. Ron *et al* established a broad experimental basis for studying ETp across proteins in a dry state, and thus, undoubtedly, at least a partially dehydrated solid-state configuration [63, 326].

Measuring the collective electrical properties of an ensemble of molecules, in the form of a monolayer, led to highly reproducible results, which indicated electrical behavior of these macromolecules, comparable to that of organic molecules. Surprisingly, the ETp efficiencies (measured as currents at a given voltage) were more like conjugated than saturated molecules [63]. One advantage of using macroscopic electrical contacts on protein monolayers over nanoscopic methods is that protein monolayers can be characterized *in situ* by various spectroscopic measurements before a top contact is made (IETS, described in section 4.3.4, is an exception). Along with obtaining information about protein structure upon assembling proteins into a device configuration, it is possible to verify protein orientation with respect to the electrodes and provide information about *in situ* structural alterations during electron transport. A systematic alteration of protein-electrode combinations allows to obtain an understanding of how protein/contact interactions can affect ETp processes.

For macroscopic contacts, a dense protein monolayer is prepared on conducting substrates, such as a highly doped Si wafer, or template-stripped gold/silver (rms roughness ⩽ 1 nm), which can serve as substrates and bottom electrode of protein-based junctions [87, 88, 148, 216]. Low roughness is important for macroscopic junctions, because otherwise the probability for electrical shorts is too high, leading to questionable results and/or low junction yields. Common top contacts are Hg or In–Ga eutectic (E-GaIn) electrodes [254, 327, 328]. The former has the advantage of being semi-noble, and with a surface that will thus be much better defined and cleaner than those of most other contacts, with the possible exception of evaporated Pb (see below). Its main disadvantage (in addition to its toxicity) is its relatively high vapor pressure, which allows for ready amalgamation with Au, unless an extra molecular layer is adsorbed on the Au.

In–Ga was used recently, to fill PDMS micro-channels, resulting in a contact configuration with a reportedly better defined junction contact area than in earlier experiments, allowing recycling these junctions *with reproducible measurements* [83, 145].

Another method for top contact formation is floating ready-made thin metal pads onto monolayers (lift-off float-on, LOFO). The pads (circular Au films with >0.1 mm diameter) are then transferred onto protein monolayers in a non-destructive way, serving as a top electrical contact [88, 148]. This protocol helps avoid possible thermal damage to the proteins and metal penetration through the monolayer, both of which are likely to occur using direct thermal evaporation of most metals. An exception is thermal evaporation of Pb, which can be done under very mild conditions and which was recently shown to allow good contact to bR monolayers, following earlier work with organic molecules [329, 330]. These contacting schemes also shield the protein layer from the surrounding atmosphere, which is advantageous because it protects the proteins. The down side, however, is that the proteins are not accessible for chemical interactions with other molecules, which is possible in the nanoscopic contacting schemes discussed above.

To obtain junctions that are intermediate between macroscopic and AFM-type nanoscopic ones, photo-lithographically patterned Au substrates and gold nanowires can serve to form solid-state molecular junctions with protein monolayers [331]. Such junctions are also of interest for monitoring optical plasmonic effects [331–336]. Gold nanowires can be trapped on molecularly modified electrodes by AC dielectrophoresis [337, 338]. As an alternative geometry, devices with electrode gaps of 10–50 nm, developed via complex (electron-beam) lithography have been used to trap proteins so as to allow transport measurements while still allowing the proteins to interact with the surrounding [30, 32, 339].

Both macroscopic and nanogap junctions demonstrate possible avenues toward the fabrication of permanent electrical junctions, where proteins can be wired without harming them. Such a development will allow studying transport mechanisms via these junctions in detail, combining different experimental techniques, interaction with the environment, and using biological activity as an active electronic function.

3.6. Measuring protein adsorption and functionality on a surface

3.6.1. Optical techniques. Linking ETp measurements across proteins, especially enzymes, to their biological electron transfer function requires studies of functional immobilized proteins that are in conformations similar to those of their native states. To interpret results obtained from immobilized proteins, it is necessary to know the protein layer thickness, density of adsorbed proteins, their orientation, secondary and tertiary structure, protein stability, and most importantly, the effect of adsorption on their biological function [170]. Many studies of immobilized proteins use electrochemical techniques, in particular cyclic voltammetry (see figure 1), to ensure their electroactivity after immobilization. These studies can show if immobilized proteins are still capable of catalytic turnover, i.e. small molecule transformation. An example can be seen in studies of currents through [Fe–Fe]-hydrogenase, immobilized on Au (1 1 1), after adding its specific bound ligand, H_2 in this case. The current obtained was directly proportional to the protein's catalytic turnover rate and to the electrode potential [340]. Using this approach, the turnover rate has been determined for various hydrogenases [341–343]. The finding that the immobilized protein still retains its biological activity can also be supported via measurement of products, if electrochemical techniques are coupled to standard detection techniques such as high performance liquid chromatography and liquid chromatography-coupled mass spectrometry [344].

Although these characterization methods offer no information on the orientation of the immobilized proteins, information can be obtained on the homogeneity, in terms of orientation and conformation of the adsorbed proteins, from the width of voltammogram peaks. For example, peak widths wider than 90 mV, the theoretical value for a typical single electron wave of an adsorbed protein [345], point to heterogeneous protein orientation [145].

Circular dichroism (CD) spectroscopy is a well-recognized technique for examining the secondary structure of proteins, especially the degree of helicity (essentially the presence of α-helices)[11][346]. Recent solid state CD measurements of intermolecular interactions do not give rise to large discrepancies between the L/R absorption spectra [347, 348]. Thus, no CD data that provide convincing information on the conformation of the proteins that make up the monolayer have been reported. To overcome this limitation, CD measurements in solution of nanoparticles onto which proteins are adsorbed as monolayers are sometimes used to examine possible structural alterations after immobilization [349, 350].

Some properties, such as heme spin state and binding of substrates to heme proteins, can be obtained readily with UV–vis spectroscopy in solution [351, 352]. For example myoglobin's optical absorption spectrum is characterized by its very intense Soret band (molar attenuation coefficient $\epsilon \approx 0.02 \, m^2 \, mol^{-1}$ in SI units) at 409 nm[12] [353] that can be detected even in a single monolayer with an absolute photoluminescence quantum yield spectrometer [354], and which can be used to resolve protein aggregates by monitoring peak shifts [355]. Another example is that of cytochrome P450, which exhibits a Soret band at 450 nm ($\epsilon \approx 0.0091 \, m^2 \, mol^{-1}$) in its reduced form bound to carbon monoxide [356]. This peak shifts to 420 nm ($\epsilon \approx 0.01765 \, m^2 \, mol^{-1}$) if the protein is denatured, and can be used to estimate which fractions of the protein are native or denatured [357].

A very sensitive technique for measuring attachment of ultra-thin films of atoms or molecules, including proteins, is that of a quartz crystal microbalance (QCM). The QCM technique measures changes in oscillating frequency of the substrate upon mass load to determine layer thickness [170]. Electrodes covering the QCM piezoelectric crystal can be coated with practically any desired thin film, allowing tailoring to the relevant immobilization scheme.

Optical techniques are widely used for monitoring protein structure, conformation and specific functions [358, 359]. Proteins with photo-induced conformational changes (bR, Halorhodopsin, photoreceptor-YtvA, Dronpa,) show shifts in the optical absorption band when converted between light- and dark-adapted states, not only in buffer solution but also after immobilization on quartz as a monolayer [88, 360–362]. In a few cases, a small shift in the optical absorption has been observed, which has been explained by the absence of hydration shells surrounding the optically active components upon monolayer preparation [360]. Recently, photoswitching was reported for Sn-substituted Cyt C and attributed to photoexcited hole transport [254].

Different optical techniques are employed to determine monolayer surface coverage on different substrate and protein-electrode interactions. The thickness and quality of protein monolayers, prepared by chemi- or physisorption on different solid substrate surfaces, have been routinely monitored

---

[11] A detailed review on the CD approach, its application to the study of protein structure, guidelines for obtaining reliable data and analysis method can be found at [346].

[12] According to the Beer–Lambert law, the absorbance of a material $A = \varepsilon c l$; where ε is the molar attenuation coefficient; c is the molar concentration; ℓ is the pathlength.
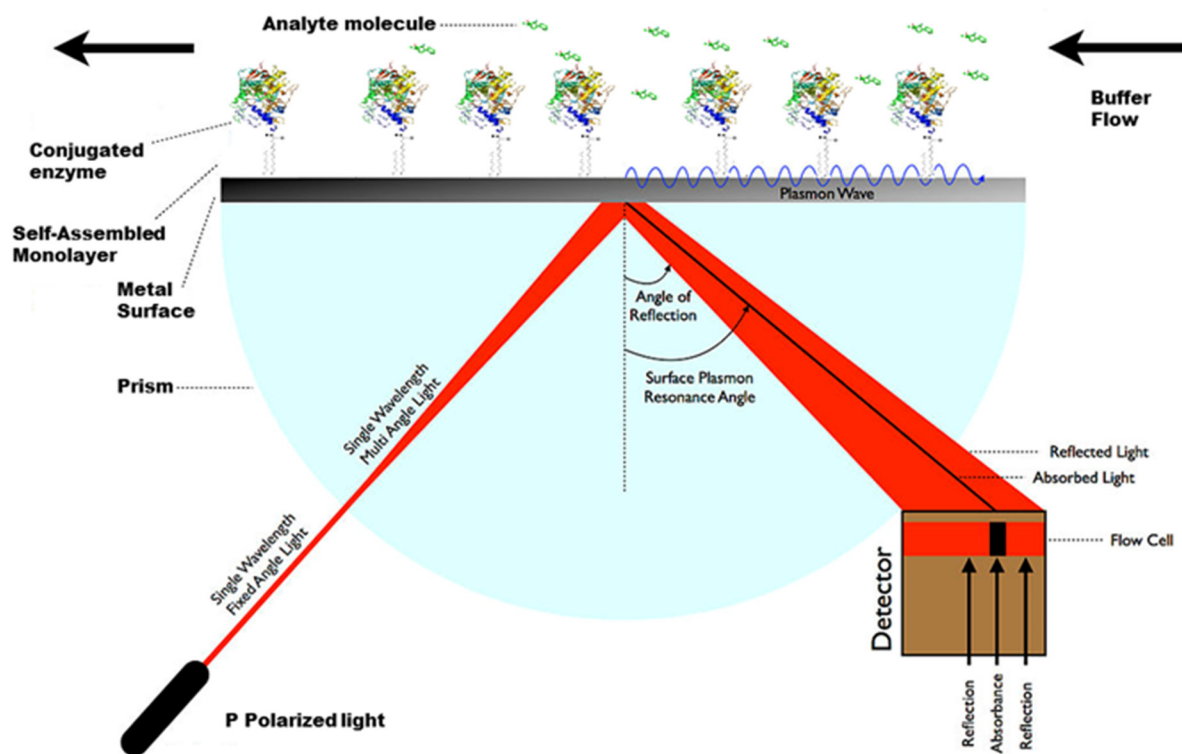
Figure 16. Diagram of surface plasmon resonance, SPR, spectroscopy with a cross-linked enzyme system. The black bar in the detector represents the resonance angle where the light is absorbed by the electrons in the metal creating the SPR dip. From [382]. CC BY-SA 3.0.

with spectroscopic ellipsometry (SE). SE is typically used for films with thickness in the range of less than a nm up to a μm or more, allowing for single protein layer resolution, and can be tailored by changing the wavelength of incoming light. However, using optical absorption often yields thickness values, that are less than the actual protein dimensions obtained from crystallography [63, 326]. The sensitivity of spectroscopy ellipsometry techniques is approximately ± 5 Å, such that changes of protein monolayer thickness (~18–90 Å) on a different substrate surface can be monitored even after multiple layer applications [362].

Other useful techniques are the earlier-mentioned PM-IRRAS and grazing angle attenuated total reflection (GATR)—FTIR spectroscopy, which can be used to characterize protein structure and orientation in thin films or monolayers on metal substrates. Surface-enhanced infrared absorption spectroscopy (SEIRA) can be used to probe a protein monolayer's functionality, such as label-free *in situ* study of biomolecular interactions [363, 364]. All of these techniques can be used to determine if protein conformation and activity are affected by immobilization. Surface-enhanced resonance Raman spectroscopy (SERRS) [365, 366] can also be used to study protein conformation and interactions by analyzing various vibrational modes of amino acids and cofactors [367, 368]. Raman spectroscopy has been used to study conformation, and cofactor coordination of heme proteins [369–371], and non-redox proteins [372–374]. SERRS can also yield information about protein stability and retention of native function. An example is a SERRS study conducted on a CY(1 0 1) immobilized on a SAM on Ag electrodes which

showed that both the ferric (Fe^{3+}) and ferrous (Fe^{2+}) states of the protein were in an inactive form [375]. A more recent study demonstrated that cytochrome P450 2D6 (CYP2D6) immobilized via a SAM on Ag electrodes was able to reversibly bind its small molecule ligand, dextromethorphan, and retained its native structure [376]. However, Raman shifts were also observed, indicative of the inactive form, and it was not possible to reduce the protein's heme group. This result is interesting given recent work, which demonstrated that biologically active CYP2D6 can be adsorbed via a SAM on Au [377], and may reveal surface-specific differences in immobilized P450 function.

Surface plasmon resonance (SPR) spectroscopy has been successfully used to study multi-layer/aggregation formation during immobilization (figure 16) [378–381]. The surface plasmon resonances are highly sensitive to the electrons' local environment. Attachment of molecules to the surface changes the local dielectric constant, and thus alters the resonance angle and finally the shape of the SPR absorption/scattering spectra.

SPR studies in conjunction with electrochemical studies are used to determine electroactivity characteristics in protein assemblies. Jin *et al* measured layer formation of alternating ds-DNA and Mb layers, and found that full electroactivity is seen only in the first layer with electron transfer occurring mainly through hopping [381]. In-depth studies by Advincula *et al* using simultaneous SPR, AFM, and electrochemical measurements allowed for collection of dielectric, surface morphology, and electrical current data (figure 17) [383, 384]. Together with electrochemical surface plasmon resonance (EC-SPR), the same group demonstrated protein
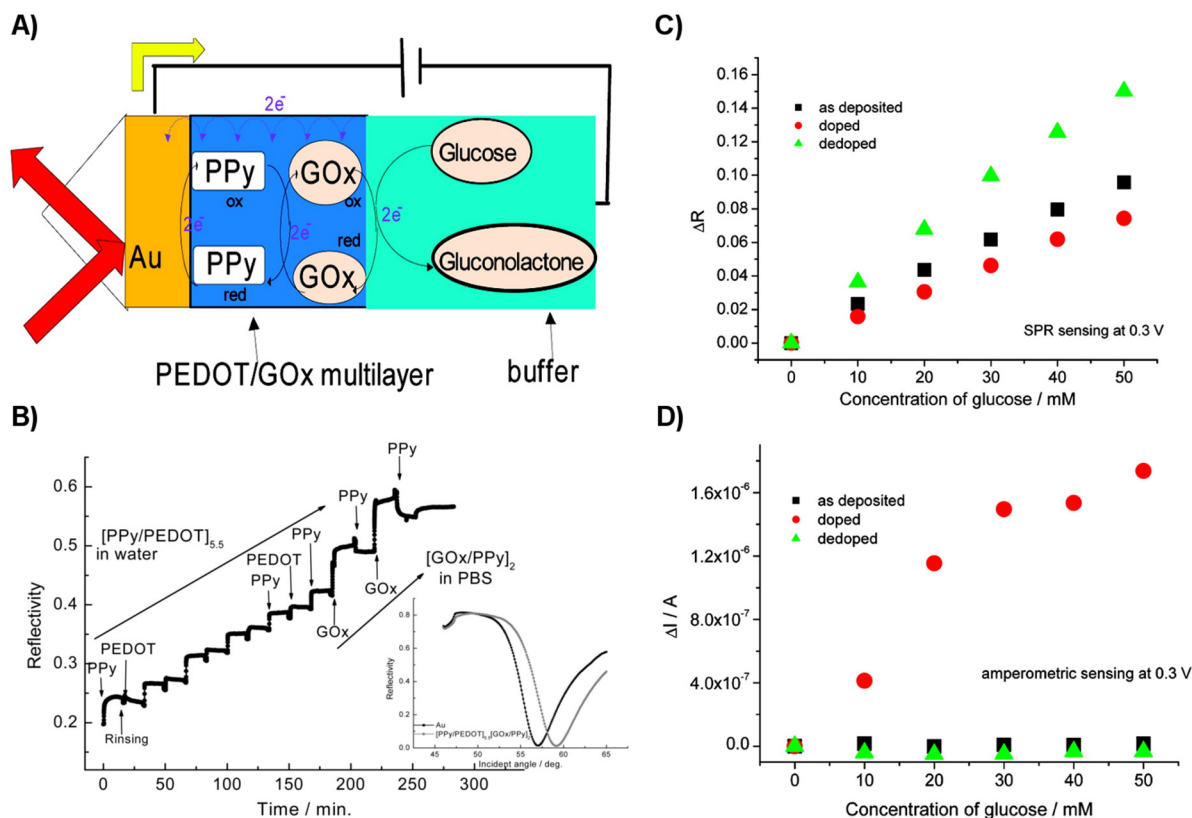
Figure 17. (A) Setup of EC-SPR, with multilayer of water-soluble polypyrrole, poly(N, N-dimethylethyl-3-(1H-pyrrol-1-yl)propan-1-ammoniumchloride) or (PPy), poly(3,4-ethylene dioxythiophene) (PEDOT), and glucose oxidase (GO_x) immobilized onto a dielectric SPR platform (Au on glass). Buffer is phosphate-buffered saline (PBS). (B) Real-time SPR plot showing changes in reflectivity upon adsorption of layers. Inset shows the change in SPR absorption dip, due to layer formation. (C) SPR glucose sensing as a function of glucose concentration for doped and de-doped states of PPy. (D) Amperometric glucose sensing as a function of glucose concentration for doped and de-doped states of PPy. Reprinted (adapted) with permission from [384]. Copyright (2010) American Chemical Society.

adsorption of a soluble polypyrrole-terminated with the glucose oxidase (GO_x) enzyme (figure 17(B)). When exposed to glucose, GOx is reduced and glucose in turn is oxidized and converted to gluconolactone and hydrogen peroxide. Of note in this study is the difference in glucose sensing, determined optically (figure 17(C)) and electrochemically (figure 17(D)), which reveals that the choice of layer composition should be based on the relevant downstream application. In the present case, to create an optical sensor, an undoped polymer would allow for glucose sensing with higher sensitivity, whereas a doped polymer allows for enhanced electrochemical sensing. In other words, even when biological viability upon attachment is demonstrated, the details are important when a bioelectronic device is the desired end product.

3.6.2. Scanning probe techniques. Scanning probe techniques have revealed a great deal of information about immobilized proteins due to their high spatial resolution. Scanning tunneling microscopy (STM) has a lateral resolution down to the atomic level, allowing single protein measurements, and in principle can also provide information on adsorbed protein structure. The high spatial resolution has also been exploited for a better understanding of immobilized protein orientation [31, 177, 195, 316].

Electrochemical STM (EC-STM) combines conventional STM and cyclic voltammetry [176]. The conducting substrate

and STM tip act as working electrodes in an electrolyte solution, allowing measurement of ET. Reference and counter electrodes are located in the solution on opposite sides of the tip. The reference electrode is often an Ag wire, whose potential is measured to obtain a measurement that can be referred to the standard hydrogen electrode potential. A bipotentiostat allows independent control of the potential of the two working electrodes, the substrate and the tip, with respect to the reference electrode, and their potential difference represents the STM's tunneling bias. The counter electrode allows the current to flow.

In EC-STM, electrons tunnel between the working electrodes via the protein due to alignment of energy levels of the protein with the Fermi levels of the contact electrodes. This alignment can be obtained through application of a bias voltage or nuclear fluctuations of the protein [171, 315]. The first single molecule studies of a redox-active molecule by EC-STM were conducted by Tao, who investigated the oxidized (hemin) form of the redox-active prosthetic group of heme proteins, Fe(III)-protoporphyrin (FePP), and the redox-inactive protoporphyrin (PP) which lacks the Fe ion [385]. Using PP as a reference, Tao demonstrated the apparent STM-measured height of FePP with respect to PP as a function of substrate potential that gave resonant tunneling-like behavior. In addition, in an STM image FePP had a larger apparent height than the reference PP at a substrate potential near the redox potential of FePP, resulting from the increase

in tunneling current of the FePP, demonstrating the usefulness of this technique [385].

Extensive work by Ulstrup and co-workers combined cyclic voltammetry and STM to study a diheme protein, cyt c4 [386]. STM demonstrated a controlled adsorption of cyt c4 (a di-heme protein, i.e. with one heme on each side) on a SAM in an orientation perpendicular to the substrate, with the heme at the C-terminal (i.e. the carboxyl group peptide's chain end) adjacent to the electrode and the heme at the N-terminal above it, and observed an interheme k_{ET} of 8000–30 000 s^{-1}. These values are much higher than those previously obtained by the same group using standard cyclic voltammetry (1600 s^{-1}), a result that the authors explain was plagued with experimental error due to diffusion of the adsorbed protein, and lower current density due to an inability to generate well-oriented monolayers [387].

EC-STM measurements have also provided mechanistic information about ET in redox proteins and changes in redox potential and conformation. For example, there have been extensive studies of azurin using EC-STM, which have yielded mechanistic information on ET [176]. Gorostiza and co-workers used EC-STM to monitor changes in the barrier height for transport in relation to the copper redox state, and to calculate β from current distance measurements (see equation (3) in section 2.1) [316]. EC-STM experiments were performed also on other classes of immobilized proteins, including hydrogenases and oxidases [341, 388, 389]. Madden *et al* [341] measured the rate of the reduction of a single H_2 molecule by a hydrogenase, C*a*HydA, immobilized as SAM onto Au(1 1 1), as a function of the applied potential.

Atomic force microscopy (AFM) is another scanning probe technique extensively used in protein surface characterization [390]. AFM measures the topography of a surface using a tip consisting of a small probe attached to a cantilever. Depending on the AFM method, the tip either makes direct contact with the surface (contact mode), or oscillates while driven close to its resonance frequency near the surface so that van der Waals forces cause changes in its oscillation phase and amplitude (tapping mode). AFM has been used to monitor protein interaction with lipid bilayers [391, 392], to determine protein surface coverage [306, 391, 393, 394], and to demonstrate protein–protein interactions [395, 396].

Conductive probe AFM (CP-AFM) is used to measure the local conductivity of a sample in contact mode. In CP-AFM, an electric potential is applied between the tip and the sample (generally via a conducting substrate for the sample), and the current that flows can then be used to measure ETp locally. Current images can also be obtained if the imaging mode is used. An important feature of CP-AFM is its ability to conduct electrical measurements as a function of applied force, which can be used not only to change the distance between the electrodes, but also to measure the effect of compression on the measured object. Proteins are relatively soft and their stability under compressive (and tensile) stress can affect ETp [179, 183]. For example, force-dependent *I–V* studies have shown that holo-azurin, i.e. with the Cu redox group present, retains higher stability with increasing force (until ~30 nN) than the protein from which the Cu has been removed,

apo-azurin. However, even for holo-Az plastic deformation sets in at an applied force above ~10 nN [53, 179, 183]. For a more complex protein such as bR, oriented with its long axis perpendicular to the substrate, and in ether one of the two possible remaining orientations, junction conductance linearly increases in the 3–10 nN applied force range reversibly, confirming retention of its native conformation. Under higher applied forces (>10 nN), the protein exhibits structural deformations and the change in conductance with force is no longer reversible, i.e. plastic deformation occurs (figure 18) [360]. Force-dependent ETp investigations of Az, bR, CYP2C9, and other proteins after immobilizing onto gold substrates, have demonstrated added protein stability in the presence of cofactors or small molecule binders [53, 143].

The response to an applied force of the conductance of an Az monolayer under cyclic mechanical loading (with CP-AFM) resembled memristive behavior, which could be modeled empirically using the viscoelastic property of the protein. Importantly, the Az conductance was found to depend not only on the force magnitude, but also on loading time. A possible general conclusion could be that conductance, measured by CP-AFM, is process-related and dominated by the time integral of the applied force [397].

Nanoscopic ETp using CP-AFM measurements showed high reproducibility if applied to the indexed nanopillar structure discussed in section 3 (figure 19(a)) even on different days after P450 protein immobilization. The ability to complete repeated studies on the same enzyme demonstrated that ETp correlates with rates of metabolism, i.e. the biological function of the cytochrome P450, and that competitive inhibitors not only block the active site, but also inhibit transfer of electrons through the protein (figure 19(b)) [142, 143]. This exciting technique, which combines the high spatial resolution of CP-AFM with the high reproducibility of the indexed nanopillar architecture, allows for precise measurement of effects of small molecule interactions with proteins on ETp.

3.7. Artifacts in ET and ETp measurements

Artifacts are associated with electron transfer and transport measurements, both in solution electrochemistry and solid-state experimental configurations. Artifacts in STM and CP-AFM measurements generally originate from protein denaturation and conformational rearrangements during the force application by sharp probes [179, 183]. In some cases it is possible to detect changes in protein conformation *in situ* by IR-absorption measurements, Raman scattering, fluorescence and/or electrochemical characterization [398, 399]. Gold substrate topography influences ET rates (investigated with interfacial electrochemical method) across cytochrome c, when adsorbed on carboxylic acid-terminated self-assembled monolayers [400, 401]. With smoother topography, SAMs exhibit an increased ability to block a solution probe molecule, which decreases spurious signals from direct contact between the electrode and solution molecules [400]. The extent of physisorption and the magnitude of the electrochemical response of chemisorbed redox-proteins decrease significantly with decreasing substrate roughness. Roughness limits the electrostatically driven adsorption of
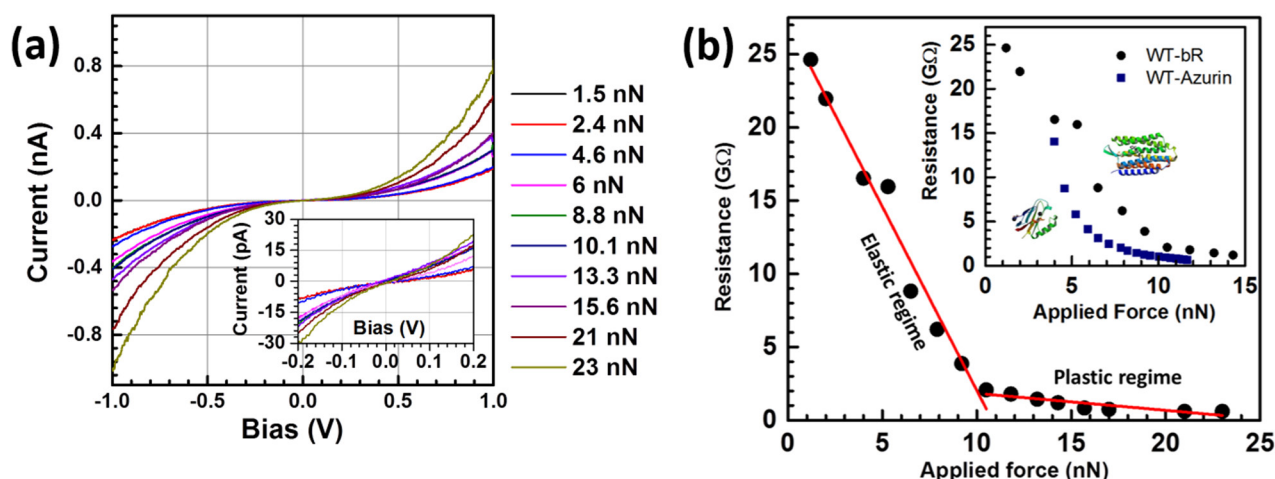
Figure 18. (a) Variation in ETp efficiency expressed by *I–V* characteristics, with applied force in protein-based conducting AFM junctions. (b) Resistance of bR-protein-based CP-AFM junction with applied force (along with adhesion force of 3 nN). Inset shows same variation with proteins of different secondary structures. Reprinted (adapted) with permission from [360]. Copyright (2014) American Chemical Society.
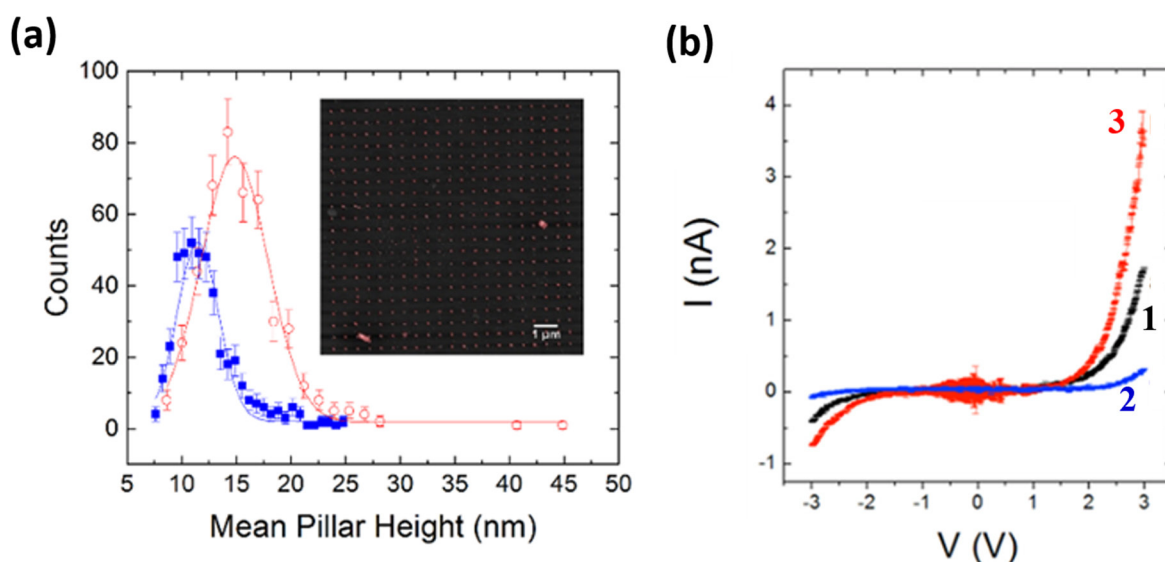

Figure 19. (a) Height distributions (fitted with a Gaussian model) for Au pillars before (blue squares) and after (red circles) cytochrome P450 (CYP2C9) attachment via tethering to a SAM of linker molecules. Inset: AFM height image of array with 421 Au pillars (20–40 nm diameter), used for protein attachment. The increased peak width indicates an increase in surface heterogeneity [143]. (b) Measured *I–V* curves (with standard error) for one pillar with (1) nanopillar with attached CYP2C9, (2) the same protein as in (1) exposed to sulfaphenazole, a small molecule that specifically binds *and inhibits its function,* and (3) the same protein as in (1) exposed to flurbiprofen + dapsone, small molecules that specifically bind to this protein and coordinate with its heme group. A wash step with doubly deionized water was used to remove small molecules in between exposures. Adapted from [143]. © IOP Publishing Ltd. All rights reserved.

proteins onto a SAM-covered surface and the effectiveness of the protein's electronic coupling to the SAM-covered substrate [400]. Substrate roughness also leads to artifacts in experimental electrochemical studies from topography-dependent acid/base properties of the SAMs [400, 401].

In macroscopic transport studies, most of the artifacts originate from defects of the self-assembled monolayer, including pinholes and the random orientation of proteins in monolayers. In general, current density (at high bias) across the chemisorbed linker monolayer is ~10^3 times larger than that across a monolayer of proteins that is connected to the substrate surface via a monolayer of a <1 nm long linker molecule, or directly.

Considering simple tunneling transport (equation (2)), a decay length constant of $\beta \sim 0.12$–0.3 Å^{-1} is obtained from

solid-state electron transport (ETp) measurements across protein monolayers [326]. We note that this value is several times smaller than that obtained for ET [65, 95, 119]. Conduction through pinholes in a protein monolayer can only compete with direct transport via the proteins if the gap between the two electrodes is ~3 Å. Given that this will be a vacuum-, air- or maybe (adventitious) hydrocarbon-filled gap, this is extremely unlikely with protein monolayers of ~2.5–7 nm thickness considering the mechanical stiffness of the top electrode or the surface tension of Hg (inset in figure 20), as explained in the next paragraph [88].

In the lower inset of figure 20 we show a representation of a monolayer-covered surface, which as an empirical grid, where each pixel represents a unit of a tunneling element, proteins
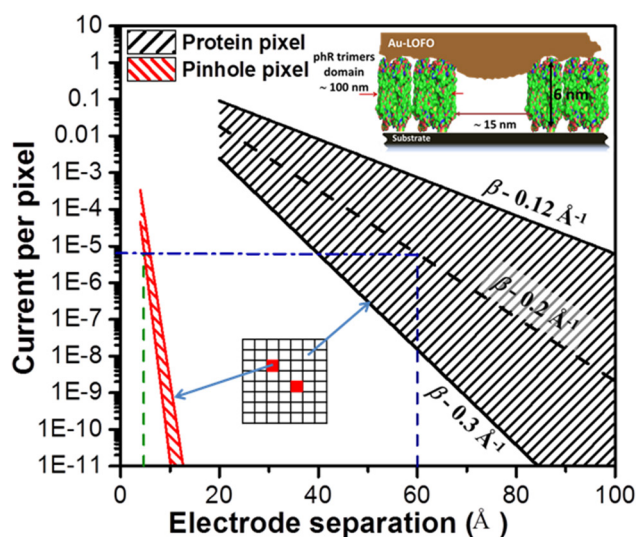
Figure 20. (a) Calculated approximate current (in normalized form) decay profiles over varying tunneling distances (defined by electrode separation) for pinholes and proteins. The *y*-axis is in units of amperes. *Lower inset* shows an empirical grid where each pixel represents a unit of tunneling elements. A red filled pixel represents a pinhole pixel whereas a white one is a protein pixel. *Upper inset* shows a schematic illustration of a pinhole as deduced from high resolution AFM scans. Reprinted (adapted) with permission from [88]. Copyright (2015) American Chemical Society.

(white) or pinholes (red). This is illustrated more graphically in the upper-right inset of the figure. The figure itself shows the tunneling currents per pixel, as a function of the tunneling distance (*x*-axis), where the pinholes are filled with hydrocarbon, i.e. the medium with the smallest tunneling decay constant, compared to those of vacuum or air ($\beta \sim 1$ Å^{-1}). The plots start at tunneling lengths of 3 Å for pinholes with hydrocarbon impurity (red-white arched region, defined by a range of possible β values of 0.6–1 Å^{-1}) and 20 Å for protein (black-white arced region, defined by β values of 0.12–0.3) [63]. It is clear that currents through hydrocarbon-filled pinholes in a protein monolayer (red-arced) will not be significant for a ~30–60 Å deep pinhole, compared to the currents through the proteins (black-arced). Thus, most of the current must flow through protein domains rather than through small pinholes with impurities in protein SAMs. If the pinholes are filled with air or are empty, i.e. in vacuum, the probability decreases even further.

It is relatively straightforward to calculate that the ability of liquid Hg (used for electrical contacts) to penetrate pinholes with diameters of ~15 nm between ~100 nm protein domains (as found from high-resolution AFM) is negligible compared to the few nm protein monolayer thickness, because of Hg's high surface tension. With solid contacts, such penetration is impossible because of their stiffness.

The next issue to consider for possible conduction artifacts that bypass the proteins is the roughness of the substrate (see section 3.5). Here rms roughness is not a good indicator, but rather, maximum roughness information is needed over μm^2 to tenths of mm^2 areas. To assure minimal roughness, highly polished doped Si and template-stripped noble metals are desirable conducting substrates.

4. Electronic and structural properties of immobilized proteins

4.1. What can be expected experimentally from electronic and structural studies of properties by computational methods?

The ETp mechanisms discussed in section 2.1 and illustrated in figure 7 suggest that a variety of combined paths may exist in a given protein structure that connects donor and acceptor residues in an ET process. In computational models, after defining donor and acceptor residues in a protein structure, an algorithm is used to calculate the attenuation factors for a large number of paths that connect these two specific residues. The path with the smallest attenuation factor is selected as the preferred path. In this '*pathway*' method, protein structure and composition are computationally analyzed to determine electron transfer with exponential length attenuation factors that take into account the atomic structure of the protein. The method is derived from the protein physics: electronic interactions decay much more rapidly through vacuum than through chemical bonds, and the protein is viewed as fully coarse-grained, described by way of a dielectric permittivity of the medium and local environment. The simplest structured protein models employ tunneling pathway and average packing density analyses to identify specific tunneling paths and transport-mediating protein residues; the outcomes can be experimentally tested by protein mutation studies [402].

Another interesting question is whether electron tunneling paths, selected by evolution are defined solely by donor–acceptor separation distance, or by other factors. Electrochemical studies on smaller bio-molecules, such as peptides and cysteine-linked peptide nucleic acids (PNA) immobilized on conducting electrodes, demonstrate that peptide backbones, and even amino acid side chains, affect electron transfer processes. Experiments have verified that backbone rigidity and electron-rich side chains increase ET efficiency across peptide monolayers, supporting the idea that electronic state localization occurs on amino acid side chains [403]. The difference between the Fermi level of the gold electrodes and the nearest peptide orbital energy, determined from density functional theory (DFT) gas phase computations, has been interpreted as a transport barrier height for ETp studies across different homopeptide junctions. A direct comparison was made between a DFT-computed transport barrier and experimental results from a solid state system (monolayer on Au surface) obtained from ultraviolet photoelectron spectroscopy (UPS) [403, 404]. Detailed ETp studies with a nanowire junction configuration (see figure 27, below) showed that ETp efficiency across a series of different homopeptides directly correlated with the computed electronic barrier and UPS observations.

Preferred pathways for ET (in biologically-relevant, electrolyte solution conditions) via the peptide backbone might exist, depending on the peptide's secondary structure [405]. The effect of secondary structure on electronic transport has been experimentally demonstrated with molecular junctions of extended helical Ala and Lys homopeptide monolayers. Monolayers of 20-mer alanine and 20-mer lysine

(neutral), which have a high propensity to form a helix, are only 4 Å longer than the respective extended hepta-peptides. Nevertheless, ETp comparisons showed that conduction via the helices was substantially higher than via the extended peptides [152, 404]. In further work, coupling to the electrode contact was found to be critical for ETp efficiency across Au/7-peptide/Au junctions, as shown by comparing ETp between peptides with tryptophan (an amino acid with an aromatic indole side chain) in different positions along the chain.

In most biological ET processes, the cofactor of the protein is thought to enhance the electron tunneling probability with respect to vacuum tunneling. Protein cofactor-mediated tunneling is generally described by superexchange, with the assumption that electron tunneling between donor and acceptor is mediated by unoccupied energy levels (for electron tunneling) or occupied states (for hole tunneling) of the cofactor, but the electrons that tunnel this way do not have any significant residence time on the bridge at any time. Similar to the pathway model, important amino acids or cofactors between donors and acceptors need to be selected to model superexchange-mediated tunneling in protein ET. This ET mechanism was developed assuming that the energy gaps between highest occupied/lowest unoccupied electronic energy levels of the bridging units and the redox-active donor and acceptor levels are large compared to the electronic coupling energy between donor/acceptor and the bridge [57]. Naturally, charge transfer can also occur via hole transfer (HT) superexchange. As an example, a bridge site close to the oxidized acceptor donates an electron to the acceptor and the resultant hole tunnels through occupied bridge states to the donor. In early studies involving periodic alkane bridges, Beratan and Hopfield showed that both electron- and hole-mediated propagation could be explored to model distance-dependent transfer decay [406].

Theoretical models of ET processes (in solution) can be used to simulate ETp, in a solid state configuration, across proteins that connect two electronically conducting electrodes. Single proteins or monolayers of azurin, cytochrome-c, and myoglobin were modeled by a square potential barrier with an effective barrier height [47, 85, 148, 326]. Tunneling can describe protein-mediated solid state ETp over length scales up to a few tens of Å, but it is not clear how it can serve to describe electron transport over longer distances ($\geqslant$50 Å) [407]. Very long-range ($>$100 Å) ET in biological systems occurs via redox-active cofactors using chains with close cofactor spacing of typically 15–20 Å. Transport across photosynthetic and mitochondrial membranes includes protein–protein ET, and, within a protein or protein complex, is generally described as multi-step hopping between multiple redox cofactors, or via multiple aromatic residues [61, 65, 95, 134]. Metal-containing cofactors, protein residues of tryptophan, tyrosine, or cysteines may act as electron relays, in e.g. ribonucleotide reductase, photosystem II, DNA photolyase, and cytochrome c/cytochrome c peroxidase [65].

Identifying the transition between coherent single-step transport (tunneling) and incoherent multistep tunneling (hopping) theoretically and experimentally remains a great challenge. Recent computational studies on charge recombination between hemes in the cytochrome c/cytochrome c peroxidase complexes explored the tunneling versus hopping transition as function of transport distance [408]. The analysis indicates that even for moderate donor–acceptor separation, hopping involving a tryptophan (residue 191) governs ET. Experimental ET studies of complex mutants with varying donor–acceptor distance indicate that coupling pathways and reorganization energies dictate ET kinetics and also reveal how hopping through aromatic residues can accelerate ET [409].

Open questions remain concerning electron transport in biology over much larger distances. As a rather ad hoc speculation, band-like coherent conduction was proposed as an alternative to hopping for transport along biological nanowires (see figure 21) [410]. Such an idea is problematic using an electronic band model, because electronic bands originate in solid-state physics for systems that obey the Bloch condition of periodicity, and is described in its simplest (1D) form by the Kronig–Penney model. Possibly models like those used for liquid metals and semiconductors may need to be revisited, but to the best of our knowledge, that has not yet been done for extra long-range ETp in biology [411]. A very recent report argues, based on experimental evidence, that the mechanisms for all long-range transport reports are electrochemical nature [412].

Flickering resonance (FR), mentioned in sections 2.1 and 2.2, and in the discussions of figures 5 and 7, has been used to describe multistate biological electron transport across a chain of biological redox active units with donor, acceptor, and bridge levels that are similar in energy [132]. The transport efficiencies expected from this model were compared with those of the established superexchange (SE) and hopping models [108, 132, 133]. To understand FR, we note that site vibrational energies in biological systems can broaden electronic energy levels on a scale of 100s of meV. Thus, short-lived (fs scale) coherences could form among multiple electronic states and create band-like states. Such transient situations would contribute to ET charge transport rates with a soft exponential distance dependence (small β values). This is the process that lies at the heart of the flickering resonance idea and could be important in the 1–10 nm range, before incoherent hopping becomes the more efficient transport process. In the FR model, the medium between donor and acceptor is not only a bridge enhancing electronic coupling (as in the superexchange model), but is also a chain of redox sites, each of which can participate in electron or hole transport ***when in resonance***. Long-range transport is assumed to take place when thermal fluctuations bring the redox-active energy levels of donor, bridge, and acceptor sites simultaneously in resonance. In contrast to charge hopping, where the carrier moves sequentially from one site to the next with nuclear relaxation at each step, charges in flickering resonance are assumed to move through the 'in resonance intermediate-states' without further nuclear relaxation until they reach the acceptor (figures 5 and 7) [108].

The FR model accounts for both exponential distance dependence and partial excess charge location on the bridge. It has been successfully implemented to analyze experimental results obtained for short-range transport in DNA instead of the superexchange model.
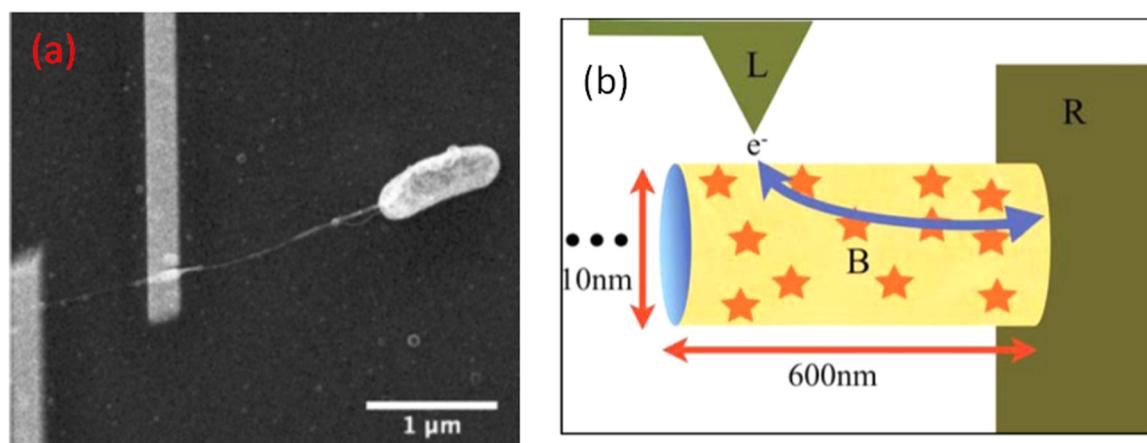
Figure 21. (a) ETp studies across bacterial nanowire (extensions of the membrane of the bacterium) from a *Shewanella oneidensis* MR-1 cell with Pt electrodes as macroscopic contact. (b) Cartoon of possible efficient ETp process in bacterial nanowires via hopping sites (star shapes) which mainly originate from closely spaced heme groups. Reproduced from [133] with permission of The Royal Society of Chemistry.

The riddle of transport across bacterial nanowires (essentially parts of the *Shewanella oneidensis* membrane) [410] and across pili (hair-like bacterial structures) [413] of *Geobacter sulfurreducens,* inspired a flickering resonance model to explore the physical constraints under which high currents could flow across such wires (figure 21) [413, 414]. It was found that a combination of thermal fluctuations and hopping-like transport could reproduce the experimental *I–V* curves, with plausible values of reaction free energies, reorganization energies, and a packing density for redox cofactors (e.g. hemes), consistent with that of multi-heme proteins found on the bacterial cell surface [131, 133, 415, 416]. However, one could argue that FR should be less relevant for ET along heme wires in proteins because of the relatively small electronic coupling between heme cofactors. While clearly the last word on ET (and ETp?) across bacterial nanowires and pili has not been written [410, 413, 414], we paraphrase Blumberger [108] and note that it is highly desirable to design experiments, motivated and guided by theory, that can elucidate the true mechanism(s) of electron flow in proteins.

There is no *a priori* reason to think that nuclear relaxation could not occur during resonant tunneling processes itself. As an example, consider the resonant tunneling in a metalloprotein discussed in section 3.4 above. If tunneling occurs via resonance with a heme group, when the electron reduces the Fe atom during the tunneling process, a structural change could occur, depending on how fast is the tunneling process. If the resonant tunneling process is slow, a nuclear configurational change could occur which changes the energy level of the resonance. This is analogous to Franck-Condon transitions in molecules in which electronic transitions (induced optically, for example) result in a change in the nuclear configuration and an excited vibronic state. In ETp, if the occupation of the excited electronic state by the tunneling electron is long enough, this causes the nuclear configuration change. Li *et al* have shown that theoretically this could be identified in a single electron transistor (SET) measurement by a gap in the SET Coulomb triangles, that is, there would be a vertical separation between Coulomb triangles at the point where they

join to normally give a non-zero differential conductance at zero bias (see figure 15) [32]. However, the experimental data are somewhat unclear about this [32], and so far this Franck-Condon-like effect in tunneling phenomena in proteins has not been unambiguously identified.

Recently, solid state conduction efficiency and existence of multiple transport pathways across bacteriorhodopsin, bR, were investigated theoretically using the extended Marcus–Hush theory [417]. The computed electronic charge mobilities of bR (1.3×10^{-2} and 9.7×10^{-4} cm^2 V^{-1} s^{-1} for holes and electrons, respectively) based on a hopping mechanism were remarkably similar to the experimentally obtained average electron mobility of 9×10^{-4} cm^2 V^{-1} s^{-1} for a system consisting of bR, bound to a TiO$_2$ nanowire [418].

Overall, it seems that only a combination of models described in section 2 and earlier in this section can quantitatively describe some of the experimental ETp data well, which indicates that our fundamental understanding is incomplete. Further control experiments, together with sophisticated computational work, are needed to improve our understanding of ETp in proteins. Obtaining detailed, microscopic information about the protein's structure in the experiments may be necessary to determine which of the models fits the electrical conductivity data best. The ideal experiment should use samples where the protein structure is well understood, the protein is not denatured, and the protein binding configuration can be measured and varied independently of the ETp measurements. While the various conditions have been met separately, realizing such an experiment remains one of the great challenges of the field. In this section, we describe various efforts aimed at dealing with these problems.

4.2. Effects of immobilization on protein structure and electronic properties

Protein immobilization on metal surfaces appears to be advantageous for the study and use of a protein's biological activities under solid-state conditions. In most cases, proteins retain their biological functionality when assembled
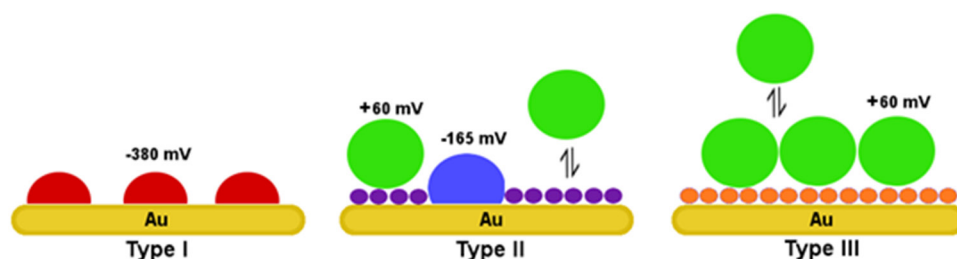
Figure 22. Schematic presentation of Cyt C (circles) adsorbed to a Au electrode without modifiers (Type I), co-adsorbed with 4,4′-bipyridyl (purple, Type II), and co-adsorbed with bis(4-pyridyl) disulfide (orange, Type III). In Type I and Type II adsorption denaturing of the protein (depicted as flattening of the circle that represents the protein) is seen, due to interaction with the electrode. Red depicts highly denatured Cyt C, while the blue depicts partially denatured Cyt C. In Type II we see some, and in Type III complete preservation of the native conformation (green) through interaction with the modifier on top of the electrode. Denaturing of Cyt C strongly affects the protein's redox potential. Reprinted with permission from [431]. Copyright (1990) American Chemical Society.

on metal electrodes functionalized with self-assembled monolayers (SAMs) via electrostatic and hydrophobic interactions as well as by covalent cross-linking. A few studies report conformational transitions and redox potential shifts of redox active proteins. For example, the redox potential of the electrostatically adsorbed P450 protein decreases upon shortening of the length of the carboxyl-terminated SAMs, i.e. upon increasing the strength of the local electric field [375]. Thus, it is important to summarize how immobilization affects protein structure and electrical properties. Upon immobilization, two competing effects modulate the redox potential of the adsorbed protein. First, the increased hydrophobicity of the redox environment brought about by immobilization on the SAM tends to increase the redox potential by stabilizing the formally neutral form. Second, increasing the electric field tends to stabilize the positively charged oxidized form, thus reducing the redox potential. From the device perspective, here we summarize ongoing research of immobilization effects on protein's redox and electrical properties.

4.2.1. Effects of choice of modified substrate surfaces on electron transfer. Few proteins directly adsorb on a solid-state substrate without substrate or protein modification. As discussed above, direct binding offers poor control of protein conformation and often results in reduced biological activity due to denaturation, and in the case of enzymes, by blocking active sites. These issues not only hinder protein functionality, but also hamper analysis of results due to the ambiguous nature of the protein state on the electrode surface.

A commonly used method allowing some protein conformational control is the direct immobilization on bare gold using surface-exposed cysteine groups of the protein via the formation of Au–S bonds. This has been used successfully implemented in yeast cytochrome c (YCC) to achieve electroactivity of immobilized species, as measured by cyclic voltammetry on a polycrystalline bare gold wire [189, 419]. Studies of cytochrome c immobilized on Au (1 1 1) via Cys102 (cysteine at position 102 in the protein amino acid sequence) [420] yielded a $k_{ET} = 1.8 \times 10^3$ s^{-1}; work on the immobilization of cytochrome C$_{555m}$ via Cys18 yielded a $k_{ET} = 1.4 \times 10^4$ s^{-1} [421]. Thus, extremely fast ET, with a large k_{ET},

is possible through direct electron transfer between the electrode and the covalently immobilized protein.

Azurin, which has a surface disulfide (Cys3-Cys26) that is suitable for covalent linking to Au (1 1 1), has been immobilized on Au via these disulfide groups while retaining its structure [50, 116]. This has allowed azurin to be probed electrochemically by both CP-AFM [179, 183] and EC-STM [176]. However, several studies have shown that immobilization of azurin on Au (1 1 1) by this method produces an electrochemically-inactive protein with k_{ET} values (30 s^{-1} and 300–400 s^{-1}) [116, 422] that are significantly slower than that of azurin adsorbed onto pyrolytic edge-plane graphite, for which k_{ET} values are as high as 5000 s^{-1} [221]. Davis and co-workers have demonstrated the importance of the orientation by measuring electrochemically active azurin on Au (1 1 1) with the cysteine residues that bind to Au on different parts of the protein's surface, with limited perturbation of the native structure [422, 423]. Of note is that the fastest $k_{ET} = 300–570$ s^{-1}, obtained for an Az mutant with a cysteine near the copper center (S118C), is still an order of magnitude slower than for azurin, adsorbed to pyrolytic edge-plane graphite electrodes. These observations indicate that, along with protein orientation, adsorption modes on specific substrates do effect ET [116].

Direct absorption of cytochrome P450 proteins, first reported by Hill and co-workers who immobilized CYP101 to edge-plane pyrolytic graphite (PG) electrodes [424], has been less successful. The study concluded that electrostatic interactions by positively charged amino acids (Arg-72, Arg-112, Lys-344, and Arg-364) located near the redox center with the negative charges on edge-plane PG allowed for electrochemically driven catalysis yielding substrate potentials. Work by Fantuzzi *et al* [425] demonstrated that P450 CYP2E1 adsorbed directly to bare glassy carbon electrodes is more electrochemically active, but with very slow k_{ET} (5 s^{-1}). In a recent study, the electrochemical (redox) activity of WT CYP101 was compared to that of mutants with all surface cysteines replaced by inert alanines (surface cysteine-free, SCF) and a mutant containing only one surface cysteine near to the redox center (SCF-K334C) [426]. The single cysteine mutant yielded anodic (−50 mV versus SCE) and cathodic (−170 mV versus SCE) peaks in cyclic voltammograms (see figure 1), while no difference from background was observed
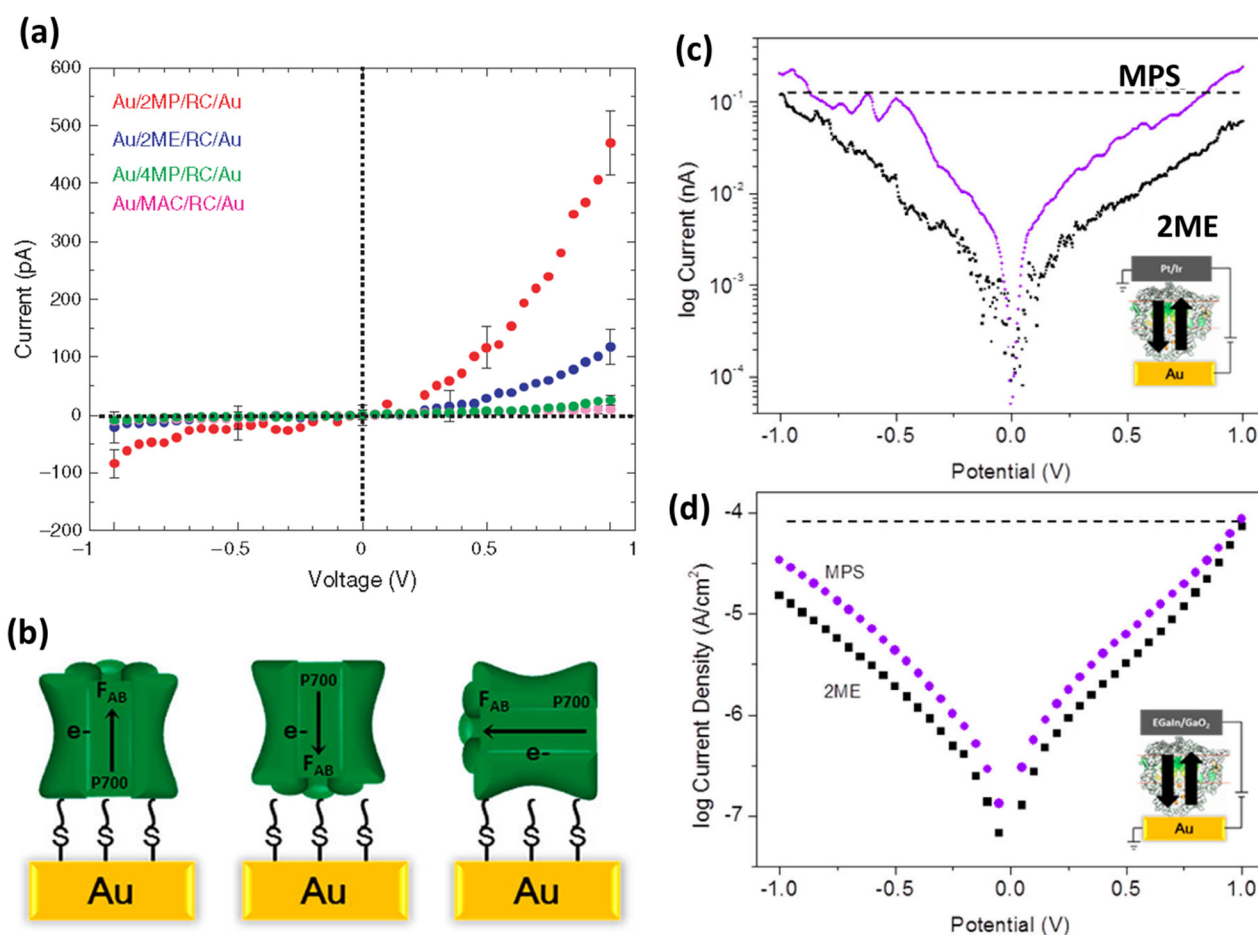
Figure 23. (a) *I–V* curves of bacterial reaction centers of photosystem I, PSI, deposited onto Au substrates modified with different linker molecules including 2-mercaptopyridine (2MP), 2-mercaptoethanol (2ME), 4-mercaptopyridine (4MP), 2-mercaptoacetic acid (MAC); error bars indicate the variability between different sets of *I–V* curves. (b) Schematic of possible orientations of PSI on chemically modified Au surfaces. Semi-log plots of current (c) and current density (d) versus voltage for junctions measured using CP-AFM (c) and EGaIn (d) for SAMs of PSI on sodium 3-mercapto-1-propanesulfonate, MPS (purple) and 2ME (black), respectively. Black arrows in inset schematic indicate the two different orientations of the PSI complexes on the surface. (a) Reproduced with permission from [436]. Copyright @ American Scientific Publishers. (b–d) Reprinted with permission from [83]. Copyright (2015) American Chemical Society.

in the WT and SCF mutant. The result indicates that multiple inactive conformations of the WT P450 protein may exist, and that the enhanced electroactivity of SCF P450 may originate from the differences in P450 orientation. In general, protein immobilization in a controlled orientation helps to bypass difficulties such as electroactive prosthetic groups buried within the protein, denaturation of proteins upon adsorption, and unfavorable protein conformations/orientation at electrodes [218, 286, 427].

Studies by Waldeck and co-workers have demonstrated that the k_{ET} of cytochrome c varies from $\leqslant 10^{-4}$ to $\sim 10^{-1}$ cm s^{-1}, depending on the type of SAM used [240, 428]. Using alkanethiol linker molecules to tether the protein to the Au electrode increased k_{ET} because the orientation of the protein was changed so that the redox center faced the gold electrode upon adsorption. In contrast, when the protein is adsorbed on bare gold, the redox center is close to the protein side opposite to the gold electrode. In addition, by changing the alkanethiol length, the interfacial k_{ET} could be controlled [50, 116, 429]. Hydrophobic surfaces, obtained from adsorption of methyl-terminated hexanethiol on gold, have been exploited to mimic

the interaction of a biological redox partner, binding to the protein, thus preserving native conformations and enhancing conduction [430].

Using various 4-pyridyl derivatives as linker molecules, it was confirmed that two scenarios exist, one in which the protein adsorbs on top of the surface modifier and retains its native confirmation, and another where the protein adsorbs both on the modifier and on the electrode surface [431]. Therefore, denaturation of the protein can be mitigated by modifying the electrode, and a proper choice of modifier is necessary to retain full protein functionality. Also, changes in the redox potential are linked to the amount of unfolding of cytochrome c caused by adsorption (figure 22) [431]. While the k_{ET} of myoglobin on bare PG has been shown to be so small and irreversible that it is almost impossible to measure [273, 432], the reversible ET rate in myoglobin on PG, modified by a positively charged polymer (poly(ester sulfonic acid)), was sufficiently fast to be measured ($k_{ET} = 52 \pm 6$ s^{-1}) [292]. Using Nafion cast from aqueous mixtures on to the basal plane pyrolytic graphite, reversible CV peaks were measured for cytochrome c$_{551}$, cytochrome b$_5$, and azurin films [433].
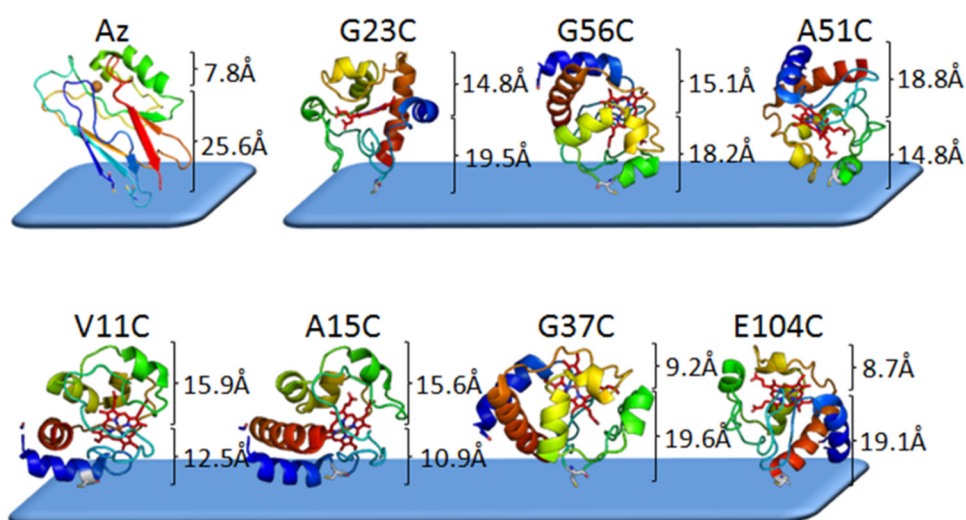
Figure 24. Molecular schemes of the different CytC mutants along with WT azurin, bound to the bottom electrode where the position and orientation of the heme cofactor is systemically modified with respect to the bottom electrode. The calculated distances between where the Cys thiolate is bound to the bottom electrode to the Fe in the heme cofactor, and from there to the other end of the protein (in contact with the top electrode), are indicated. Reproduced with permission from [156]. *Proc. Natl. Acad. Sci* (2014).

This demonstrates that surfaces can be specifically tailored through modification to promote effective conduction in different proteins.

With glassy carbon electrodes (GCE), immobilized CYP101 has a positive shift of the redox potential (-361 mV versus Ag/AgCl) in comparison to CYP101 in solution (-525 mV versus Ag/AgCl). Immobilization on hydrophobic substrate causes partial dehydration of CYP101, excluding water from the heme pocket changing the coordination of the heme iron following shift from low to high spin [67]. Sodium montmorillonite modified GCE with immobilized myoglobin also yielded redox-active protein with quasi-reversible CV peaks, and the ability to detect nitric oxide concentration through changes in heme coordination [276]. The examples discussed above demonstrate heterogeneous values of k_{ET}, which were not found to be influenced by the co-adsorption of the second heme protein, leading to the possibility of developing biosensors capable of simultaneously measuring different analytes.

A quartz crystal microbalance method is another important technique to demonstrate regular and reproducible layer formation via alternating layers of proteins utilizing polyions such as cationic poly(ethyleneimine) (PEI) or anionic poly(styrenesulfonate) (PSS) on gold [111, 434]. It has been experimentally demonstrated that styrene epoxidation enhances turnover on a carbon cloth electrode when functionalized with a protein multilayer, which could be used as a sensitive protein multilayer device.

4.2.2. Effects of modified substrate surfaces on protein conformation and electron transport. Two fundamental issues for the field of bioelectronics are (i) how to order proteins on the electrodes with respect to their conformation, position of active sites and (ii) how to affirm electrical contact area between the protein and the electrode. Immobilized protein orientation and electrical contacts significantly alter electron transport mechanisms and junction properties in ETp measurements. Macroscopic and nanoscopic measurements of

photosynthesis proteins immobilized on metal substrates show different electrical conductivities based on protein orientation [83, 435, 436]. Control over the orientation of the photosystem I (PSI) protein complex and especially of its reaction center (RC I; this is the protein part without the majority of chlorophyll molecules, which are used for light-harvesting) on surfaces can be achieved by its direct covalent attachment. This control can be achieved by mutations which provide an exposed cysteine amino acid (has an SH group available for binding) and/or by modification of the surface with functional groups that can bind to exposed amino acids or interact electrostatically with different parts of the protein complex [435, 437].

ETp has been measured across the RC from *Rhodobacter sphaeroides* on SAM-modified Au (1 1 1) substrates using CP-AFM. Orientation-dependent ETp efficiency was determined using different linkers to the Au substrate, as shown in figures 23(a) and (b). The large tunneling distance (~ 7.5 nm) rules out direct tunneling as an ETp mechanism, and the variations in the tunneling current thus support the existence of alternative electron transport pathways and electronic states (localized or delocalized over the entire structure) across the protein complex. Slight rectification (at negative bias range) in the cases of the mercaptoethanol SAM-modified Au (1 1 1) electrode (figures 23(a) and (c)) reflects preferential adsorption of the RC such that electrons from the Au-coated AFM probe flow to the chemically modified Au(1 1 1) [436]. The variations in transport efficiency with PSI and RC orientation mainly originate from electronic interactions between protein complexes and substrate energy levels, which affect the electron injection barrier [83]. For efficient electron injection into proteins, the work function of the electrode has to match the energy level of the lowest unoccupied molecular orbital (LUMO) or highest occupied molecular orbital (HOMO) of the conducting species [439], taking into account that the work function of the electrode will be affected by the SAM. In these studies, electrode modification was carried out only
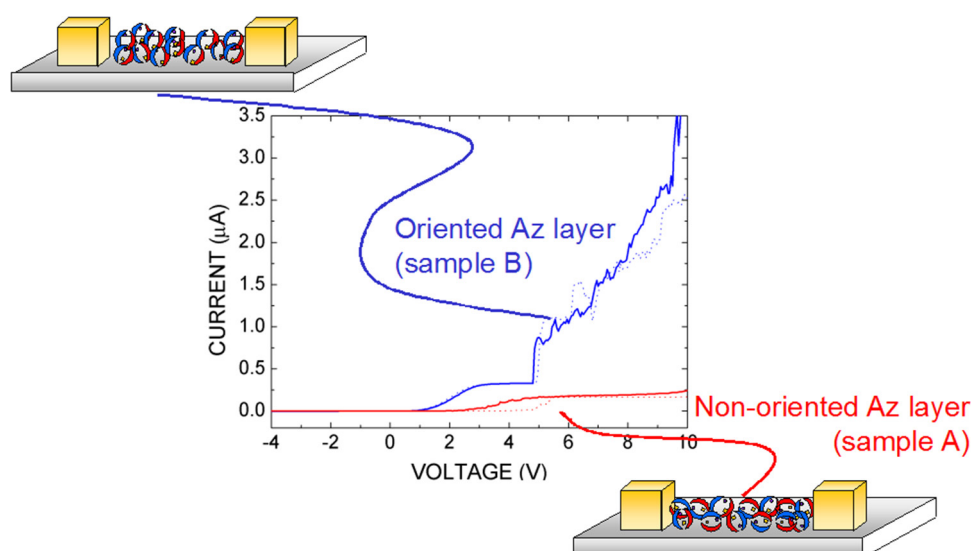
Figure 25. *I–V* curves of non-oriented azurin bound by electrostatics (sample A) and oriented azurin covalently bonded by surface-exposed cysteins (sample B), both over a remarkably wide gap of > 60 nm! [194] John Wiley & Sons. © 2002 WILEY-VCH Verlag GmbH & Co. KGaA, Weinheim.

on the conducting substrates, which seems to contradict the effect of orientation on ETp. Orientation-dependent conductance effects need to be determined by measurements that combine modified-Au (1 1 1) substrates and modified-Au-coated probes, which eliminate the effect of lowering carrier injection barrier only at the substrate-protein interfaces.

An investigation of CytC protein monolayers in a sandwich configuration indicates that covalent protein–electrode binding significantly enhances electronic interactions, as currents across CytC mutants bound covalently to the electrode via a cysteine thiolate are orders of magnitude higher than those through electrostatically adsorbed CytC [147, 153]. Seven different mutants of CytC, where a cysteine (Cys) residue was incorporated at different locations on the protein's surface, were bound covalently to the electrode, forming seven different orientations of CytC with distinct electrode–heme distances (figure 24). The differences in electrical current magnitude efficiency with different CytC mutants indicate that ETp mostly depends on electrode–heme distance rather than on the separation distance between electrodes [440, 441]. A configuration with small electrode–heme distance provides efficient electronic interaction/coupling, allowing for more efficient tunneling from the heme to one of the contacts at low *T* (80–130 K) and thermally activated transport dominated via electrode (silicon wafer)-protein coupling at higher *T* (>150 K) [84, 440].

4.3. Electronic measurements: interpreting results in terms of ET and ETp

4.3.1. Electron transfer and transport across immobilized proteins. The ability to conduct controlled measurements of ETp on immobilized proteins has allowed mechanistic interrogation of ETp in a variety of proteins with different functionalities. Studies ranging from nanometer to macroscopic scales have demonstrated that ETp at low temperatures (<150–200 K) occurs mainly by tunneling, and can switch to thermally activated transport originating primarily in electrode–protein

coupling at higher temperatures (>200 K) [47]. By combining these ETp measurements with the structural characterization of immobilized proteins, it is possible to determine at least some of the crucial factors that modulate the electronic transport behavior of these proteins. Aside from the cases discussed in section 4.2.2 above, another example is work by Rinaldi *et al* [194] which demonstrates that the orientation of azurin immobilized on a SiO₂ substrate strongly affects the measured current intensity. Oriented azurin was approximately ten times more conducting than randomly oriented azurin, as depicted in figure 25. Remarkably, electrical conductance was measured over a huge 60–100 nm gap. We suggest that this might be explained by the at least 50% relative ambient humidity. Parallel orientations of the azurin Cys3-Cys26 bridge result in a distribution of parallel dipoles that favors conduction, while random electrostatic interactions on the non-oriented layer result in random dipole orientations, and thus a reduced total dipole field and a lower ETp efficiency [194].

In STM-based molecular junctions, the orientation of cytochrome b₅₆₂ was engineered by introducing two thiol groups spanning different axes of the protein for controlled binding to gold electrodes, which yielded a larger conductance than the wild type (WT) protein immobilized through electrostatic interactions [178, 191]. In macroscopic configurations, covalent attachment to both electrodes offers higher conduction and reduced thermal activation energy compared to one-side chemical attachments or electrostatically bound proteins [153]. As in the Cyt C experiments described above, these studies indicate that currents, i.e. ETp efficiencies, are mostly affected by heme-electrode distance rather than by electrode's separation distance, illustrating the importance of redox cofactors in ETp [153, 191]. These and the previous results also demonstrate experimentally a connection between ETp and ET (pathways).

Given the importance of redox-active prosthetic groups in ETp, studies of modified proteins which replace redox cofactors with non-redox place fillers, or which remove prosthetic groups/cofactors entirely, have been carried out to understand

the role of these metal centers in metalloproteins [84, 147, 151, 153]. Findings from these studies have demonstrated that redox centers are not only important for maintaining protein conformation, but also for mediating the ET and ETp mechanism. Mukhopadhyay and co-workers conducted solid-state electron transport through holo- and apo-ferritin as well as three metal core-reconstituted ferritins including Mn(III)-ferritin, Co(III)-ferritin, and Cu(II)-ferritin using CP-AFM [146]. The study concludes that the metal core has a direct effect on electronic conductivities of the ferritins [146]. In further work, they concluded that the ferritins behave as n-type semiconductors with variable bandgaps (0.8–2.6 eV) determined from differential conductance data, with the largest gap found in apo-ferritin [216]. ETp studies across holo- and apo-ferritin by the Davis group and Nijhuis group also show increased conductivity of the holo protein over the apo-protein [86, 145]. Macroscopic and break junction experiments on apo- and holo- heme-proteins such as CytC and myoglobin conclude that ETp depends on the relative position of the heme group with respect to the electrodes [29, 32, 85]. In the solid-state, the porphyrin ring of the heme-proteins (with and without iron ion) contributes significantly to determining the protein's ETp characteristics, perhaps acting as a tunneling resonant center. In this scenario, solid-state transport processes differ significantly from electrochemical charge transfer mechanism, which center only on the metal ion for redox reactions. We discuss this issue in more detail in the next section.

4.3.2. Biological relevance of electron transfer and transport measurements. Theoretical studies of biological electron transfer aim to understand the effect of molecular and solvent properties on observed rates and yields, mostly following Marcus theory (section 2.1). The connections between molecular charge transfer (ET) kinetics and molecular conductance (ETp) in protein-based molecular junctions may be unravelled by a fundamental understanding of electronic conduction channels (ETp pathways in the pathway model) across macromolecular structures.

ETp in proteins shares common mechanisms with ET, such as superexchange mediated tunneling or hopping via protein residues and/or cofactors (sections 2.1 and 4.1). A hypothetical relation between protein ET and ETp could be obtained by comparing WT and modified forms of proteins with/without their biological activities. ET and ETp of holo- and apo-proteins have been studied in cytochrome c [84, 147], azurin [53, 151], and myoglobin [85], with increased conductance (*G*)/turnover rates in the holo proteins. Other relevant results include those from the study of macroscopic ETp of holo-CytC compared to CytC without its Fe ion (porphyrin-CytC), and apo-CytC (without heme) [84].

Chemical 'doping' of human serum albumin (HSA) with hemin reveals similar electrochemical and solid-state ETp as CytC [147]. While removal of Fe from heme eliminates ET activity in both CytC and hemin-doped HSA, it has almost no effect on solid-state ETp measurements, demonstrating a clear difference between ETp and ET [147]. A likely reason is that ET requires redox activity of the protein which depends

on electrochemical potentials, reflecting the thermodynamic and kinetic dispersion of protein response, whereas ETp does not require it. We compared ET rates with ETp currents (also rates!) after correcting for ~10^3–10^4 ratios between actual and geometric contact area in macroscopic measurements and for protein lengths, solid-state ETp measurements with different proteins overlap, covering a range of rates [47]. The obtained ETp rate is at least an order of magnitude larger than those determined from spectroscopic ET data. Experimentally obtained electrochemical ET rate data are even lower, likely because of the additional electronic to ionic transport step at the protein/solution interface.

Temperature-dependent (~10–360 K) transport studies can be a powerful tool to identify possible transport mechanisms. Such studies were carried out for ET (mostly on frozen solutions, in a glassy state) some time ago and were surprisingly independent of temperature in some cases [442, 443]. Temperature-dependent ETp studies are relatively straightforward if suitable device structures that are stable under temperature cycling are used. Two-electrode, sandwich-configuration devices have been used for such measurements on azurin [148], cytochrome C [153], human and bovine serum albumin [87, 150], ferritin [145], and on membrane proteins such as bacteriorhodopsin [87], halorhodopsin (phR) [88] and PS-1 [83]. Temperature-independent transport over a wide temperature range (160–320 K and 200–300 K) was found for PS-I, azurin, phR and ferritin proteins [53, 83, 88, 145, 148], although [216] suggests ferritin is a semiconductor, which would be incompatible with temperature- independent transport. Indeed, temperature-independent transport behavior is surprising because while azurin is a relatively small protein (~3.5 nm along its largest dimension, some 2–2.5 nm between electrodes because of tilt), all others are large (⩾6 nm) and form monolayers that are well over 5 nm thick. These distances exceed the maximum length over which ETp across conjugated organic molecules was found to be temperature-independent (via tunneling) [444, 445].

Recent data have shown that it is the coupling of the protein to the electrodes that determines if there is temperature dependence, likely because of the absence/presence of an electrostatic barrier [446]. Thus, strong electrode-protein coupling in azurin and halorhodopsin junctions could allow superexchange-mediated tunneling, which is temperature-independent, except for the small temperature dependence due to thermal broadening of the Fermi–Dirac distribution of the electrons in the contacts (although [447] argues to the contrary for strong temperature dependence). This hypothesis is supported by the study of ETp in different CytC mutants (discussed earlier in this review) with different electrode-protein couplings, due to different orientations between the protein and the electrodes imposed by the location of the binding cysteine [153].

In addition to the redox protein examples, given above, modifications of the non-redox photoactive proteins bacteriorhodopsin [87] and halorhodopsin [99, 360] have demonstrated the importance of cofactors for the temperature-dependent ETp, and by inference, for the dominant electron transport mechanism. ETp efficiency decreases for bacteriorhodopsin
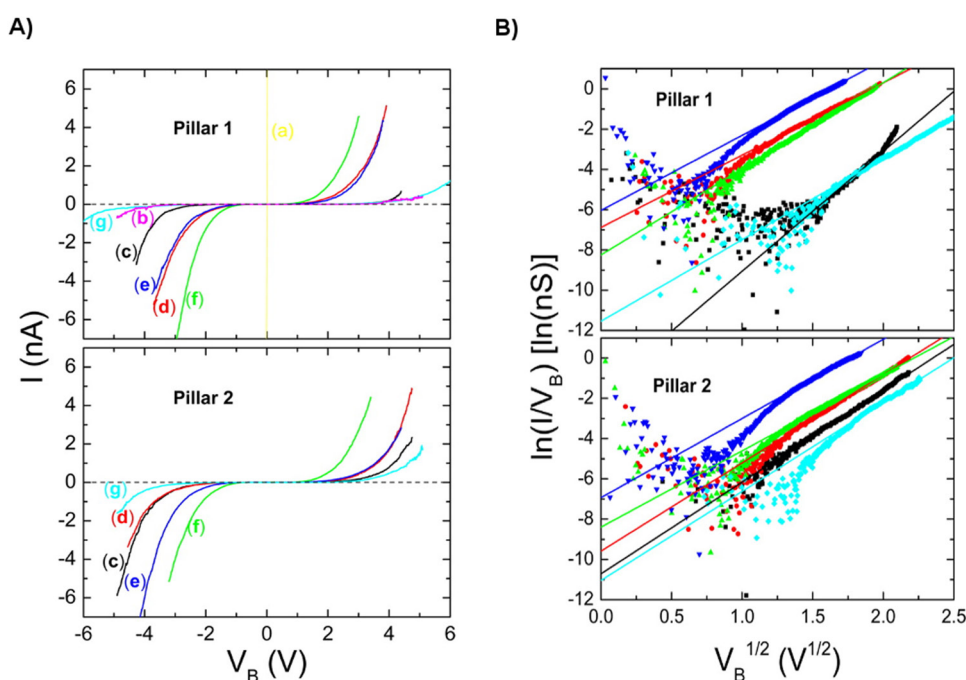
Figure 26. (A) *I–V* curves measured for two nanopillars through the course of an experiment. Curve (a) shows the bare gold nanopillars prior to any attachment; curve (b) is after attachment of a thiol SAM (MUA: OT), curve (c) is after covalent bonding of CYP2C9 to SAM. The remaining curves represent covalently tethered CYP2C9 exposed to small molecule binders flurbiprofen (d), dapsone (e), to both flurbiprofen and dapsone simultaneously (f), and to inhibitor aniline (g). The gold and SAM data are not shown for nanopillar 2 for clarity. (B) shows Poole–Frenkel plots for the data obtained in A) for positive bias voltages using the same color scheme. The symbols are the data and the lines are fits to a straight line. Reprinted with permission from [142]. Copyright (2013) American Chemical Society.

(bR)-based junctions upon retinal removal, similar to what happens in azurin upon Cu removal. Replacement with retinal oxime (RO) results in a different temperature dependence, suggesting a different dominant ETp mechanism than in WT bR [87]. Halorhodopsin (phR) contains two cofactors, which are chromophores, and which undergo a conformational change following visible light absorption. These chromophore cofactors are directly responsible for halorhodopsin's biological function as a chloride ion pump. In halorhodopsin the removal of conjugated cofactors led to a change of ETp from a temperature independent to a temperature dependent behavior [87, 88]. The alterations of the ETp pathway upon removal of cofactors were not the result of conformational changes, as CD measurements showed minimal changes in secondary structure, but, in view of the experimentally found role of electrode-protein coupling for ETp temperature (in)dependence in the above-mentioned recent data, *it is likely that the surface charge density distribution changed*. In the case of phR, it was necessary to have both cofactors for maximal ETp efficiency and to retain temperature-independent transport [88].

In conclusion, macroscopic ETp measurements down to low temperatures with different protein monolayers show that temperature-independent transport always dominates <150 K, even though junction currents differ markedly in their magnitude for different proteins [47, 85, 87, 153]. As the temperature increases, currents in different types of proteins converge to a similar magnitude [151]. Temperature-dependent ETp is in keeping with hopping as the dominant mechanism for transport and can occur if a barrier exists at the electrode-contact interface. Thus, given temperature-independent coupling to the electrodes, ETp across proteins is temperature-independent, a conclusion that will require careful experimental scrutiny, as it challenges our present understanding of electron transport.

One can view the α-helices and β-sheets that make up about ¾ of proteins as possible bridges with multiple hopping sites, each site with vibronic broadening. As the temperature increases, the phonon–electron coupling increases, as well as level broadening. Thus, coupling between adjacent sites can be strong enough to create efficient conduction paths that do not involve the cofactor moiety. The convergence of the currents at room temperature implies that at elevated temperatures the proteins interact strongly with the electrodes, which dominates the measurements, and there is no dependence on the protein's exact composition. At low temperatures, molecular vibrations are quenched or, at least, strongly suppressed, and therefore other pathways can dominate ETp. Judging from the differences in currents at lower temperature, we presume that those pathways depend strongly on the presence of the cofactors. Cofactors with delocalized electronic states can be viewed as a 'dopant' of the peptide skeleton. Such a picture is consistent with super-exchange-mediated off-resonance tunneling as a mechanism for temperature-independent ETp.

At low temperatures, ETp efficiency across a dry protein monolayer that is covalently bound to an electrode is significantly higher if the protein is oriented with respect to the electrode than if it is randomly oriented [85]. This is apparently due to the stronger protein-electrode electronic coupling via covalent bonding of the protein to the substrate, and via cofactors for the case of oriented proteins that may allow highly efficient protein-electrode electronic coupling.
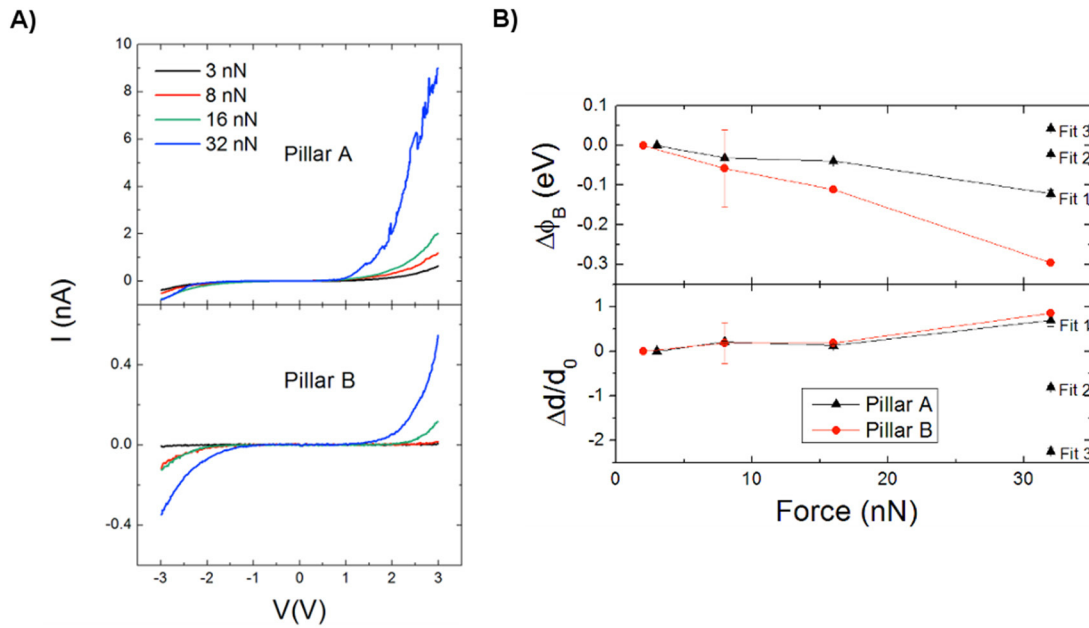
Figure 27. *I–V* curves for two nanopillars with CYP2C9 immobilized via thiol SAM. (A) Curves for a nanopillar with CYP2C9 alone (Pillar A) and CYP2C9 exposed to small molecule binder flurbiprofen (Pillar B) for the different tip forces shown in the legend. All curves were measured on the same pillar and therefore the same CYP2C9 protein. (B) Changes in the energy barrier height φ_B and the relative change in the distance between hopping sites d relative to the distance at a tip force of 3 nN (d_0) as a function of force for nanopillars in (A) showing decreasing barrier height with force, but increasing d/d_0. Data points at 32 nN were extracted for fits for different bias voltage regions using the Poole–Frenkel model, with Fit 1 (measured between 1.6 and 1.8 $V^{1/2}$) being consistent with the rest of the data obtained at lower forces. Reproduced from [143]. © IOP Publishing Ltd. All rights reserved.

4.3.3. Protein structure and electron transport measurements. Conformational changes, especially if they affect a protein's active site, can have large effects on ETp. Stabilization of a protein's active site prior to immobilization on a substrate is necessary to retain substrate binding specificity, metabolic functionality, and activity levels comparable to its solution metabolism [144, 306, 448]. This is important because immobilizing the protein has been shown to alter functionality even while stabilizing the protein's native structure [306]. The method of an indexed array (of gold nanopillars) allows sequential measurements of the same protein under varied conditions (addition and removal of small molecules) when a protein is covalently tethered to the pillars [142, 143]. It was demonstrated that the addition of small molecules greatly impact ETp in immobilized P450 CYP2C9 through analysis of *I–V* plots, fitted to the Poole–Frenkel (PF) emission model (figure 26) [142, 143]. The PF model consists of electrons conducting from one localized state to another within an insulating layer [449], and in this sense is akin to the hopping mechanism discussed in section 2.1 (figure 5). In the PF model, the current *I* is described by

$$I = CV \exp\left[-q\left(\frac{\Phi_B - \sqrt{qV/\pi d\varepsilon_0\varepsilon_s}}{kT}\right)\right], \quad (9)$$

where *V* is the applied (bias) voltage, *q* is the charge of an electron, Φ_B is the effective voltage barrier that the electron must overcome to move from one localized state to another, *d* is the distance across which the voltage is applied, ε_o is the permittivity of free space, and ε_s is the relative permeability of the material (immobilized protein) at high frequencies, assuming that there is no local polarization induced, *k* is Boltzmann's

constant, *T* is the absolute temperature, and *C* is a constant that depends on the intrinsic mobility of the charge carriers, the effective area of the electrical contact, and the effective distance *d* across which *V* is applied. Taking the natural log of both sides results in

$$\ln\left(\frac{I}{V}\right) = \ln C - \frac{q_B}{kT} + \frac{q}{kT}\left(\frac{q}{\pi d\varepsilon_0\varepsilon_s}\right)^{1/2} V^{1/2}, \quad (10)$$

so that a plot of $\ln(I/V)$ as a function of $V^{1/2}$ yields a straight line with an intercept component proportional to Φ_B (figure 26). Using this model, changes in Φ_B were measured in the same CYP2C9 protein after exposure to different small molecules with known impact on CYP2C9 functionality. These studies demonstrated ETp is enhanced by known CYP2C9 small molecule ligands, and reduced by a known CYP2C9 inhibitor. Furthermore, ETp results correlated well with the known biological activity of the protein for activators compared to non-activators.

We previously noted that ETp need not be limited to the same pathways as ET, and thus it is possible that ET and ETp phenomena are not correlated. However, in this study there was a clear correlation of ET efficiency and ETp as related to biological function of the measured protein. This is especially relevant in the case of flurbiprofen and dapsone, two small molecules that are readily transformed by CYP2C9, and which have different effects on the spin state of the heme iron. Flurbiprofen is known to promote a high spin state of the heme iron, while dapsone has no effect on the spin state, but no correlation is observed between ETp and spin state (see section 4.3.6 for spintronic effects in proteins). These small molecules have, however, been shown to bind simultaneously
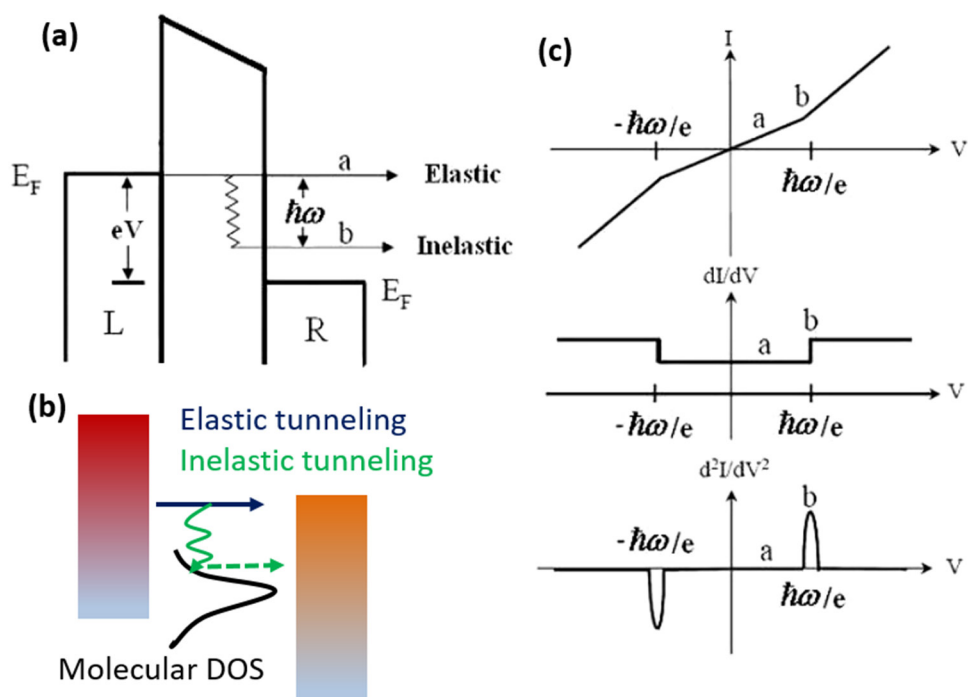
Figure 28. (a) and (b) Schematic of metal-molecule-metal junctions and energy band diagram with a vibrational mode of frequency ω localized inside the junction. 'a' represents the elastic tunneling process; 'b' is the inelastic tunneling process. (c) Corresponding $I(V)$, dI/dV, and d^2I/dV^2 characteristics. Reprinted with permission from [453]. Copyright (2002), AIP Publishing LLC.
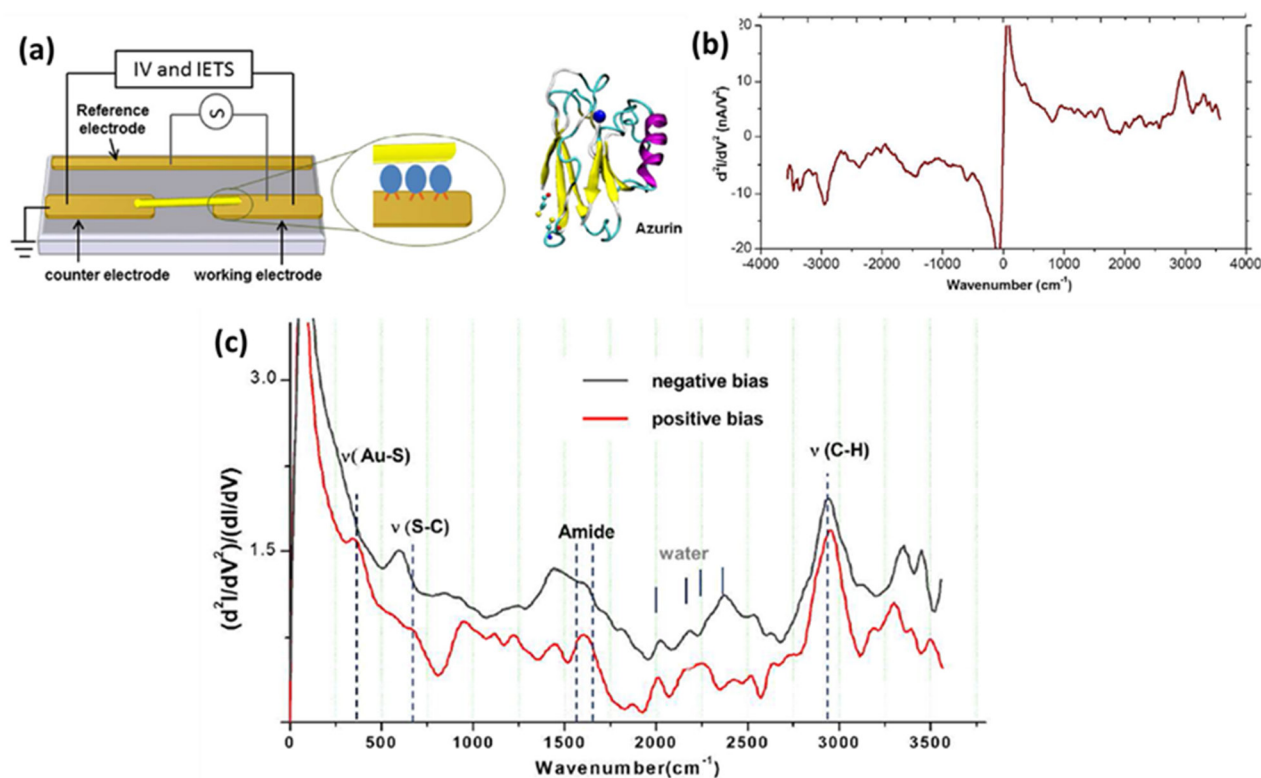

Figure 29. (a) Scheme of the azurin junction fabricated by trapping nanowires by ac electric field. (b) IETS spectrum for the azurin junction (c) IETS spectrum of azurin junction at around 5.5 K with 6 mV ac modulation amplitude, with tentative assignments of the peaks, are based on previously reported IR spectra of the protein. Reprinted with permission from [337]. Copyright (2015) American Chemical Society.
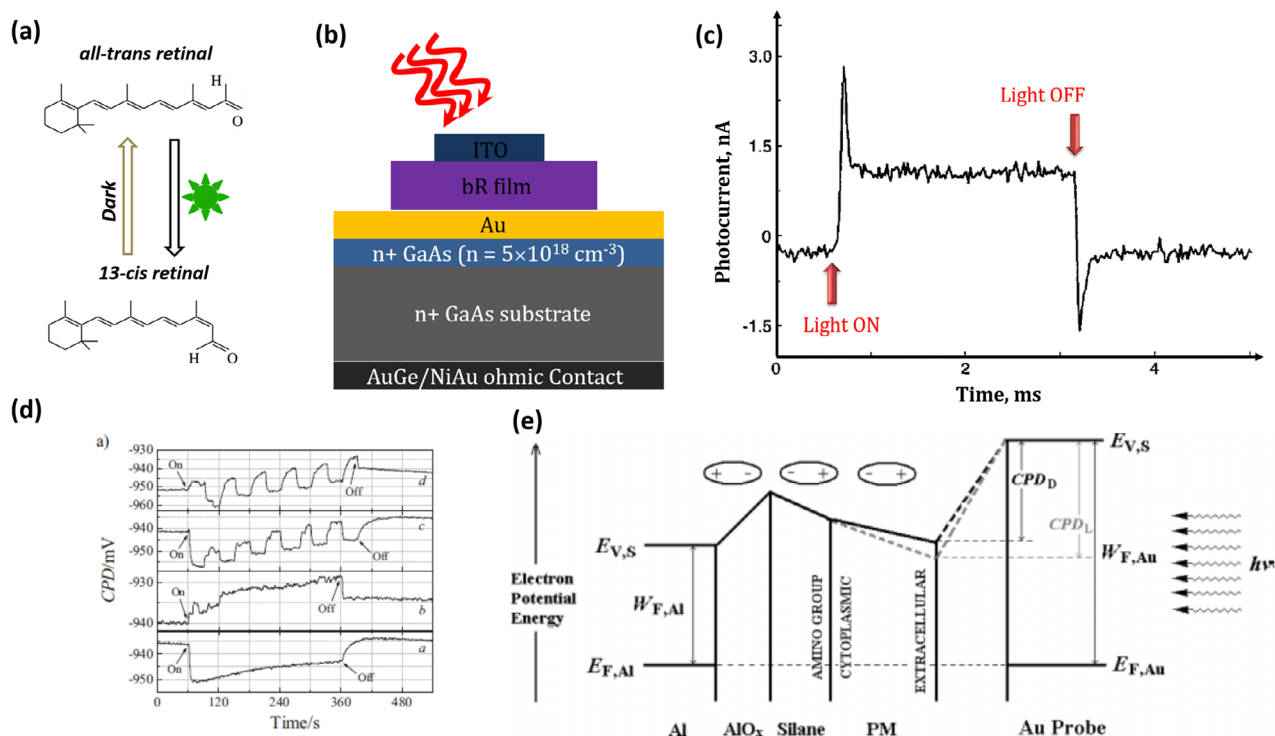
Figure 30. (a) Conformation alteration of retinal cofactor in bacteriorhodopsin upon light absorption. (b) Schematic device configuration for ITO/bR/Au/GaAs heterostructure showing terminal connection for measuring photoconduction; (c) measured photoresponse with 630 nm light modulation for device under ambient humidity conditions. (d) Time trace of contact potential difference (CPD) from bR layer on solid support (Si/Al/AlO$_x$/APS/bR) with green light modulation. (e) Empirical energy level diagram explains the results from CPD measurement, with the polarity of the dipole for each layer shown above the diagram. Dashed lines indicate experimentally observed shifts after irradiation with green light. (a–c) Reproduced with permission from [457]. © Copyright 2001 IEEE. (d, e) [459] John Wiley & Sons. Copyright © 2005 WILEY-VCH Verlag GmbH & Co. KGaA, Weinheim.

and greatly promote CYP2C9 activity [450], which correlates well with the observed changes in Φ_B. The conductance related to the addition of the small molecules themselves cannot explain differences in the observed electrical conduction, leading to the assumption that induced conformational changes of the protein or heme may lead to altered ETp pathways. Evidence for this comes from *I–V* studies as a function of tip force which reveal an apparent phase transition at high force (32 nN) in proteins not containing a small molecule within the active site, but absent in the presence of a small molecule possibly due to protein stabilization (figure 27(A)) [143]. Using the Poole–Frenkel model, changes in the ETp pathway as a function of force can be estimated using a very low force as a baseline. From this analysis, an increase in the pathway length with increasing force was deduced, possibly explained by a zig-zag pathway upon compression of the protein (figure 27(B)).

Lastly, these studies demonstrated for the first time that two known inhibitors, thought to function only by blocking the entrance into the protein's active site, both lower ETp conductance [142, 143]. This may provide mechanistic insight on how CYP2C9 is inhibited, and could also delineate key structural features of small molecules that keep them from being transformed, which is of great importance in drug design.

Taken together, these results also suggest that functional groups within proteins play an important part in determining mechanisms and pathways for ETp, and those ETp characteristics correlate with protein biological function. Protein conformation is a crucial factor for determining electron transport pathways. When proteins are in known active conformations, studies have shown higher conductivities. This implies that there is some correlation between conformations with higher ETp and conformations for biological activity. This work is another example that cofactors impact electron transport with minimal changes in secondary structure, showing that cofactors play a larger role than just stabilizing conformations. The ability to study holo- and apo-proteins, or proteins with known small molecule ligands, will allow better correlation of ETp measurements with biological functionality in the future. These studies provide a glimpse of how results from ETp measurements can inform on mechanisms of protein activity for proteins whose functionality is dependent upon ET.

4.3.4. Molecular vibration contribution to electron transport measurements. Molecular vibrations within proteins, which are sensitive to the protein's atomic conformations, sometimes alter the tunneling matrix element during charge transport [451, 452]. When a molecular vibrational mode with a characteristic frequency $f_{vib} = \omega/2\pi$ is involved in the transport, depending on the applied bias, the electron can lose or gain a quantum of energy $E_{vib} = \hbar\omega$ to (de)excite the vibrational mode during transport (figure 28(a)). This opens an inelastic tunneling channel when the energy difference between the Fermi levels of the electrodes is greater than $\hbar\omega$, which increases the total conductance. Thus, the total junction-current shows a kink as a function of the applied bias for $|eV_{bias}| > \hbar\omega$. This kink results
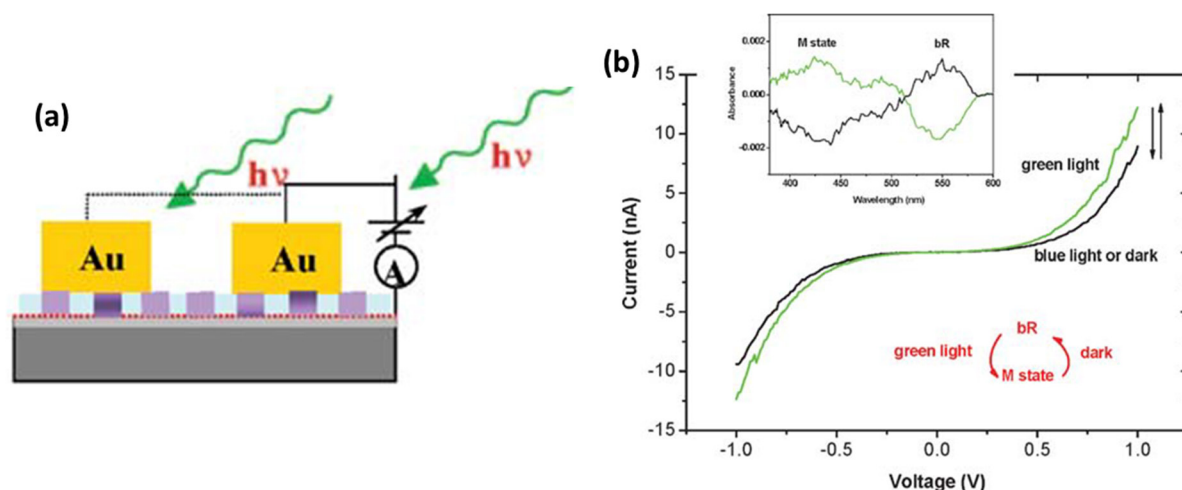
Figure 31. (a) Schematic of Au/WT-bR (oriented)/APTMS/AlO$_x$/Al junction, with geometric area ~2 × 10^{-3} cm^2. Measurements were carried out upon illumination with green light ($\lambda > 550$ nm), and after varying times in the dark, after this illumination, (b) Reversible *I–V* curves upon illumination at $\lambda > 550$ nm (green) and upon illumination with (380 nm $< \lambda < 440$ nm; black) light. Inset represents differential-adsorption spectra of bacteriorhodopsin monolayers. The black curve shows the irradiated–dark measurements; the green curve shows the (dark after illumination)–irradiated measurements. (a) [465] John Wiley & Sons. Copyright © 2007 WILEY-VCH Verlag GmbH & Co. KGaA, Weinheim. (b) Reproduced from [466] with permission of The Royal Society of Chemisty.

in a step-like signal in the differential conductance (d*I*/d*V*) plot, and becomes a peak in a d^2*I*/d*V*^{2} plot. Since only a small fraction of electrons are transported inelastically, the conductance step is small. A phase-sensitive ('lock-in') second harmonic detection technique can be used to directly measure the d^2*I*/d*V*^{2} peaks (due to inelastic electron tunneling; hence the name Inelastic Electron Tunneling Spectroscopy, IETS) with more sensitivity than taking numerical derivatives of *I*(*V*) data.

Early IETS research included studies of biologically important molecules such as RNA and DNA, and even myoglobin, by Hansma and co-workers [454]. A porous (inorganic) insulator, doped with the (bio)organic molecule of interest, was used in a metal-insulator-metal junction configuration. While indeed IETS measurements on molecular junctions provide information on the vibrational modes of the molecules involved in transport, the ill-defined coverage and random orientations of molecules in the junctions of these pioneering studies made them act as dopants of the main (inorganic) tunneling barrier. Thus, it was difficult to draw conclusions about the ETp properties of the molecules. Recently, the IETS of an azurin-based molecular junction was measured where the most prominent inelastic transport peak was the C–H stretching mode around 2900 cm^{-1} [337]. Because of the special conformation of the junction (azurin between two Au electrodes; see figure 29(a)) this could be a double junction, in which case the applied voltage would be divided and cause the C–H stretching peak to appear at a higher applied voltage of ~5800 cm^{-1}. Other IETS peaks were observed around 1600 cm^{-1}, corresponding to amide I and II vibrational modes with significant amplitudes, i.e. the intensity ratio was quite different from that seen in the IR (infrared) spectrum of a monolayer on Au (using PM-IRRAS) [337].The other peaks could be assigned to modes of the side groups of amino acids, such as the NH$_2$ in-plane bending and C=C or CN bonds in aromatic side groups present in tyrosine, phenylalanine, and tryptophan. These findings confirm that the side groups of the amino acids play a role in the inelastic part

of the transport (which is at most a few percent of the total current in the case of the azurin junction) across proteins.

4.3.5. Opto-electronic properties of immobilized proteins. The development of optoelectronic biomaterials has been driven by the convergence of biochemical techniques for peptide/protein engineering. Multilayers of photoactive rhodopsin families of (mutated) proteins have been explored over the last three decades as optical sensors and memory devices [58]. To date, much of the protein-based optoelectronics research has focused on the photoresponse characteristics of the light-sensitive protein bacteriorhodopsin (bR) with the aim of developing light switches, or modulators using semiconductor-based photonic crystals [455]. No membrane protein has been studied as extensively as bR, where the reversible photocycle is triggered by light-induced trans $\rightarrow$ cis retinal double bond isomerization, as occurs in human visual pigments. The configuration alteration of the retinal chromophore, which is covalently bound to the protein and in located at the center of the protein, results in a conformational change of the surrounding protein and in the proton pumping action (figure 30(a)) [456]. Transient (photo-voltage/-current) and steady-state photoconduction with bR, acting as the light-sensitive material across an indium tin oxide (ITO)/bR/Au/GaAs heterostructure, has been reported (figure 30(a)–(c)) [457]. Light-induced optical memory elements have been realized with a genetically engineered or chemically modified bR, with long excited state lifetimes (~minutes) [458]. Photoinduced surface potential alteration of bR patches has been employed as electrostatic memory using scanning surface potential microscopy (figures 30(d) and (e)) [459, 460]. bR-FET-VCSEL monolithically integrated bio-photo-receivers and photo-transceiver arrays have been successfully designed, fabricated, and characterized for standard communication applications [461]. The large electro-optic effect in bR films can in principle be used in other novel all-optical light switches in bio-hybrid semiconductor photonic crystals [462].
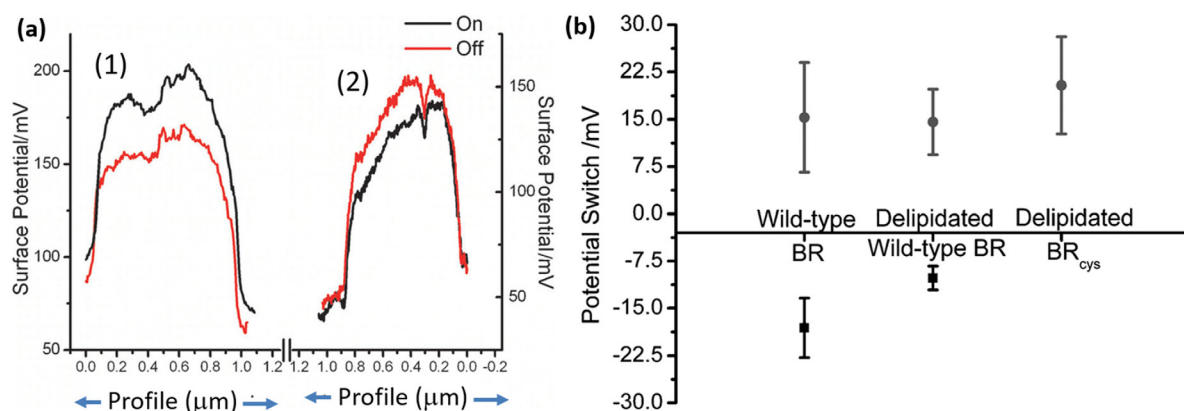
Figure 32. (a) Surface potential cross-section of wild-type purple membrane, PM, patches, immobilized on gold, as mapped by KPFM, in the dark (red line) and under illumination of $\lambda > 495$ nm (black line). The difference between the left and right hand traces in the figure are attributed to probing the extracellular and cytoplasmic sides of the membrane patch, respectively. (b) Comparison of light-induced surface potential modulation for wild-type bR in PM, delipidated wild-type bR and delipidated bR, oriented onto the substrate via a cysteine mutation. [468] John Wiley & Sons. Copyright © 2012 WILEY-VCH Verlag GmbH & Co. KGaA, Weinheim.
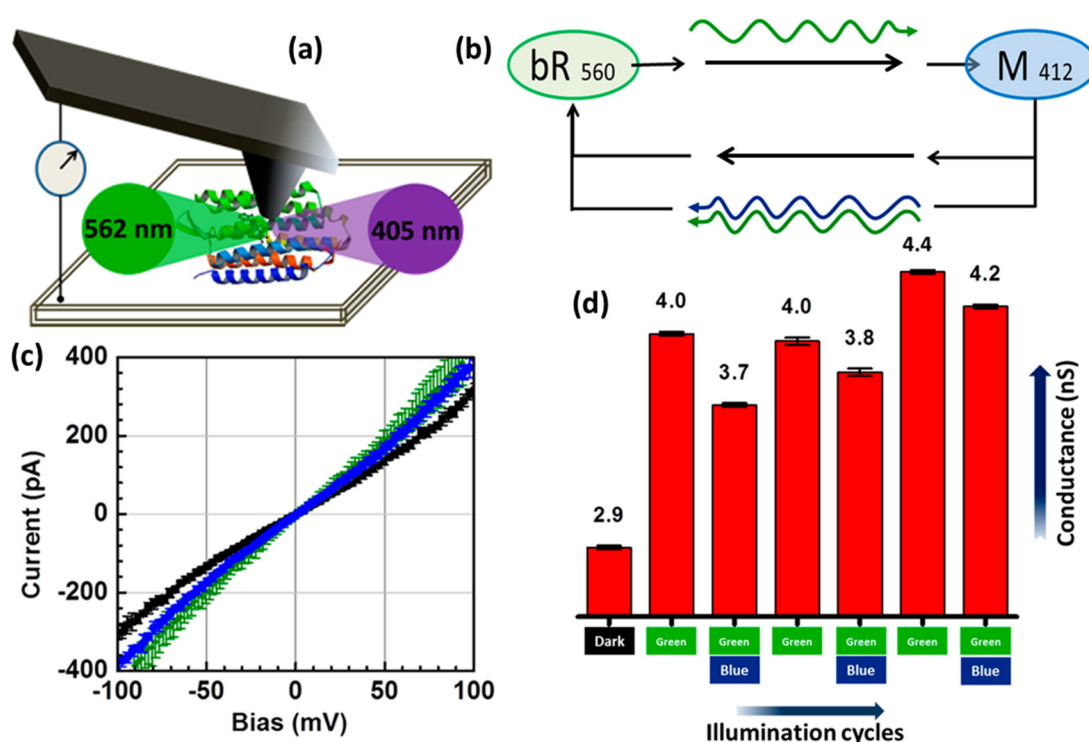

Figure 33. (a) Schematic of electron transport measurement across bR momoners with conducting probe atomic force microscopy. (b) Schematic of bR photocycle in dry dehydrated condition, (c) typical light-induced conduction modulation of a junction with delipidated bR, dLbR, i.e. bR with most of the lipids removed. *I–V* characteristics of a dLbR junction in the dark (black), under green illumination (green), and with blue+green illumination (blue). (d) Conductance modulation of a dLbR junction (numbers on top of bars, in nS) under different illumination conditions (shown at bottom). Reprinted with permission from [360]. Copyright (2014) American Chemical Society.

Monolayers of bR could be more suitable for optoelectronic transport studies than multilayers because the protein structure and orientation in monolayers are better defined. The transient photocurrent of bR monolayers in an aqueous environment has been measured in a photo-electrochemical cell where a bR monolayer was created at the interface between a transparent conductive electrode and an aqueous electrolyte gel [463, 464]. Systematic optoelectronic transport studies (at 293 K and 40% RH) were reported with monolayers of bR that were prepared as follows: bR was extracted from its natural purple membrane and reconstituted with a detergent

to form membranes with the detergent, containing ~ 80 % bR in terms of area. Such membranes close on themselves to form spherical vesicles. These vesicles were self-assembled on a suitable solid support, such as surface-modified silicon or gold, and spontaneously opened when incubated in water (pH −7). By using positively charged silicon surfaces as electrically conducting supports with semi-transparent (30–50%) gold-pads as top electrodes, planar junction structures were fabricated, as shown schematically in the inset of figure 31(b) [465]. Those junctions were then used to test if the so-called photocycle, i.e. the photochromic activity of bR that is central to its biological
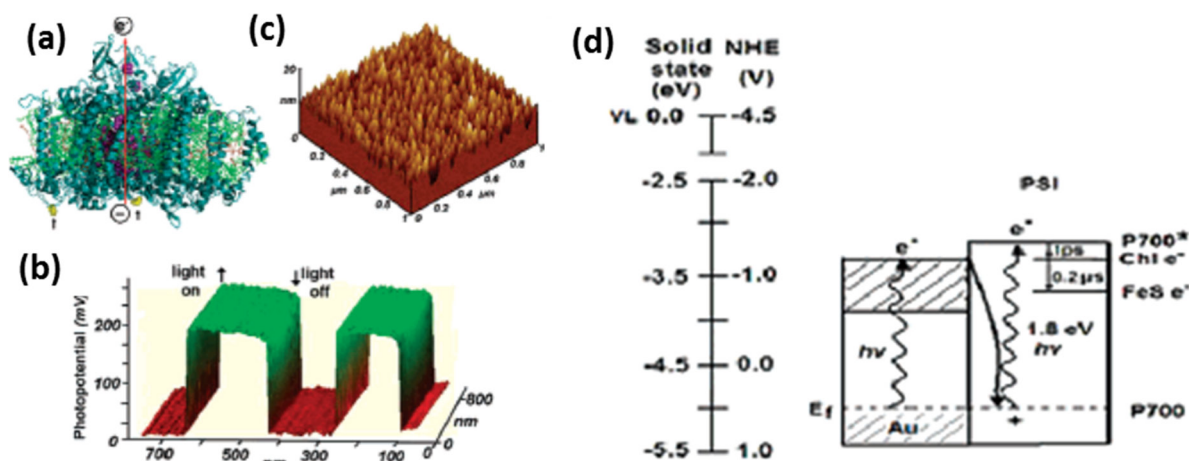
Figure 34. (a) Structure of photosynthetic reaction center I (RC I) based upon crystallographic data (PDB 2O01). (b) and (c) Scanning Kelvin probe force microscopy, SKPFM (see figure 35(b)), images of the PS I monolayer on a gold surface and corresponding topography images of oriented PS I monolayer. Reprinted with permission from [439]. Copyright (2007) American Chemical Society. (d) Schematic energy level diagram of the gold-PS I junction based on experimentally determined contact potential difference. Reprinted with permission from [471]. Copyright (2000) American Chemical Society.

proton-pumping action (see figures 30(a) and 33(b)), is preserved in a dry solid-state monolayer configuration.

As shown in figure 31, the electrical current could indeed be optically modulated in a dry, solid-state bR monolayer junction with electrostatically favorable protein orientations, following the photocycle of the protein. The origin of photo-induced current enhancement was further confirmed via UV–visible absorption of bR monolayer in the presence of green light (abs. maximum around ~560 nm). Upon green light (>495 nm) illumination the 560 nm absorption peak of bR disappeared and a new band appeared at ~420 nm, indicating the formation of the so-called M-state, which results from the retinal in the bR undergoing the trans-cis isomerization that triggers the photocycle (figures 30(a) and 31(b), inset).

The photochemically induced intermediate M-state thermally decayed to the ground state in a few msec, as deduced from the re-appearance of the 560 nm band and the disappearance of the 420 nm band. The enhancement, induced by green light of the junction conduction can then be directly associated with the bR photocycle, implying more efficient conduction via the photochemically induced M intermediate state protein conformation which occurs upon irradiating the junction with green light. M-state involvement in photoconduction was further confirmed through control experiments with apo-retinal bR, where no photocurrent enhancement was obtained, which at least correlates with the known lack of M-state formation in the apo-form of bR [466].

Davis, Watts, and coworkers studied largely lipid-free (25% of endogenous lipid remaining) bR and reported reproducible, robust and controlled interfacial assembly [467–469]. They explored both partial delipidation and single-site mutation of bacteriorhodopsin (bR$_{cys}$) where one of the amino acids, methione (Met-163), located on the cytoplasmic side of bR (i.e. the side exposed to the bacteria's inside cytoplasm in the purple membrane), was replaced with a cysteine. This allows for direct binding of the protein to Au via a Au–S bond, resulting in a unidirectional uniform orientation of the protein

on a gold substrate (figure 31). Along with the photo-cycle, proton flux movement across protein structure-induced potential changes was mapped out by scanning probe microscopy [460]. The magnitude of the surface potential switch upon illumination is consistently larger for bR$_{cys}$ (delipidated or PM embedded) than with the WT-type bR. Strikingly, the photoinduced surface potential switch was solely unidirectional (positive direction), which confirms the designed and confined surface molecular orientation (figure 32).

The study concludes that the process of freeing the protein from its associated lipid and introducing a reactive surface cysteine residue preserves the protein's photophysical characteristics, while enabling a more intimate interfacial sampling on gold electrodes compared to purple membrane. The modulated, wavelength-specific irradiation of a bR$_{cys}$ monolayer generates current transients similar to those naturally observed during the native membrane's proton pumping activities [43]. The chemical binding of functional, delipidated bR$_{cys}$ onto solid surfaces allowed analysis of potential photoswitching, which may be relevant to the development of derived nanoscale photoresponsive devices (the 'molecular pixel') [467].

To enhance photoconduction across bR-containing monolayers, ETp was probed across higher protein concentrations in partially delipidated WT-bR, where ~75% of the PM lipids were removed [360]. bR was immobilized as a monolayer, taking advantage of interactions of the WT surfaces, which are normally in contact with lipids, with the surface of highly ordered pyrolytic graphite (HOPG) used as a conducting substrate (figure 33(a)). The hydrophobic interaction induces bR to a 'lying down' configuration rather than 'standing up' like on gold or silicon substrate. This junction configuration reduces the tunneling barrier height from 6 nm, as for bR$_{cys}$, to 2.5 nm, thus enhancing junction current and light-induced conductance variations with electro-optical modulation.

The conductance of bR monomer junctions was significantly enhanced under green light illumination compared to that measured in the dark, as long as junctions were probed with
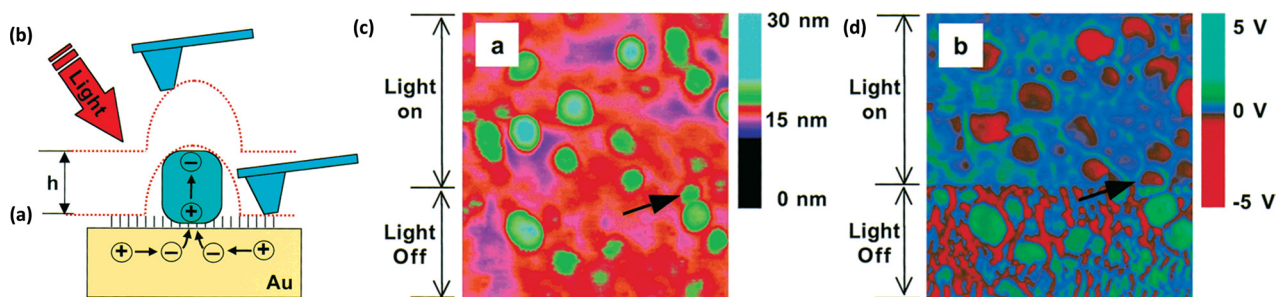
Figure 35. Schematic illustration of SKPFM technique used for photovoltage measurement of single reaction centers of Photosystem I, RC I. Dual measurements employed (a) tapping mode AFM for topographic imaging and (b) lift-mode Kelvin Probe Force mode for voltage imaging. (c) Topographic and (d) electric potential image maps (500×500 nm) of the same set of isolated and oriented PS I reaction centers on a 2-mercaptoethanolmodified gold surface. (d) Demonstrates a clear light-induced PS I electric potential reversal from positive voltage to negative upon illumination. The scanning directions for each raster of the constructed images were from left to right and top to bottom. Reprinted with permission from [471]. Copyright (2000) American Chemical Society.
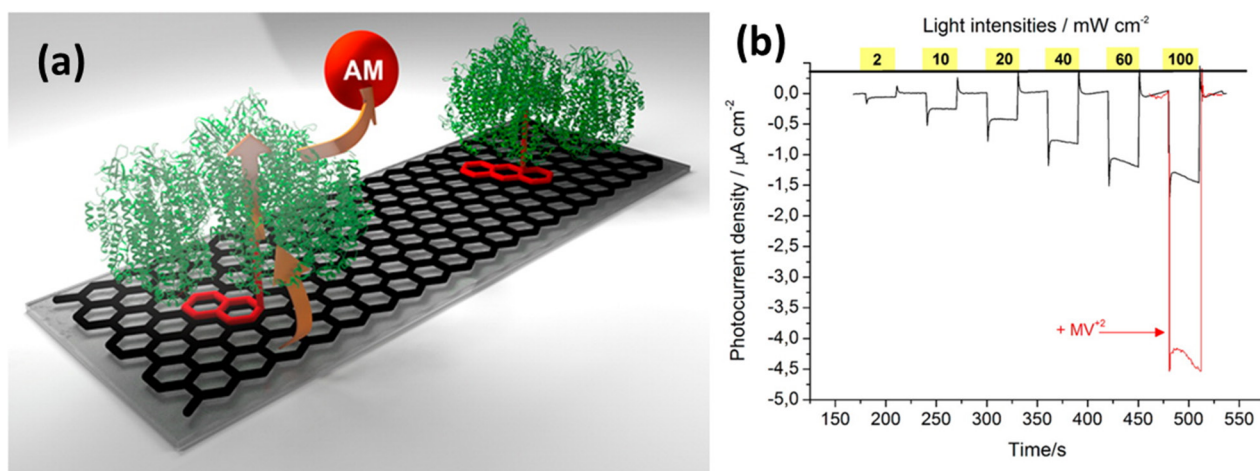

Figure 36. (a) Construction of graphene-based biohybrid light-harvesting architectures consisting of RC I adsorbed onto π-system-modified graphene interfaces. (b) Photochronoamperometric examination of a graphene·dicarboxylic-anthracene-PSI electrode, recorded with different light intensities (2, 10, 20, 40, 60, 100 mW cm^{-2}). Cathodic photocurrents are shown in the figure; all measurements have been performed under air saturation. Reprinted with permission from [472]. Copyright (2015) American Chemical Society.

an applied force within the elastic force range (2–10 nN; see figure 18(b)) (figures 33(a) and (b)). In the elastic force regime, the relative photo-conductance, $\Delta G/G_{dark}$, induced by green illumination does not depend on tip force and $G_{green}/G_{dark} = 2$ (i.e. $\Delta G/G_{dark} = 1$).

At higher applied forces (>10 nN; see figure 18(a)), in the plastic regime, the change in the relative photo-induced conductance decreases, and $\Delta G/G_{dark}$ reduces to as little as 0.2, decreasing monotonically with force (see section 3.6.2). This behavior can be interpreted as follows: at low forces, there is efficient conversion of the ground state to the M-like intermediate under green illumination and minor structural perturbation of the bR monomer (figure 33(b)). In the plastic range bR monomers are under higher applied force, which hinders the light-induced conformational changes and impedes M-like state formation (figure 33(b)), leading to a decrease in photoconductance. During successive green and (blue+green) illumination cycles, a reproducible conductance variation was observed over typically three to four full cycles (figures 33(c) and (d)). These results rule out junction heating upon illumination as the cause of the conductance changes and strongly

support the interpretation of photochemically induced M-like intermediate accumulation during green light illumination, which increases the conductance (refer to figure 31). Exposure to blue light, on top of the green light, decreases the fraction of M-like intermediate in the mixture by accelerating its conversion back to the initial dark bR state, which further decreases the conductance (figures 33(c) and (d)). Humidity-dependent light responses at two distinct applied forces, in the elastic (9 nN) and in the plastic (23 nN) regimes, demonstrate relative current enhancement with increasing humidity followed by saturation above 70% relative humidity.

Like bacteriorhodopsin, a dry photosystem I protein (PS I) monolayer on a linker-modified gold surface retains its fundamental optoelectronic properties, as deduced from the optical absorption spectra and the surface photovoltage spectral response (SPV) [439]. However, the SPV spectrum was broad and slightly blue-shifted (~10–20nm) when compared to the absorption spectrum, which can be due to electronic coupling of PS I to the electronic energy states of the gold, i.e. substantial mixing between the molecular and substrate wave functions [470]. Illumination of the PS I monolayer with
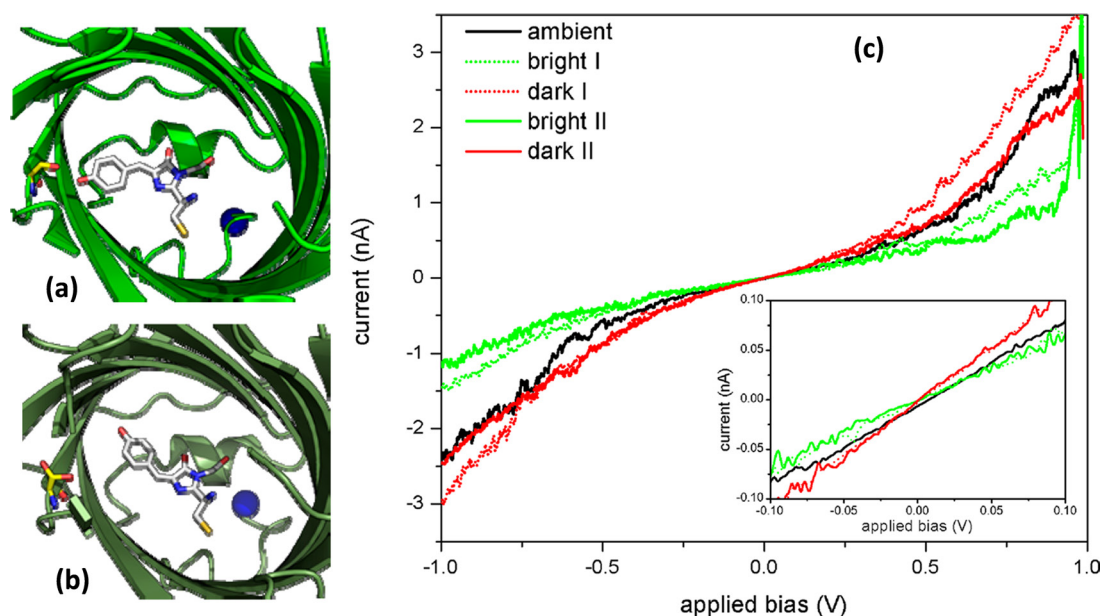
Figure 37. (a) and (b) Structure of bright state and dark state of Dronpa (PDB ID: 2Z1O and 2POX) with N-terminus highlighted in blue. The chromophore, which is represented in white, resides at different positions of the β-barrel in different states, (c) averaged STS *I–V* spectra of His-tagged Dronpa as the protein is cycled through dark and bright states. Inset—showing ohmic region (-0.1 V to $+0.1$ V) of *I–V* spectra. An increase in conductance is visible upon switching from the bright state to the dark state. Reprinted with permission from [473]. Copyright (2012) American Chemical Society.

632 nm (some 50 nm below the peak, but within the absorption band of PS I) caused a dramatic reversible increase of ~0.45 V in the contact potential difference (figure 34). This photovoltage modification was explained by the light-induced charge separation that drives electron transfer across the reaction center, resulting in the appearance of a negative charge at the reducing end of the protein away from the gold surface. The explanation implies that PS I protein was highly orientated on the linker-modified gold substrate, possibly due to the intrinsic dipole moment of protein itself. In the dark, charge recombination takes place and the photovoltage nulls to original levels.

Scanning Kelvin force probe microscopy was used to study the electrostatic potentials generated at single PS I reaction centers (RC I), immobilized on linker-modified atomically flat gold (figure 35) [471]. The photovoltage at the central region of the PS I domains was more positive than at the peripheral envelop area by 240–360 meV. This energy difference suggests a possible mechanism following the Calvin–Benson cycle, whereby negatively charged ferredoxin, the soluble electron carrier from RC I, is anchored and positioned at the reducing end of RC I for electron transfer. Under illumination, the electric potentials of RC I acceptors develop a negative voltage following electron capture, whereas in the dark, the potential is positive.

Unidirectional photocurrent of RC I on π-system-modified graphene electrodes has been pursued in the quest for developing functional photobiohybrid systems (figure 36) [472]. Naphthalene derivatives provide a suitable surface for the adsorption of RC I, and their combination yield, already at (the dark) open-circuit potential, a high cathodic photocurrent output of 4.5 ± 0.1 μA cm^{-2}, which is significant for bio-hybrid device applications.

What were likely close to monolayers of cytochrome c, with Sn instead of Fe, were found to act as reversible and efficient photo-switches in hexane-immersed solid-state junctions. Excitations in either the longer wavelength (Q-)band, @ 535 nm, or in the Soret band @ 405 nm led to significant on/off ratios of up to 25. While no mechanistic studies were done, it was suggested that intramolecular excitations, rather than photo-induced conformational changes, opened new transport channels [252].

Conductance switching in the photoswitchable protein dronpa (similar to GFP, green fluorescent protein) self-assembled onto gold substrates (1 1 1), was measured using scanning tunneling microscopy (STM) and scanning tunneling spectroscopy (STS) methods before and after the protein was reversibly switched to a non-fluorescent dark state and to the fluorescent bright state in a cyclic fashion using 488 and 405 nm light (figure 37) [473].

ETp studies on photoreceptor proteins containing a flavin chromophore have shown that chromophore-protein interactions, and the electronic environment (which mostly originates from protein residues) around the chromophore, plays an important in light-induced transport enhancements [361].

To use proteins as tunable soft-matter building blocks for optoelectronic applications, they must be modified to generate properties beyond their native biological functions, which is possible using biochemistry and via mutations. A further level in functionality can be reached by combining proteins, as indeed occurs in several cases in nature (e.g. in the photosynthetic and mitochondrial electron transport chains). An example, demonstrated in an electrochemical set-up by Lee *et al* [474] is an artificial photosynthetic cascade, where a monolayer of the redox-active electron transfer, ET protein CytC is attached, by chemical modification, to a monolayer of
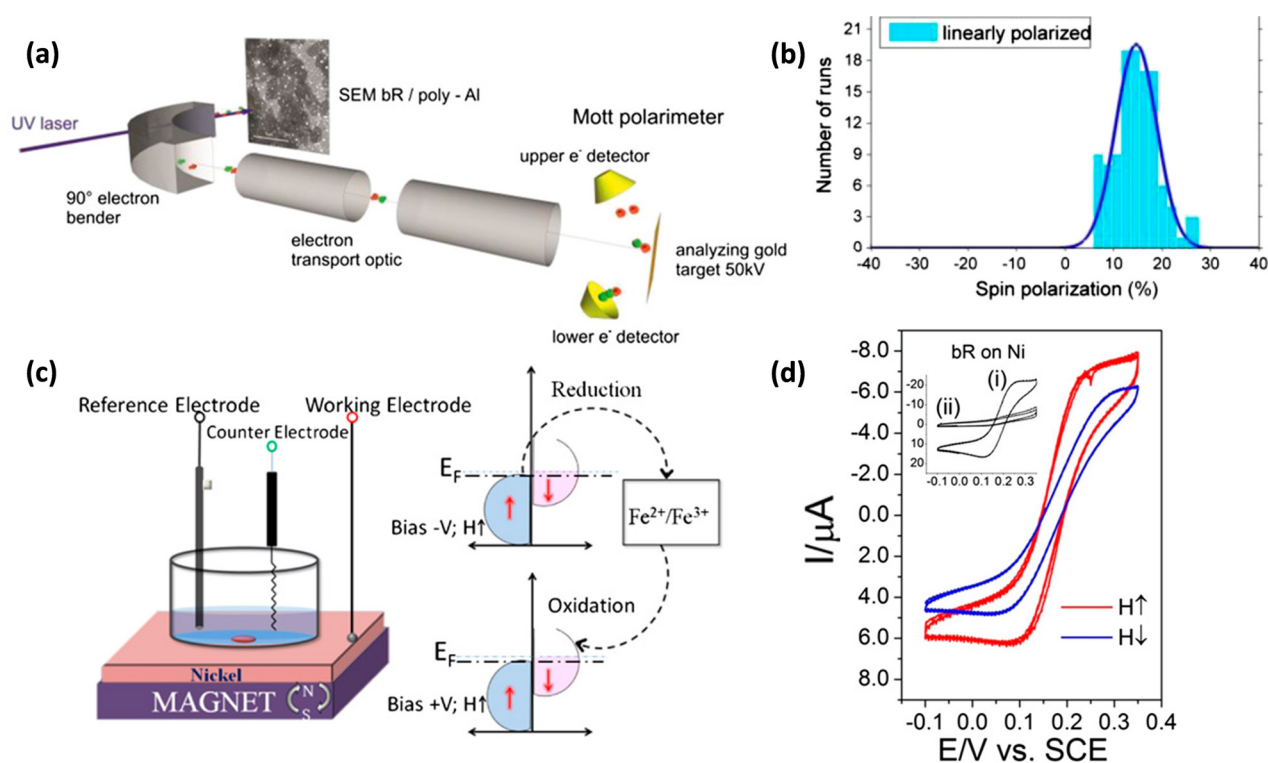
Figure 38. (a) Schematic of spin-dependent photoelectron experimental setup. UV laser radiation (blue) excites photoelectrons from a bR-coated poly-Al substrate (a scanning electron microscope image of a partial monolayer is shown). The excited electrons are extracted antiparallel to the light incidence, bent by 90°, and guided into the Mott polarimeter to determine their longitudinal spin polarization (green and red dots indicate electrons with different polarizations). (b) Spin polarization of photoelectrons ejected by linearly polarized UV excitation from an aluminum substrate after having traversed a purple membrane containing bR 10% in volume. When the electrons were ejected from aluminum substrates, a spin polarization of about 15% was measured. (c) Spin-dependent electrochemistry setup where the working electrode was made from nickel; a permanent magnet was used to control the magnetic direction of substrate. (d) Spin-dependent electrochemical studies as obtained, using a thin film of bR, physisorbed on the Ni working electrode; arrows in the figures indicate the two possible directions (conventionally UP and DOWN) of the magnetic field ($H = 0.35$ T), which is orthogonal to the surface of the working electrode. (Inset) CVs of a bR/Ni thin film without magnetic field (i) freshly deposited bR on Ni and (ii) after the electrochemical burning of the bR. Reproduced from [486–488] with permission from *Proc. Natl. Acad. Sci.* (2013).

the redox-active ET protein azurin. Future work may allow to extend this approach to the solid state by sandwiching the protein bilayer between an electron- and a transparent hole-selective electrode. In their natural environment, protein–protein docking enables electron transfer between these two proteins.

To date, the challenge in bio-*opto*-electronics has been to be able to choose and chemically modify proteins to get predictable ETp modulation characteristics with illumination. To that end, the origin of dominant ETp modulation mechanisms must be identified and parameters crucial for tailoring the optoelectronic properties of these biomolecules, such as the relations between ETp and protein structure and composition, will have to be determined.

4.3.6. Spintronic properties. The possible role of the electron spin electronics, or spintronics, in chemistry and biology has received much attention recently (see also section 4.3.3. and discussion of figures 26 and 27). For example, it was recently discovered that the earth's magnetic field has a significant effect on bird and fish navigation [475, 476]. A general spin-selectivity effect, due to electrons passing through chiral molecules, the so-called chiral-induced spin selectivity, CISS, was observed first in electron transmission

(i.e. photoemission) through organic molecules and DNA attached to gold electrodes [477–479]. Later, a similar effect was observed in electrochemical ET experiments [480], and in a few cases also in solid state (CP-AFM) ETp studies [481, 482]. Spin filtering by chiral molecules has been suggested to be a result of evolution, which would increase the conductance of one spin channel (e.g. spin-up) while decreasing the conductance of the other spin channel (e.g. spin-down) [478, 483, 484]. Spin selectivity in biological electron transfer was first observed in an oriented monolayer of PSI protein monolayers [485]. Spin polarization in ET across PSI was evaluated following photo-induced charge transport in PSI, from the primary electron donor, P700, to a tightly bound phylloquinone molecule, through the primary acceptor, chlorophyll a. Spin-selective measurements with different orientations of the PSI protein complex show that spin polarization is dependent on the ET path in PSI. Different substrate magnetizations also demonstrate that light-induced electron transfer through oriented PSI is spin selective and that the favorable electron spin is aligned parallel to the ET direction in the protein [485].

Recent studies also demonstrate spin-dependent electron transmission through helical structured bR proteins embedded

in their native membrane environment (figure 38) [486]. The results point to the possibility that the spin degree of freedom may play a role in ETp in biological systems. Both spin-filtered photoelectron transmission through an adsorbed protein membrane film and spin-dependent cyclic voltammetry across patches of purple membranes, deposited on externally magnetized Ni substrates, showed efficient spin filtering by a bR layer.

The efficiency of electron spin filtering through purple membranes films and its mutant was controlled by illumination with green light, in line with the bR photocycle [487, 488]. Whereas significant spin-dependent electron transmission through the native membranes was observed, illumination with green light dramatically reduced the spin filtering of a bR mutant. These studies are consistent with the idea that the accumulation of the M-intermediate state in films upon illumination opens, or facilitates transport along pathways for spin-down electrons, thus resulting in lower electron spin filtering efficiency.

5. Summary and future outlook

In this report, we have we have summarized what we view as some of the important new findings in the field of protein-based biomolecular electronics, in recent years. While formidable progress has been made in towards a fundamental understanding of ET, the understanding of the solid-state analogue, ETp, is far less advanced. Further measurements that incorporate more detailed interrogation at the single molecule level, and more advanced control of variables, related to protein conformation and orientation, may provide parameters needed to optimize the use of proteins in bioelectronics. The remarkable electronic transport efficiencies of proteins might be an unintended consequence of properties that evolved, over billions of years of evolution, for other purposes. The solid-state junction (ETp) approach to contacting proteins might be more similar to what happens in nature (i.e. ET processes) than would seem to be the case at first sight (see section 4.1, discussion of figure 21). If this is not accidental, then the reasons for it are not (yet) clear. Understanding of ETp and any fundamental relationships with ET, and finding conditions when these two can be combined, may well become possible in the near future.

Proteins already represent refined structures capable of complex and specific reactions. By exploiting the electronic properties of protein-based molecular junctions in various environments, we foresee the creation of advanced solid-state biosensing devices and bio-circuits that integrate such sensing devices. Implantable electronics for real-time monitoring has been a reality for some time (e.g. heart pace makers), and, using organic electronics, flexible electronic implants are rapidly developing towards widespread use. The ability to use proteins as electronic components can avoid biocompatibility concerns that are present with artificial electronic components, and may allow easier integration into biological systems. However, before proteins can be used in these applications, it is crucial to control how they interact with the solid-state platforms to which they will likely be coupled to communicate with the outside world. Such connections should preserve their functionality in downstream platforms, and this requires understanding the fundamental electronic transport properties.

There are many aspects in the selection of the solid-state substrate and binding methodologies that need to be considered for successful immobilization of active proteins. An important conclusion is that protein conformation plays a key role in maintaining protein stability and function after immobilization and can play a decisive role in the measurement of reproducible electron transport characteristics. In nature, proteins have evolved to function in very specific ways. To use these functionalities, protein function must be preserved on solid supports, and specifically must preserve the integrity of what are known or assumed to be important functional groups. Although maintaining protein structural integrity is challenging in the experimental work discussed here, the results reveal that immobilization methodology can be tailored to obtain useful results.

Our review of the literature shows that immobilization schemes that mimic the protein's biological attachment (e.g. figures 6 and 10) and which allow for interrogation of desired aspects is an effective way to retain protein function and to obtain reproducible results. Different proteins assume a variety of conformations that are necessary for biological functionality, and using this information to immobilize the proteins can yield optimal protein function. For example, if the goal of an experiment is to measure transport involving a particular site of the protein known to participate in ET with a partner (small molecule, ion etc), immobilization onto the electrode for *in situ* electrochemical ET measurements or solid-state ETp measurements after *ex situ* binding should be optimized to assure that the natural binding surface remains exposed for interaction. If the protein of interest is membrane-bound in nature, it is likely to retain its function if covalently tethered using a SAM, rather than directly bound to a solid surface. Taking these steps allows for retention of protein activity, which can then be used in bioelectronic devices. By determining protein orientation and conformation when immobilized, the ability to correlate ETp with biological activity will be enhanced. For example, when optically active cofactors of the membrane-bound proteins bacteriorhodopsin and halorhodopsin, were modified through chemical reactions, the alteration in their optical absorptions was directly correlated to their ETp efficiencies. Altering or removing metal-ion containing cofactors was directly manifested in both their ET and ETp behavior and in their optical absorption properties. Bacteriorhodopsin, immobilized on a ferromagnetic substrate, serves as a spin-filter for electrons that are transmitted across it, which has been ascribed to the 7 left-handed α-helices that define its secondary conformation. Combining spin-filtering with optoelectronic properties of proteins, which rely strongly on their conformations, is a fascinating opportunity to understand the role of spin in biology and, possibly, to future 'biospintronic' devices.

Quite a few studies of protein ETp both at the nanoscale and macroscale have been made, as discussed in this report. Large area monolayer structures can in principle be integrated in future devices, in contrast to what seems (at least presently) possible for single proteins. Therefore, the fabrication of macroscopic electrical junctions, described in this report, which use protein monolayers of geometric areas ranging from 10^2 to 2×10^5 μm^2 (as defined by the smallest electrode), constitute an important step towards using proteins as electronic components. In the future, further miniaturization to a few μm^2 areas may well become possible. At the same time working at the nanoscale and probing ETp of single (or few) proteins can elucidate details about protein function that may be averaged out in macroscopic measurements of the ensemble. In a biological system, proteins are usually not in a monolayer structure, and are often isolated (non-aggregated), implying that single molecule studies could offer more accurate information on actual protein function if it is present in an environment that mimics their natural state (e.g. a membrane protein in low concentrations in a monolayer of detergent). Thus, while unlikely to become part of bioelectronic devices in the near future, studies at the single protein level are important for obtaining fundamental understanding to make bioelectronic devices.

Presently most single molecule studies rely on nanoscale SPM techniques, apart of some studies on break junctions described above. However, the conductance data for proteins (and those for conjugated organic molecules) have a much larger degree of variability for nanoscopic junctions than for macroscopic ones [47], even though both show the same trends. ETp efficiency of proteins is remarkably high when compared to ET rates in proteins and to the transport efficiency through conjugated molecules.

While the ETp studies reviewed here provide information that may well be necessary for incorporating proteins into solid-state platforms, the question remains what have we learned, and what can we learn about the transport mechanism across these proteins from these measurements. Compared to organic molecules, what allows electron transport across proteins to be more efficient than expected? How does electrode-protein (and protein–protein) coupling affect solid-state electronic transport? How can electron transport across relatively long distances ($\geqslant 6$ nm) observed in proteins be temperature-independent? Although it is too ambitious to hope that solid state bioelectronics research can answer all these questions in the short term, progress towards understanding the connections between transport efficiency, protein–electrode coupling, and temperature-independent transport are good places to start.

While there is a clear difference between the ionic transport-coupled electron transfer in biology and all-electronic transport in the artificial solid-state - like systems for future bioelectronics, an understanding of ETp may be relevant to ET because the presence of efficient transport channels in a protein can be expected to affect both. This possibility is intriguing within the context of the earlier mentioned (section 4.1), surprising long-distance electron transport in pili of *G. sulfurreducens* and in nanowires *of S. oneidensis*.

Findings in various report on ETp in/through proteins can be linked back to the proteins' innate function, strengthening the notion that at least some of the biological functionality can be studied with ETp. The importance of cofactors has been demonstrated in redox-active and redox-inactive proteins, illustrating that cofactors are not simple hopping sites. Possibly, the cofactors' effects are related to the conformation and/or charge envelope, as well as to the electronic energy levels of the protein, relevant to transport. The interactions of cofactors with proteins that affect ETp may be relevant to protein function, and understanding how these changes occur may shed light on transport mechanisms and pathways. An important step to understand the effects of cofactors will be to develop the ability to apply gate voltages to protein electronic junctions. While some reports of this exist (and are discussed in this report), it has not yet been possible to achieve gating in a manner that is clear enough so that it can be readily reproduced.

We have experimentally demonstrated that the interaction of proteins with biological binding partners influences ETp characteristics. A possible next step is to determine if ETp changes are related to the degree of conformational change caused by binding, and to determine how ETp pathways are altered.

Although high-resolution SPM imaging allows observing single proteins, it does not always guarantee isolation. This is important not only to prevent aggregation, but also to enable future studies where the same protein can be studied under different conditions, as is usually the case in biology. Nanolithography has helped create nanoarrays that allow both isolation and indexing for enhanced studies, but control of protein conformation remains a challenge. In-depth understanding of protein structure and conformation after immobilization is indeed a great challenge. Protein conformation is highly dynamic around room temperature, and movements of different structural elements have been demonstrated to affect ETp. Currently, spectroscopic techniques can offer snapshots of some general structural elements, but this is far from the ability to trace pathways of electronic transfer or transport. To understand real-time conformational changes, and how they relate to ETp, more quantitative molecular modeling of the protein conformation in the monolayer environment will be required.

In closing, we note that, although the worlds of molecular life sciences and electronics are often separated by a large divide, the growing mutual interest of these areas in each other to address common challenges, is contributing to the creation of new scientific and technological disciplines. Harnessing the unique chemical and physical properties of proteins could allow devices that can be fully integrated with biological systems. We hope that this report will boost interdisciplinary discussions and studies of topics that include bio- and bio-inspired -electronics, with an eye also towards future implantable bio-compatible integrated circuits and innovative healthcare applications.

Acknowledgments

Note added in proof During the final corrections to the proofs amn interesting report by [489] appeared, which shows how another electrochemically inactive protein, integrin, passes pulses of nA currents during msecs between two electrodes over ~ 5 nm, using peptides to bind the protein to the tip and electrode. transitions from low to high cnductance were observed, aupon bias application. Accompanying computational theory results of energy levels were interpreted as indicative of a possible quantum-critical state of the protein, between loclized and band-like electronics states.

References

[1] Davis J J *et al* 2005 Molecular bioelectronics *J. Mater. Chem.* **15** 2160–74

[2] Finkelstein J 2009 Metalloproteins *Nature* **460** 813

[3] Lu Y, Yeung N, Sieracki N and Marshall N M 2009 Design of functional metalloproteins *Nature* **460** 855–62

[4] Pessarakli M 2005 *Handbook of Photosynthesis* (Boca Raton, FL: Taylor and Francis)

[5] Chakraborty T 2007 *Charge Migration in DNA* (Berlin: Springer)

[6] Clarke M J *et al* 1991 *Long-Range Electron Transfer in Biology* (Berlin: Springer)

[7] Jortner J and Bixon M 1999 *Electron Transfer—from Isolated Molecules to Biomolecules, Part 1* (New York: Wiley)

[8] Rasor J P and Voss E 2001 Enzyme-catalyzed processes in pharmaceutical industry *Appl. Catal. Gen.* **221** 145–58

[9] Van Beilen J B, Duetz W A, Schmid A and Witholt B 2003 Practical issues in the application of oxygenases *Trends Biotechnol.* **21** 170–7

[10] Vilker V L, Reipa V, Mayhew M and Holden M J 1999 Challenges in capturing oxygenase activity *in vitro J. Am. Oil Chem. Soc.* **76** 1283–9

[11] Zaks A and Dodds D R 1997 Application of biocatalysis and biotransformations to the synthesis of pharmaceuticals *Drug Discov. Today* **2** 513–31

[12] Schulze B and Wubbolts M G 1999 Biocatalysis for industrial production of fine chemicals *Curr. Opin. Biotechnol.* **10** 609–15

[13] Tao J A, Lin G Q and Liese A 2009 *Biocatalysis for the Pharmaceutical Industry: Discovery, Development, and Manufacturing* (New York: Wiley)

[14] Lamb S B, Lamb D C, Kelly S L and Stuckey D C 1998 Cytochrome P450 immobilisation as a route to bioremediation/biocatalysis *FEBS Lett.* **431** 343–6

[15] Leung A, Shankar P M and Mutharasan R 2007 A review of fiber-optic biosensors *Sensors Actuators* B **125** 688–703

[16] Wolfbeis O S 2008 Fiber-optic chemical sensors and biosensors *Anal. Chem.* **80** 4269–83

[17] Kimmel D W, LeBlanc G, Meschievitz M E and Cliffel D E 2012 Electrochemical sensors and biosensors *Anal. Chem.* **84** 685–707

[18] Kuila T *et al* 2011 Recent advances in graphene-based biosensors *Biosens. Bioelectron.* **26** 4637–48

[19] Wang J 2005 Carbon-nanotube based electrochemical biosensors: a review *Electroanalysis* **17** 7–14

[20] Carrara S, Baj-Rossi C, Boero C and De Micheli G 2014 Do carbon nanotubes contribute to electrochemical biosensing? *Electrochim. Acta* **128** 102–12

[21] Baj-Rossi C, De G and Carrar S 2011 P450-based nano-bio-sensors for personalized medicine *Biosensors—Emerging Materials and Applications* ed P A Serra (Rijeka: InTech) (https://doi.org/10.5772/16328)

[22] Palchetti I and Mascini M 2008 Electroanalytical biosensors and their potential for food pathogen and toxin detection *Anal. Bioanal. Chem.* **391** 455–71

[23] Ligler F S *et al* 2003 Array biosensor for detection of toxins *Anal. Bioanal. Chem.* **377** 469–77

[24] Carrara S, Shumyantseva V V, Archakov A I and Samorì B 2008 Screen-printed electrodes based on carbon nanotubes and cytochrome P450scc for highly sensitive cholesterol biosensors *Biosens. Bioelectron.* **24** 148–50

[25] Baj-Rossi C, Micheli G D and Carrara S 2012 Electrochemical detection of anti-breast-cancer agents in human serum by cytochrome P450-coated carbon nanotubes *Sensors* **12** 6520–37

[26] Aviram A and Ratner M A 1974 Molecular rectifiers *Chem. Phys. Lett.* **29** 277–83

[27] Salemme F R 2006 Design principles for self-assembling devices from macromolecules *Bionanotechnology* ed V Renugopalakrishnan and R V Lewis (Netherlands: Springer) pp 1–8

[28] Facci P 2002 *Single Metalloproteins At Work: Towards a Single-Protein Transistor* (Amsterdam: Elsevier)

[29] Li D 2009 Exploring electron transfer in myoglobin-based transistors *PhD Thesis* West Virginia University (DAI-B 70/11, Dissertation Abstracts International, Ann Arbor MI, USA)

[30] D'Amico S *et al* 2004 Ambipolar transistors based on azurin proteins *IEE Proc. Nanobiotechnol.* **151** 173–5

[31] Artés J M, Díez-Pérez I and Gorostiza P 2012 Transistor-like behavior of single metalloprotein junctions *Nano Lett.* **12** 2679–84

[32] Li D, Gannett P M and Lederman D 2012 An investigation into the feasibility of myoglobin-based single-electron transistors *Nanotechnology* **23** 395705

[33] Zhang T *et al* 2000 All-optical logic gates using bacteriorhodopsin films *Opt. Eng.* **39** 527–34

[34] Aguilella V M and Alcaraz A Nanobiotechnology: a fluid approach to simple circuits *Nat. Nanotechnol.* **4** 403–4

[35] Ciesielski P N *et al* 2010 Photosystem I—based biohybrid photoelectrochemical cells *Bioresour. Technol.* **101** 3047–53

[36] Ditto W L 2003 Chaos in neural systems: from epilepsy to neurocomputing *Proc. of the 25th Annual Int. Conf. of the IEEE Engineering in Medicine and Biology Society* vol 4 pp 3830–3

[37] Ha S, Wee Y and Kim J 2012 Nanobiocatalysis for enzymatic biofuel cells *Top. Catal.* **55** 1181–200

[38] Reshetilov A N 2015 Biosensors and biofuel cells: research focused on practical application (review) *Appl. Biochem. Microbiol.* **51** 264–9

[39] Calabrese Barton S, Gallaway J and Atanassov P 2004 Enzymatic biofuel cells for implantable and microscale devices *Chem. Rev.* **104** 4867–86

[40] Guiseppi-Elie A, Brahim S, Slaughter G and Ward K R 2005 Design of a subcutaneous implantable biochip for monitoring of glucose and lactate *IEEE Sens. J.* **5** 345–55

[41] Farahi R H, Ferrell T L, Guiseppi-Elie A and Hansen P 2007 Integrated electronics platforms for wireless implantable biosensors *IEEE NIH Life Sci. Systems and Application Workshop LISA* pp 27–30

[42] Carrara S, Cavallini A, Garg A and De Micheli G 2009 Dynamical spot queries to improve specificity in P450s based multi-drugs monitoring *ICME Int. Conf. on Complex Medical Engineering* pp 1–6

[43] Saga Y, Watanabe T, Koyama K and Miyasaka T 1999 Mechanism of photocurrent generation from bacteriorhodopsin on gold electrodes *J. Phys. Chem.* B **103** 234–8

[44] Berna A Z, Anderson A R and Trowell S C 2009 Bio-benchmarking of electronic nose sensors *PLoS One* **4** e6406

[45] Winkler J R, Dunn A R, Hess C R and Gray H B 2008 Electron tunneling through iron and copper proteins *Bioinorganic Electrochemistry* ed O Hammerich and J Ulstrup (Netherlands: Springer) pp 1–23

[46] Skourtis S S 2013 Review: probing protein electron transfer mechanisms from the molecular to the cellular length scales *Pept. Sci.* **100** 82–92

[47] Amdursky N *et al* 2014 Electronic transport via proteins *Adv. Mater.* **26** 7142–61

[48] Bianco P 2007 The origin of bioelectrochemistry: an overview *Encyclopedia of Electrochemistry* (New York: Wiley)

[49] Andolfi L and Cannistraro S 2005 Conductive atomic force microscopy study of plastocyanin molecules adsorbed on gold electrode *Surf. Sci.* **598** 68–77

[50] Chi Q, Zhang J, Friis E P, Andersen J E T and Ulstrup J 1999 Electrochemistry of self-assembled monolayers of the blue copper protein *Pseudomonas aeruginosa* azurin on Au(1 1 1) *Electrochem. Commun.* **1** 91–6

[51] Gray H B and Winkler J R 1996 Electron transfer in proteins *Annu. Rev. Biochem.* **65** 537–61

[52] Farver O and Pecht I 1992 Long range intramolecular electron transfer in azurins *J. Am. Chem. Soc.* **114** 5764–7

[53] Li W *et al* 2012 Temperature and force dependence of nanoscale electron transport via the Cu protein azurin *ACS Nano* **6** 10816–24

[54] Facci P 2014 *Biomolecular Electronics: Bioelectronics and the Electrical Control of Biological Systems and Reactions* (Amsterdam: Elsevier)

[55] Nicolini C 2016 *Molecular Bioelectronics: the 19 Years of Progress* (Singapore: World Scientific)

[56] Cuevas J C and Scheer E 2010 *Molecular Electronics: an Introduction to Theory and Experiment* (Singapore: World Scientific)

[57] Nitzan A 2006 *Chemical Dynamics in Condensed Phases: Relaxation, Transfer and Reactions in Condensed Molecular Systems* (Oxford : Oxford University Press)

[58] Xi B, Wise K J, Stuart J A and Birge R R 2006 Bacteriorhodopsin-based 3D optical memory *Bionanotechnology: Proteins to Nanodevices* ed

V Renugopalakrishnan and R V Lewis pp 39–59 (Netherlands: Springer)

[59] Artés J, Hihath J and Díez-Pérez I 2015 Biomolecular electronics *Molecular Electronics: an Experimental and Theoretical Approach* ed I Baldea (Singapore: Pan Stanford) pp 281–323

[60] Alessandrini A and Facci P 2016 Electron transfer in nanobiodevices *Eur. Polym. J.* **83** 450–66

[61] Gray H B and Winkler J R 2003 Electron tunneling through proteins *Q. Rev. Biophys.* **36** 341–72

[62] Waleed Shinwari M, Jamal Deen M, Starikov E B and Cuniberti G 2010 Electrical conductance in biological molecules *Adv. Funct. Mater.* **20** 1865–83

[63] Ron I, Pecht I, Sheves M and Cahen D 2010 Proteins as solid-state electronic conductors *Acc. Chem. Res.* **43** 945–53

[64] Sligar S G and Salemme F R 1992 Protein engineering for molecular electronics *Curr. Biol.* **2** 494

[65] Winkler J R and Gray H B 2014 Electron flow through metalloproteins *Chem. Rev.* **114** 3369–80

[66] Cohen S R 2007 Electron flow through molecular structures *Scanning Probe Microscopy: Electrical and Electromechanical Phenomena at the Nanoscale* ed S Kalinin and A Gruverman (New York: Springer) pp 715–45

[67] Niki K, Bard A J, Stratmann M and Wilson G 2002 *Bioelectrochemistry in Encyclopedia of Electrochemistry* vol 9 (Weinheim: Wiley)

[68] Léger C and Bertrand P 2008 Direct electrochemistry of redox enzymes as a tool for mechanistic studies *Chem. Rev.* **108** 2379–438

[69] Bockris J O, Reddy A K N and Gamboa-Aldeco M E 2007 *Modern Electrochemistry 2A: Fundamentals of Electrodics* (Berlin: Springer)

[70] Bockris J O, Reddy A K N and Gamboa-Aldeco M 2000 *Modern Electrochemistry 2B: Electrodics in Chemistry, Engineering, Biology and Environmental Science* (Berlin: Springer)

[71] Cordes M and Giese B 2009 Electron transfer in peptides and proteins *Chem. Soc. Rev.* **38** 892–901

[72] Reece S Y, Hodgkiss J M, Stubbe J and Nocera D G 2006 Proton-coupled electron transfer: the mechanistic underpinning for radical transport and catalysis in biology *Phil. Trans. R. Soc.* B **361** 1351–64

[73] Wierzbinski E *et al* 2013 The single-molecule conductance and electrochemical electron-transfer rate are related by a power law *ACS Nano* **7** 5391–401

[74] Venkatramani R, Wierzbinski E, Waldeck D H and Beratan D N 2014 Breaking the simple proportionality between molecular conductances and charge transfer rates *Faraday Discuss.* **174** 57–78

[75] Vilan A, Aswal D and Cahen D 20174 Large-area, ensemble molecular electronics: motivation and challenges *Chem. Rev.* **117** 4248–86

[76] Riess I 1997 What does a voltmeter measure? *Solid State Ion.* **95** 327–8

[77] Gerischer H and Ekardt W 1983 Fermi levels in electrolytes and the absolute scale of redox potentials *Appl. Phys. Lett.* **43** 393–5

[78] Bockris J O and Khan S U M 1984 Comment on 'Fermi levels in electrolytes and the absolute scale of redox potentials' (1983 *Appl. Phys. Lett.* **43** 393) *Appl. Phys. Lett.* **45** 913–3

[79] Gerischer H 1984 Response to 'Comment on 'Fermi levels in electrolytes and the absolute scale of redox potentials' (1984 *Appl. Phys. Lett.* **45** 913) *Appl. Phys. Lett.* **45** 913–4

[80] Reiss H 1985 The Fermi level and the redox potential *J. Phys. Chem.* **89** 3783–91

[81] Cahen D and Kahn A 2003 Electron energetics at surfaces and interfaces: concepts and experiments *Adv. Mater.* **15** 271–7

[82] Moser C C, Keske J M, Warncke K, Farid R S and Dutton P L 1992 Nature of biological electron transfer *Nature* **355** 796–802

[83] Castañeda Ocampo O E *et al* 2015 Mechanism of orientation-dependent asymmetric charge transport in tunneling junctions comprising photosystem I *J. Am. Chem. Soc.* **137** 8419–27

[84] Amdursky N, Pecht I, Sheves M and Cahen D 2013 Electron transport via cytochrome C on Si–H surfaces: roles of Fe and Heme *J. Am. Chem. Soc.* **135** 6300–6

[85] Raichlin S, Pecht I, Sheves M and Cahen D 2015 Protein electronic conductors: hemin–substrate bonding dictates transport mechanism and efficiency across myoglobin *Angew. Chem., Int. Ed.* **54** 12379–83

[86] Axford D N and Davis J J 2007 Electron flux through apo- and holoferritin *Nanotechnology* **18** 145502

[87] Sepunaru L, Friedman N, Pecht I, Sheves M and Cahen D 2012 Temperature-dependent solid-state electron transport through bacteriorhodopsin: experimental evidence for multiple transport paths through proteins *J. Am. Chem. Soc.* **134** 4169–76

[88] Mukhopadhyay S, Dutta S, Pecht I, Sheves M and Cahen D 2015 Conjugated cofactor enables efficient temperature-independent electronic transport across ~6 nm long halorhodopsin *J. Am. Chem. Soc.* **137** 11226–9

[89] Hirst J 2013 Mitochondrial complex I *Annu. Rev. Biochem.* **82** 551–75

[90] Moser C C, Page C C and Dutton P L 2006 Darwin at the molecular scale: selection and variance in electron tunnelling proteins including cytochrome c oxidase *Phil. Trans. R. Soc.* B **361** 1295–305

[91] Fleming G R, Martin J L and Breton J 1988 Rates of primary electron transfer in photosynthetic reaction centres and their mechanistic implications *Nature* **333** 190–2

[92] Gunner M R, Robertson D E and Dutton P L 1986 Kinetic studies on the reaction center protein from *Rhodopseudomonas sphaeroides*: the temperature and free energy dependence of electron transfer between various quinones in the QA site and the oxidized bacteriochlorophyll dimer *J. Phys. Chem.* **90** 3783–95

[93] Moser C C *et al* 2003 Length, time, and energy scales of photosystems *Adv. Protein Chem.* **63** 71–109

[94] De Vault D and Chance B 1966 Studies of photosynthesis using a pulsed laser *Biophys. J.* **6** 825–47

[95] Gray H B and Winkler J R 2005 Long-range electron transfer *Proc. Natl Acad. Sci. USA* **102** 3534–9

[96] McLendon G and Hake R 1992 Interprotein electron transfer *Chem. Rev.* **92** 481–90

[97] Fontecilla-Camps J C, Volbeda A, Cavazza C and Nicolet Y 2007 Structure/function relationships of [NiFe]- and [FeFe]-hydrogenases *Chem. Rev.* **107** 4273–303

[98] Dobbek H, Gremer L, Meyer O and Huber R 1999 Crystal structure and mechanism of CO dehydrogenase, a molybdo iron-sulfur flavoprotein containing S-selanylcysteine *Proc. Natl Acad. Sci. USA* **96** 8884–9

[99] Doukov T I, Blasiak L C, Seravalli J, Ragsdale S W and Drennan C L 2008 Xenon in and at the end of the tunnel of bifunctional carbon monoxide dehydrogenase/acetyl-CoA synthase *Biochemistry* **47** 3474–83

[100] Moser C C, Anderson J L R and Dutton P L 2010 Guidelines for tunneling in enzymes *Biochim. Biophys. Acta* **1797** 1573–86

[101] Marcus R A and Sutin N 1985 Electron transfers in chemistry and biology *Biochim. Biophys. Acta* **811** 265–322

[102] Marcus R A 1993 Electron transfer reactions in chemistry: theory and experiment (nobel lecture) *Angew. Chem., Int. Ed. Engl.* **32** 1111–21

[103] Bendall D S 1996 *Protein Electron Transfer* (Milton Park: BIOS Scientific Publishers)

[104] Bill N L, Trukhina O, Sessler J L and Torres T 2015 Supramolecular electron transfer-based switching involving pyrrolic macrocycles. A new approach to sensor development? *Chem. Commun.* **51** 7781–94

[105] Giese B, Graber M and Cordes M 2008 Electron transfer in peptides and proteins *Curr. Opin. Chem. Biol.* **12** 755–9

[106] Hopfield J J 1974 Electron transfer between biological molecules by thermally activated tunneling *Proc. Natl Acad. Sci.* **71** 3640–4

[107] Hush N S 1958 Adiabatic rate processes at electrodes. I. Energy-charge relationships *J. Chem. Phys.* **28** 962–72

[108] Blumberger J 2015 Recent advances in the theory and molecular simulation of biological electron transfer reactions *Chem. Rev.* **115** 11191–238

[109] Halpern J and Orgel L E 1960 The theory of electron transfer between metal ions in bridged systems *Discuss. Faraday Soc.* **29** 32–41

[110] Bortolotti C A *et al* 2007 Orientation-dependent kinetics of heterogeneous electron transfer for cytochrome c immobilized on gold: electrochemical determination and theoretical prediction *J. Phys. Chem.* C **111** 12100–5

[111] Lvov Y M, Lu Z, Schenkman J B, Zu X and Rusling J F 1998 Direct electrochemistry of myoglobin and cytochrome P450cam in alternate layer-by-layer films with DNA and other polyions *J. Am. Chem. Soc.* **120** 4073–80

[112] Zhan T, Xi M, Wang Y, Sun W and Hou W 2010 Direct electrochemistry and electrocatalysis of myoglobin immobilized on Fe₂O₃ nanoparticle–sodium alginate–ionic liquid composite-modified electrode *J. Colloid Interface Sci.* **346** 188–93

[113] Page C C, Moser C C, Chen X and Dutton P L 1999 Natural engineering principles of electron tunnelling in biological oxidation–reduction *Nature* **402** 47–52

[114] Gupta R K and Redfield A G 1970 Double nuclear magnetic resonance observation of electron exchange between ferri- and ferrocytochrome c *Science* **169** 1204–6

[115] Simonneaux G and Bondon A 2005 Mechanism of electron transfer in heme proteins and models: the NMR approach *Chem. Rev.* **105** 2627–46

[116] Chi Q *et al* 2000 Molecular monolayers and interfacial electron transfer of *pseudomonas aeruginosa* azurin on Au(1 1 1) *J. Am. Chem. Soc.* **122** 4047–55

[117] Farver O, Zhang J, Chi Q, Pecht I and Ulstrup J 2001 Deuterium isotope effect on the intramolecular electron transfer in *Pseudomonas aeruginosa* azurin *Proc. Natl Acad. Sci.* **98** 4426–30

[118] Nocera D G, Winkler J R, Yocom K M, Bordignon E and Gray H B 1984 Kinetics of intermolecular and intramolecular electron transfer from ruthenium(II) complexes to ferricytochrome c *J. Am. Chem. Soc.* **106** 5145–50

[119] Winkler J R and Gray H B 2014 Long-range electron tunneling *J. Am. Chem. Soc.* **136** 2930–9

[120] Farver O and Pecht I 2007 Elucidation of electron-transfer pathways in copper and iron proteins by pulse radiolysis experiments *Progress in Inorganic Chemistry* ed K D Karlin (New York: Wiley) pp 1–78

[121] Winkler J R, Di B A J, Farrow N A, Richards J H and Gray H B 1999 Electron tunneling in biological molecules *Pure Appl. Chem.* **71** 1753–64

[122] Farver O *et al* 2015 Long-range electron transfer in engineered azurins exhibits marcus inverted region behavior *J. Phys. Chem. Lett.* **6** 100–5

[123] Farver O, Marshall N M, Wherland S, Lu Y and Pecht I 2013 Designed azurins show lower reorganization free energies for intraprotein electron transfer *Proc. Natl Acad. Sci.* **110** 10536–40

[124] Lancaster K M *et al* 2011 Electron transfer reactivity of type zero *pseudomonas aeruginosa* azurin *J. Am. Chem. Soc.* **133** 4865–73

[125] Farver O, Hwang H J, Lu Y and Pecht I 2007 Reorganization energy of the CuA center in purple azurin: impact of the mixed valence-to-trapped valence state transition *J. Phys. Chem.* B **111** 6690–4

[126] Beratan D N, Onuchic J N and Hopfield J J 1987 Electron tunneling through covalent and noncovalent pathways in proteins *J. Chem. Phys.* **86** 4488–98

[127] Beratan D N, Betts J N and Onuchic J N 1991 Protein electron transfer rates set by the bridging secondary and tertiary structure *Science* **252** 1285–8

[128] Onuchic J N, Beratan D N, Winkler J R and Gray H B 1992 Pathway analysis of protein electron-transfer reactions *Annu. Rev. Biophys. Biomol. Struct.* **21** 349–77

[129] Prytkova T R, Kurnikov I V and Beratan D N 2007 Coupling coherence distinguishes structure sensitivity in protein electron transfer *Science* **315** 622–5

[130] Jones M L, Kurnikov I V and Beratan D N 2000 The nature of tunneling pathway and average packing density models for protein-mediated electron transfer *J. Phys. Chem.* A **106** 2002–6

[131] Beratan D N *et al* 2015 Charge transfer in dynamical biosystems, or the treachery of (static) images *Acc. Chem. Res.* **48** 474–81

[132] Zhang Y, Liu C, Balaeff A, Skourtis S S and Beratan D N 2014 Biological charge transfer via flickering resonance *Proc. Natl Acad. Sci.* **111** 10049–54

[133] Polizzi N F, Skourtis S S and Beratan D N 2012 Physical constraints on charge transport through bacterial nanowires *Faraday Discuss.* **155** 43–61

[134] Stubbe J, Nocera D G, Yee C S and Chang M C Y 2003 Radical initiation in the class I ribonucleotide reductase: long-range proton-coupled electron transfer? *Chem. Rev.* **103** 2167–202

[135] López-Pérez D E *et al* 2012 Intermolecular interactions in electron transfer through stretched helical peptides *Phys. Chem. Chem. Phys.* **14** 10332–44

[136] Zohta Y 1993 On the definition of sequential tunneling in a double-barrier resonant tunneling structure *Japan. J. Appl. Phys.* **32** L177–9

[137] Büttiker M 1988 Coherent and sequential tunneling in series barriers *IBM J. Res. Dev.* **32** 63–75

[138] Lambert C J 2015 Basic concepts of quantum interference and electron transport in single-molecule electronics *Chem. Soc. Rev.* **44** 875–88

[139] Prabhulkar S, Tian H, Wang X, Zhu J-J and Li C-Z 2012 Engineered proteins: redox properties and their applications *Antioxid. Redox Signal.* **17** 1796–822

[140] Eyer C S and Backes W L 1992 Relationship between the rate of reductase-cytochrome P450 complex formation and the rate of first electron transfer *Arch. Biochem. Biophys.* **293** 231–40

[141] Guengerich F P and Johnson W W 1997 Kinetics of ferric cytochrome P450 reduction by NADPH–cytochrome P450 reductase: rapid reduction in the absence of substrate and variations among cytochrome P450 systems *Biochemistry* **36** 14741–50

[142] Jett J E *et al* 2013 Measurement of electron transfer through cytochrome P450 protein on nanopillars and the effect of bound substrates *J. Am. Chem. Soc.* **135** 3834–40

[143] Bostick C D, Flora D R, Gannett P M, Tracy T S and Lederman D 2015 Nanoscale electron transport measurements of immobilized cytochrome P450 proteins *Nanotechnology* **26** 155102

[144] Yang M *et al* 2009 Electrocatalytic drug metabolism by CYP2C9 bonded to a self-assembled monolayer-modified electrode *Drug Metab. Dispos.* **37** 892–9

[145] Kumar K S, Pasula R R, Lim S and Nijhuis C A 2016 Long-range tunneling processes across ferritin-based junctions *Adv. Mater.* **28** 1824–30

[146] Rakshit T and Mukhopadhyay R 2012 Solid-state electron transport in Mn-, Co-, holo-, and Cu-ferritins: force-induced modulation is inversely linked to the protein conductivity *J. Colloid Interface Sci.* **388** 282–92

[147] Amdursky N, Ferber D, Pecht I, Sheves M and Cahen D 2013 Redox activity distinguishes solid-state electron transport from solution-based electron transfer in a natural and artificial protein: cytochrome C and hemin-doped human serum albumin *Phys. Chem. Chem. Phys.* **15** 17142–9

[148] Sepunaru L, Pecht I, Sheves M and Cahen D 2011 Solid-state electron transport across azurin: from a temperature-independent to a temperature-activated mechanism *J. Am. Chem. Soc.* **133** 2421–3

[149] Scheller F W *et al* 2005 Thirty years of haemoglobin electrochemistry *Adv. Colloid Interface Sci.* **116** 111–20

[150] Amdursky N, Pecht I, Sheves M and Cahen D 2012 Doping human serum albumin with retinoate markedly enhances electron transport across the protein *J. Am. Chem. Soc.* **134** 18221–4

[151] Amdursky N *et al* 2015 Electron transfer proteins as electronic conductors: significance of the metal and its binding site in the blue Cu protein, azurin *Adv. Sci.* **2** 1400026

[152] Guo C *et al* 2016 Tuning electronic transport via hepta-alanine peptides junction by tryptophan doping *Proc. Natl Acad. Sci.* **113** 10785–90

[153] Amdursky N *et al* 2014 Solid-state electron transport via cytochrome c depends on electronic coupling to electrodes and across the protein *Proc. Natl Acad. Sci. USA* **111** 5556–61

[154] DeGrado W F, Summa C M, Pavone V, Nastri F and Lombardi A 1999 De novo design and structural characterization of proteins and metalloproteins *Annu. Rev. Biochem.* **68** 779–819

[155] Case M A and McLendon G L 2004 Metal-assembled modular proteins: toward functional protein design *Acc. Chem. Res.* **37** 754–62

[156] Sasaki T and Kaiser E T 1989 Helichrome: synthesis and enzymic activity of a designed hemeprotein *J. Am. Chem. Soc.* **111** 380–1

[157] Das A and Hecht M H 2007 Peroxidase activity of de novo heme proteins immobilized on electrodes *J. Inorg. Biochem.* **101** 1820–6

[158] Koder R L *et al* 2009 Design and engineering of an O(2) transport protein *Nature* **458** 305–9

[159] Carter P 1986 Site-directed mutagenesis *Biochem. J.* **237** 1–7

[160] Nobel Media AB 2014 The Nobel Prize in Chemistry 1993 (Nobelprize.org.)

[161] Shortle D, DiMaio D and Nathans D 1981 Directed mutagenesis *Annu. Rev. Genet.* **15** 265–94

[162] Takafumi Ueno T O 2004 Molecular engineering of cytochrome P450 and myoglobin for selective oxygenations *J. Porphyr. Phthalocyanines* **8** 279–89

[163] Ozaki S, Matsui T and Watanabe Y 1996 Conversion of myoglobin into a highly stereo-specific peroxygenase by the L29H/H64L mutation *J. Am. Chem. Soc.* **118** 9784–5

[164] Yeung N and Lu Y 2008 One heme, diverse functions: using biosynthetic myoglobin models to gain insights into heme copper oxidases and nitric oxide reductases *Chem. Biodivers.* **5** 1437–48

[165] Park H-S *et al* 2006 Design and evolution of new catalytic activity with an existing protein scaffold *Science* **311** 535–8

[166] Wegner S V, Boyaci H, Chen H, Jensen M P and He C 2009 Engineering a uranyl-specific binding protein from NikR *Angew. Chem., Int. Ed Engl.* **48** 2339–41

[167] Talbert J N and Goddard J M 2012 Enzymes on material surfaces *Colloids Surf.* B **93** 8–19

[168] Secundo F 2013 Conformational changes of enzymes upon immobilisation *Chem. Soc. Rev.* **42** 6250–61

[169] Rabe M, Verdes D and Seeger S 2011 Understanding protein adsorption phenomena at solid surfaces *Adv. Colloid Interface Sci.* **162** 87–106

[170] Alessandrini A, Berti L, Gazzadi G C and Facci P 2008 Imparting chemical specificity to nanometer-spaced electrodes *Nanotechnology* **19** 355303

[171] Alessandrini A, Salerno M, Frabboni S and Facci P 2005 Single-metalloprotein wet biotransistor *Appl. Phys. Lett.* **86** 133902

[172] Carrara S, Erokhin V, Facci P and Nicolini C 1996 *On the Role of Nanoparticle Sizes in Monoelectron Conductivity* vol 18 (Dordrecht: Kluwer)

[173] Facci P, Erokhin V, Carrara S and Nicolini C 1996 Room-temperature single-electron junction *Proc. Natl Acad. Sci. USA* **93** 10556–9

[174] Petrangolini P, Alessandrini A, Navacchia M L, Capobianco M L and Facci P 2011 Electron transport properties of single-molecule-bearing multiple redox levels studied by EC-STM/STS *J. Phys. Chem.* C **115** 19971–8

[175] Vergani L *et al* 1992 Fluorescence cytometry of microtubules and nuclear-dna during cell-cycle and reverse-transformation *J. Cell. Biochem.* **50** 201–9

[176] Alessandrini A, Corni S and Facci P 2006 Unravelling single metalloprotein electron transfer by scanning probe techniques *Phys. Chem. Chem. Phys.* **8** 4383–97

[177] Alessandrini A and Facci P 2008 *Electrochemically Assisted Scanning Probe Microscopy: a powerful Tool in Nano(bio) Science* (Amsterdam: Elsevier)

[178] Della Pia E A *et al* 2012 Fast electron transfer through a single molecule natively structured redox protein *Nanoscale* **4** 7106–13

[179] Davis J J, Wang N, Morgan A, Zhang T and Zhao J 2006 Metalloprotein tunnel junctions: compressional modulation of barrier height and transport mechanism *Faraday Discuss.* **131** 167–79

[180] Davis J J, Wrathmell C L, Zhao J and Fletcher J 2004 The tunnelling conductance of molecularly ordered metalloprotein arrays *J. Mol. Recognit.* **17** 167–73

[181] Raccosta S, Baldacchini C, Rita Bizzarri A and Cannistraro S 2013 Conductive atomic force microscopy study of single molecule electron transport through the Azurin-gold nanoparticle system *Appl. Phys. Lett.* **102** 203704

[182] Lewis A *et al* 1996 Directly probing rapid membrane protein dynamics with an atomic force microscope: a study of light-induced conformational alterations in bacteriorhodopsin *Biophys. J.* **70** 2380–4

[183] Zhao J, Davis J J, Sansom M S P and Hung A 2004 Exploring the electronic and mechanical properties of protein using conducting atomic force microscopy *J. Am. Chem. Soc.* **126** 5601–9

[184] Tao N J 2006 Electron transport in molecular junctions *Nat. Nanotechnol.* **1** 173–81

[185] Boussaad S and Tao N J 1999 Electron transfer and adsorption of myoglobin on self-assembled surfactant films: an electrochemical tapping-mode AFM study *J. Am. Chem. Soc.* **121** 4510–5

[186] Richter C A, Hacker C A and Richter L J 2005 Electrical and spectroscopic characterization of metal/monolayer/Si devices *J. Phys. Chem.* B **109** 21836–41

[187] Moulton S E, Barisci J N, Bath A, Stella R and Wallace G G 2003 Investigation of protein adsorption and electrochemical behavior at a gold electrode *J. Colloid Interface Sci.* **261** 312–9

[188] Fleming B D, Praporski S, Bond A M and Martin L L 2008 Electrochemical quartz crystal microbalance study of azurin adsorption onto an alkanethiol self-assembled monolayer on gold *Langmuir* **24** 323–7

[189] Bonanni B, Alliata D, Bizzarri A R and Cannistraro S 2003 Topological and electron-transfer properties of yeast cytochrome c adsorbed on bare gold electrodes *ChemPhysChem Eur. J. Chem. Phys. Phys. Chem.* **4** 1183–8

[190] Li N, Xu J-Z, Yao H, Zhu J-J and Chen H-Y 2006 The direct electron transfer of myoglobin based on the electron tunneling in proteins *J. Phys. Chem.* B **110** 11561–5

[191] Della Pia E A, Macdonald J E, Elliott M and Jones D D 2012 Direct binding of a redox protein for single-molecule electron transfer measurements *Small* **8** 2341–4

[192] Schnyder B, Kotz R, Alliata D and Facci P 2002 Comparison of the self-chemisorption of azurin on gold and on functionalized oxide surfaces *Surf. Interface Anal.* **34** 40–4

[193] Rinaldi R *et al* 2003 Electronic rectification in protein devices *Appl. Phys. Lett.* **82** 472–4

[194] Rinaldi R *et al* 2002 Solid-state molecular rectifier based on self-organized metalloproteins *Adv. Mater.* **14** 1453–7

[195] Alessandrini A and Facci P 2015 EC-STM/STS of redox metalloproteins and co-factors *Molecular Electronics: an Experimental and Theoretical Approach* ed I Baldea (Singapore: Pan Stanford) pp 325–52

[196] Norde W 1986 Adsorption of proteins from solution at the solid-liquid interface *Adv. Colloid Interface Sci.* **25** 267–340

[197] Haynes C A and Norde W 1994 Globular proteins at solid/liquid interfaces *Colloids Surf.* B **2** 517–66

[198] Malmsten M 2003 *Biopolymers at Interfaces* 2nd edn (Boca Raton, FL: CRC Press)

[199] Malmsten M and Lassen B 1995 Competitive protein adsorption at phospholipid surfaces *Colloids Surf.* B **4** 173–84

[200] Gekko K and Hasegawa Y 1986 Compressibility-structure relationship of globular proteins *Biochemistry* **25** 6563–71

[201] Malmsten M 1998 Formation of adsorbed protein layers *J. Colloid Interface Sci.* **207** 186–99

[202] Kondo A, Murakami F and Higashitani K 1992 Circular dichroism studies on conformational changes in protein molecules upon adsorption on ultrafine polystyrene particles *Biotechnol. Bioeng.* **40** 889–94

[203] Cruz J C, Pfromm P H, Tomich J M and Rezac M E 2010 Conformational changes and catalytic competency of hydrolases adsorbing on fumed silica nanoparticles: I. Tertiary structure *Colloids Surf.* B **79** 97–104

[204] Shah S, Solanki K and Gupta M N 2007 Enhancement of lipase activity in non-aqueous media upon immobilization on multi-walled carbon nanotubes *Chem. Cent. J.* **1** 1–6

[205] Petkar M, Lali A, Caimi P and Daminati M 2006 Immobilization of lipases for non-aqueous synthesis *J. Mol. Catal.* B **39** 83–90

[206] Asuri P *et al* 2006 Increasing protein stability through control of the nanoscale environment *Langmuir* **22** 5833–6

[207] Shang W, Nuffer J H, Dordick J S and Siegel R W 2007 Unfolding of ribonuclease A on silica nanoparticle surfaces *Nano Lett.* **7** 1991–5

[208] Shang W *et al* 2009 Cytochrome C on silica nanoparticles: influence of nanoparticle size on protein structure, stability, and activity *Small Weinh. Bergstr. Ger.* **5** 470–6

[209] Vertegel A A, Siegel R W and Dordick J S 2004 Silica nanoparticle size influences the structure and enzymatic activity of adsorbed lysozyme *Langmuir* **20** 6800–7

[210] Vilan A and Cahen D 2017 Chemical modification of semiconductor surfaces for molecular electronics *Chem. Rev.* **117** 4624–66

[211] Samanta D and Sarkar A 2011 Immobilization of bio-macromolecules on self-assembled monolayers: methods and sensor applications *Chem. Soc. Rev.* **40** 2567–92

[212] Bonasio R *et al* 2007 Specific and covalent labeling of a membrane protein with organic fluorochromes and quantum dots *Proc. Natl Acad. Sci.* **104** 14753–8

[213] Wammes A E M *et al* 2013 Site-specific peptide and protein immobilization on surface plasmon resonance chips via strain-promoted cycloaddition *Lab. Chip* **13** 1863–7

[214] Rusmini F, Zhong Z and Feijen J 2007 Protein immobilization strategies for protein biochips *Biomacromolecules* **8** 1775–89

[215] Murugan P, Krishnamurthy M, Jaisankar S N, Samanta D and Mandal A B 2015 Controlled decoration of the surface with macromolecules: polymerization on a self-assembled monolayer (SAM) *Chem. Soc. Rev.* **44** 3212–43

[216] Bera S, Kolay J, Banerjee S and Mukhopadhyay R 2017 Nanoscale on-silico electron transport via ferritins *Langmuir* **33** 1951–8

[217] Armstrong F A 2005 Recent developments in dynamic electrochemical studies of adsorbed enzymes and their active sites *Curr. Opin. Chem. Biol.* **9** 110–7

[218] Armstrong F A, Heering H A and Hirst J 1997 Reaction of complex metalloproteins studied by protein-film voltammetry *Chem. Soc. Rev.* **26** 169–79

[219] Ferapontova E E *et al* 2005 Direct electrochemistry of proteins and enzymes *Perspectives in Bioanalysis* vol 1, ed F S Emil Paleček and J Wang (Amsterdam: Elsevier) pp 517–98

[220] Guo L-H, Allen H and Hill O 1991 Direct electrochemistry of proteins and enzymes *Advances in Inorganic Chemistry* vol 36, ed A G Sykes (New York: Academic) pp 341–75

[221] Hirst J and Armstrong F A 1998 Fast-scan cyclic voltammetry of protein films on pyrolytic graphite edge electrodes: characteristics of electron exchange *Anal. Chem.* **70** 5062–71

[222] Yeh P and Kuwana T 1977 Reversible electrode reaction of cytochrome c *Chem. Lett.* **6** 1145–8

[223] Eddowes M J and Hill H A O 1977 Novel method for the investigation of the electrochemistry of metalloproteins: cytochrome c *J. Chem. Soc. Chem. Commun.* 771–2

[224] Angove H A, Cole J A, Richardson D J and Butt J N 2002 Protein film voltammetry reveals distinctive fingerprints of nitrite and hydroxylamine reduction by a cytochrome c nitrite reductase *J. Biol. Chem.* **277** 23374–81

[225] Gwyer J D, Angove H C, Richardson D J and Butt J N 2004 Redox-triggered events in cytochrome c nitrite reductase *Bioelectrochem. Amst. Neth.* **63** 43–7

[226] Léger C *et al* 2001 Enzyme electrokinetics: energetics of succinate oxidation by fumarate reductase and succinate dehydrogenase *Biochemistry* **40** 11234–45

[227] Sucheta A, Cammack R, Weiner J and Armstrong F A 1993 Reversible electrochemistry of fumarate reductase immobilized on an electrode surface. Direct voltammetric observations of redox centers and their participation in rapid catalytic electron transport *Biochemistry* **32** 5455–65

[228] Heering H A, Weiner J H and Armstrong F A 1997 Direct detection and measurement of electron relays in a multicentered enzyme: voltammetry of electrode-surface films of *E. Coli* fumarate reductase, an iron–sulfur flavoprotein *J. Am. Chem. Soc.* **119** 11628–38

[229] Turner K L *et al* 1999 Redox properties of flavocytochrome c3 from Shewanella frigidimarina NCIMB400 *Biochemistry* **38** 3302–9

[230] Léger C *et al* 2003 Enzyme electrokinetics: using protein film voltammetry to investigate redox enzymes and their mechanisms *Biochemistry* **42** 865362

[231] Murgida D H and Hildebrandt P 2005 Redox and redox-coupled processes of heme proteins and enzymes at electrochemical interfaces *Phys. Chem. Chem. Phys.* **7** 3773–84

[232] Murgida D H and Hildebrandt P 2001 Active-site structure and dynamics of cytochrome c immobilized on self-assembled monolayers—a time-resolved surface enhanced resonance Raman spectroscopic study *Angew. Chem., Int. Ed.* **40** 728–31

[233] Albrecht T, Li W, Ulstrup J, Haehnel W and Hildebrandt P 2005 Electrochemical and spectroscopic investigations of immobilized de novo designed heme proteins on metal electrodes *ChemPhysChem* **6** 961–70

[234] Freire R S, Pessoa C A, Mello L D and Kubota L T 2003 Direct electron transfer: an approach for electrochemical biosensors with higher selectivity and sensitivity *J. Braz. Chem. Soc.* **14** 230–43

[235] Fischer M J E 2010 Amine coupling through EDC/NHS: a practical approach *Surface Plasmon Resonance: Methods and Protocols* ed N J Mol and M J E Fischer (New York: Humana Press) pp 55–73

[236] Love J C, Estroff L A, Kriebel J K, Nuzzo R G and Whitesides G M 2005 Self-assembled monolayers of thiolates on metals as a form of nanotechnology *Chem. Rev.* **105** 1103–70

[237] Wadu-Mesthrige K, Amro N A and Liu G-Y 2000 Immobilization of proteins on self-assembled monolayers *Scanning* **22** 380–8

[238] Kim D and Herr A E 2013 Protein immobilization techniques for microfluidic assays *Biomicrofluidics* **7** 41501

[239] Hodneland C D, Lee Y-S, Min D-H and Mrksich M 2002 Selective immobilization of proteins to self-assembled monolayers presenting active site-directed capture ligands *Proc. Natl Acad. Sci.* **99** 5048–52

[240] Liu H, Yamamoto H, Wei J and Waldeck D H 2003 Control of the electron transfer rate between cytochrome c and gold electrodes by the manipulation of the electrode's hydrogen bonding character *Langmuir* **19** 2378–87

[241] van de Kamp M *et al* 1990 Involvement of the hydrophobic patch of azurin in the electron-transfer reactions with cytochrome c551 and nitrite reductase *Eur. J. Biochem.* **194** 109–18

[242] van de Kamp M, Floris R, Hali F C and Canters G W 1990 Site-directed mutagenesis reveals that the hydrophobic patch of azurin mediates electron transfer *J. Am. Chem. Soc.* **112** 907–8

[243] Kenaan C, Zhang H, Shea E V and Hollenberg P F 2011 Uncovering the role of hydrophobic residues in cytochrome P450-cytochrome P450 reductase interactions *Biochemistry* **50** 3957–67

[244] Wang M *et al* 1997 Three-dimensional structure of NADPH–cytochrome P450 reductase: prototype for FMN- and FAD-containing enzymes *Proc. Natl Acad. Sci. USA* **94** 8411–6

[245] Maneg O, Malatesta F, Ludwig B and Drosou V 2004 Interaction of cytochrome c with cytochrome oxidase: two different docking scenarios *Biochim. Biophys. Acta* **1655** 274–81

[246] Allen P M, Allen H, Hill O and Walton N J 1984 Surface modifiers for the promotion of direct electrochemistry of cytochrome c *J. Electroanal. Chem. Interfacial Electrochem.* **178** 69–86

[247] Taniguchi I, Higo N, Umekita K and Yasukouchi K 1986 Electrochemical behavior of horse heart cytochrome c in acid solutions using a 6-mercaptopurine-modified gold electrode *J. Electroanal. Chem. Interfacial Electrochem.* **206** 341–8

[248] Ruzgas T, Wong L, Gaigalas A K and Vilker V L 1998 Electron transfer between surface-confined cytochrome c and an N-acetylcysteine-modified gold electrode *Langmuir* **14** 7298–7305

[249] Avila A, Gregory B W, Niki K and Cotton T M 2000 An electrochemical approach to investigate gated electron

[249] transfer using a physiological model system: cytochrome c immobilized on carboxylic acid-terminated alkanethiol self-assembled monolayers on gold electrodes *J. Phys. Chem.* B **104** 2759–2766

[250] Wu Y and Hu S 2006 Voltammetric investigation of cytochrome c on gold coated with a self-assembled glutathione monolayer *Bioelectrochemistry* **68** 105–12

[251] Liu H-H, Lu J-L, Zhang M, Pang D-W and Abruña H D 2003 Direct electrochemistry of cytochrome c surface-confined on DNA-modified gold electrodes *J. Electroanal. Chem.* **544** 93–100

[252] Chen S-M and Chen S-V 2003 The bioelectrocatalytic properties of cytochrome C by direct electrochemistry on DNA film modified electrode *Electrochim. Acta* **48** 513–29

[253] Tarlov M J and Bowden E F 1991 Electron-transfer reaction of cytochrome c adsorbed on carboxylic acid terminated alkanethiol monolayer electrodes *J. Am. Chem. Soc.* **113** 1847–9

[254] Nakamaru S, Scholz F, Ford W E, Goto Y and von Wrochem F 2017 Photoswitchable Sn-cyt c solid-state devices *Adv. Mater.* **29** 1605924

[255] Bigelow W C, Pickett D L and Zisman W A 1946 Oleophobic monolayers *J. Colloid Sci.* **1** 513–38

[256] Grumezescu A 2016 *Fabrication and Self-Assembly of Nanobiomaterials: Applications of Nanobiomaterials* (Amsterdam: Elsevier)

[257] Shafrin E G and Zisman W 1949 Hydrophobic monolayers adsorbed from aqueous solutions *J. Colloid Sci.* **4** 571–90

[258] Du X and Hlady V 2002 Monolayer formation on silicon and mica surfaces rearranged from N-hexadecanoyl-l-alanine supramolecular structures *J. Phys. Chem.* B **106** 7295–9

[259] Nuzzo R G and Allara D L 1983 Adsorption of bifunctional organic disulfides on gold surfaces *J. Am. Chem. Soc.* **105** 4481–3

[260] Haimov B *et al* 2016 Kinetics of nanoscale self-assembly measured on liquid drops by macroscopic optical tensiometry: from mercury to water and fluorocarbons *J. Am. Chem. Soc.* **138** 2585–91

[261] Andrews A M, Liao W-S and Weiss P S 2016 Double-sided opportunities using chemical lift-off lithography *Acc. Chem. Res.* (https://doi.org/10.1021/acs.accounts.6b00034)

[262] González-Granados Z *et al* 2013 Formation of mixed monolayers from 11-mercaptoundecanoic acid and octanethiol on Au(1 1 1) single crystal electrode under electrochemical control *J. Phys. Chem.* C **117** 24307–16

[263] Yan C, Zharnikov M, Gölzhäuser A and Grunze M 2000 Preparation and characterization of self-assembled monolayers on indium tin oxide *Langmuir* **16** 6208–15

[264] Arya S K, Solanki P R, Datta M and Malhotra B D 2009 Recent advances in self-assembled monolayers based biomolecular electronic devices *Biosens. Bioelectron.* **24** 2810–7

[265] Mak L H, Sadeghi S J, Fantuzzi A and Gilardi G 2010 Control of human cytochrome P450 2E1 electrocatalytic response as a result of unique orientation on gold electrodes *Anal. Chem.* **82** 5357–62

[266] Patel N *et al* 1997 Immobilization of protein molecules onto homogeneous and mixed carboxylate-terminated self-assembled monolayers *Langmuir* **13** 6485–90

[267] Chapman R G, Ostuni E, Yan L and Whitesides G M 2000 Preparation of mixed self-assembled monolayers (SAMs) that resist adsorption of proteins using the reaction of amines with a SAM that presents interchain carboxylic anhydride groups *Langmuir* **16** 6927–36

[268] Cui X D *et al* 2002 Making electrical contacts to molecular monolayers *Nanotechnology* **13** 5

[269] Bruening M and Dotzauer D 2009 Polymer films: just spray it *Nat. Mater.* **8** 449–50

[270] Ma H, Hu N and Rusling J F 2000 Electroactive myoglobin films grown layer-by-layer with poly(styrenesulfonate) on pyrolytic graphite electrodes *Langmuir* **16** 4969–75

[271] Cosnier S 1999 Biomolecule immobilization on electrode surfaces by entrapment or attachment to electrochemically polymerized films. A review *Biosens. Bioelectron.* **14** 443–56

[272] Ho D, Chu B, Lee H and Montemagno C D 2004 Protein-driven energy transduction across polymeric biomembranes *Nanotechnology* **15** 1084

[273] Nassar A E, Willis W S and Rusling J F 1995 Electron transfer from electrodes to myoglobin: facilitated in surfactant films and blocked by adsorbed biomacromolecules *Anal. Chem.* **67** 2386–92

[274] Zhang Z, Nassar A-E F, Lu Z, Schenkman J B and Rusling J F 1997 Direct electron injection from electrodes to cytochromeP450cam in biomembrane-like films *J. Chem. Soc. Faraday Trans.* **93** 1769–74

[275] Shumyantseva V V *et al* 2004 Direct electron transfer of cytochrome P450 2B4 at electrodes modified with nonionic detergent and colloidal clay nanoparticles *Anal. Chem.* **76** 6046–52

[276] Kröning S, Scheller F W, Wollenberger U and Lisdat F 2004 Myoglobin-clay electrode for nitric oxide (NO) detection in solution *Electroanalysis* **16** 253–9

[277] Lei C, Lisdat F, Wollenberger U and Scheller F W 1999 Cytochrome c/clay-modified electrode *Electroanalysis* **11** 274–6

[278] Zhou Y, Hu N, Zeng Y and Rusling J F 2002 Heme protein–clay films: direct electrochemistry and electrochemical catalysis *Langmuir* **18** 211–9

[279] Chen X, Hu N, Zeng Y, Rusling J F and Yang J 1999 Ordered electrochemically active films of hemoglobin, didodecyldimethylammonium ions, and clay *Langmuir* **15** 7022–30

[280] Song Y *et al* 2013 Direct electrochemistry of cytochrome c based on poly(diallyldimethylammonium chloride)-graphene nanosheets/gold nanoparticles hybrid nanocomposites and its biosensing *Electroanalysis* **25** 1400–9

[281] Dinesh B, Mani V, Saraswathi R and Chen S-M 2014 Direct electrochemistry of cytochrome c immobilized on a graphene oxide–carbon nanotube composite for picomolar detection of hydrogen peroxide *RSC Adv.* **4** 28229–37

[282] Tanne J, Dietzel B, Scheller F W and Bier F 2014 Nanohybrid materials consisting of poly[(3-aminobenzoic acid)-co-(3-aminobenzenesulfonic acid)-co-aniline] and multiwalled carbon nanotubes for immobilization of redox active cytochrome c *Electroanalysis* **26** 732–8

[283] He P and Hu N 2004 Electrocatalytic properties of heme proteins in layer-by-layer films assembled with SiO$_2$ nanoparticles *Electroanalysis* **16** 1122–31

[284] Li Z and Hu N 2003 Direct electrochemistry of heme proteins in their layer-by-layer films with clay nanoparticles *J. Electroanal. Chem.* **558** 155–65

[285] Zhou Y, Li Z, Hu N, Zeng Y and Rusling J F 2002 Layer-by-layer assembly of ultrathin films of hemoglobin and clay nanoparticles with electrochemical and catalytic activity *Langmuir* **18** 8573–9

[286] Rusling J F 1998 Enzyme bioelectrochemistry in cast biomembrane-like films *Acc. Chem. Res.* **31** 363–9

[287] Hu N 2001 Direct electrochemistry of redox proteins or enzymes at various film electrodes and their possible applications in monitoring some pollutants *Pure Appl. Chem.* **73** 1979–91

[288] Chapman D 1990 Biophysical chemistry of membrane function Kotyk A, Janáček K and Koryta J; John Wiley, Chichester, 1988; xvii + 377 pages; £45.00 *FEBS Lett.* **268** 435–6

[289] Rusling J F 2003 *Biomolecular Films: Design, Function, and Applications* (Boca Raton, FL: CRC Press)

[290] Oliver B N, Egekeze J O and Murray R W 1988 Solid-state voltammetry of a protein in a polymer solvent *J. Am. Chem. Soc.* **110** 2321–2

[291] Sun H, Hu N and Ma H 2000 Direct electrochemistry of hemoglobin in polyacrylamide hydrogel films on pyrolytic graphite electrodes *Electroanalysis* **12** 1064–70

[292] Hu N and Rusling J F 1997 Electrochemistry and catalysis with myoglobin in hydrated poly(ester sulfonic acid) ionomer films *Langmuir* **13** 4119–25

[293] Datta S, Christena L R and Rajaram Y R S 2013 Enzyme immobilization: an overview on techniques and support materials *3 Biotech.* **3** 1–9

[294] Sallez Y, Bianco P and Lojou E 2000 Electrochemical behavior of c-type cytochromes at clay-modified carbon electrodes: a model for the interaction between proteins and soils *J. Electroanal. Chem.* **493** 37–49

[295] Lei C, Wollenberger U, Jung C and Scheller F W 2000 Clay-bridged electron transfer between cytochrome P450cam and electrode *Biochem. Biophys. Res. Commun.* 740–4

[296] Iler R K 1966 Multilayers of colloidal particles *J. Colloid Interface Sci.* **21** 569–94

[297] Lvov Y and Mohwald H 1999 *Protein Architecture: Interfacing Molecular Assemblies and Immobilization Biotechnology* (Boca Raton, FL: CRC Press)

[298] Kimizuka N, Tanaka M and Kunitake T 1999 Spatially controlled synthesis of protein/inorganic nano-assembly: alternate molecular layers of Cyt c and TiO$_2$ nanoparticles *Chem. Lett.* **28** 1333–4

[299] Lvov Y and Caruso F 2001 Biocolloids with ordered urease multilayer shells as enzymatic reactors *Anal. Chem.* **73** 4212–7

[300] McKenzie K J and Marken F 2003 Accumulation and reactivity of the redox protein cytochrome c in mesoporous films of TiO$_2$ phytate *Langmuir* **19** 4327–31

[301] Lvov Y *et al* 2000 Films of manganese oxide nanoparticles with polycations or myoglobin from alternate-layer adsorption *Langmuir* **16** 8850–7

[302] Gaigalas A K and Niaura G 1997 Measurement of electron transfer rates between adsorbed azurin and a gold electrode modified with a hexanethiol layer *J. Colloid Interface Sci.* **193** 60–70

[303] Wong L S, Khan F and Micklefield J 2009 Selective covalent protein immobilization: strategies and applications *Chem. Rev.* **109** 4025–53

[304] Frey B L and Corn R M 1996 Covalent attachment and derivatization of poly(l-lysine) monolayers on gold surfaces as characterized by polarization-modulation FT-IR spectroscopy *Anal. Chem.* **68** 3187–93

[305] Chittur K K 1998 FTIR/ATR for protein adsorption to biomaterial surfaces *Biomaterials* **19** 357–69

[306] Gannett P M *et al* 2006 Preparation, characterization, and substrate metabolism of gold-immobilized cytochrome P450 2C9 *J. Am. Chem. Soc.* **128** 8374–5

[307] Zheng Z and Gunner M R 2009 Analysis of the electrochemistry of hemes with Ems spanning 800 mV *Proteins* **75** 719–34

[308] Lang D and Böcker R 1995 Highly sensitive and specific high-performance liquid chromatographic analysis of 7-hydroxywarfarin, a marker for human cytochrome P-4502C9 activity *J. Chromatogr.* B **672** 305–9

[309] Fantuzzi A *et al* 2011 A new standardized electrochemical array for drug metabolic profiling with human cytochromes P450 *Anal. Chem.* **83** 3831–9

[310] Panicco P, Dodhia V R, Fantuzzi A and Gilardi G 2011 Enzyme-based amperometric platform to determine the polymorphic response in drug metabolism by cytochromes P450 *Anal. Chem.* **83** 2179–86

[311] Rzeźnicka I I *et al* 2009 Observation of photoactive yellow protein anchored to a modified Au(1 1 1) surface by scanning tunneling microscopy *Chem. Phys. Lett.* **472** 113–7

[312] Manickam A, Johnson C A, Kavusi S and Hassibi A 2012 Interface design for CMOS-integrated electrochemical impedance spectroscopy (EIS) biosensors *Sensors* **12** 14467–88

[313] Wollenberg L A *et al* 2012 Selective filling of nanowells in nanowell arrays fabricated using polystyrene nanosphere lithography with cytochrome P450 enzymes *Nanotechnology* **23** 385101

[314] Smaali K, Clément N, Patriarche G and Vuillaume D 2012 Conductance statistics from a large array of sub-10 nm molecular junctions *ACS Nano* **6** 4639–47

[315] Chi Q, Farver O and Ulstrup J 2005 Long-range protein electron transfer observed at the single-molecule level: *in situ* mapping of redox-gated tunneling resonance *Proc. Natl Acad. Sci. USA* **102** 16203–8

[316] Artés J M, Díez-Pérez I, Sanz F and Gorostiza P 2011 Direct measurement of electron transfer distance decay constants of single redox proteins by electrochemical tunneling spectroscopy *ACS Nano* **5** 2060–6

[317] Muthusubramanian N *et al* 2016 Insulator-protected mechanically controlled break junctions for measuring single-molecule conductance in aqueous environments *Appl. Phys. Lett.* **109** 13102

[318] Schukfeh M I *et al* 2016 Towards nanometer-spaced silicon contacts to proteins *Nanotechnology* **27** 115302

[319] Reed M A, Zhou C, Muller C J, Burgin T P and Tour J M 1997 Conductance of a molecular junction *Science* **278** 252–4

[320] Kergueris C *et al* 1999 Electron transport through a metal-molecule-metal junction *Phys. Rev.* B **59** 12505–13

[321] Park J *et al* 2002 Coulomb blockade and the Kondo effect in single-atom transistors *Nature* **417** 722–5

[322] Galperin M and Ratner M A and Nitzan A 2007 Molecular transport junctions: vibrational effects *J. Phys.: Condens. Matter* **19** 103201

[323] Kubatkin S *et al* 2003 Single-electron transistor of a single organic molecule with access to several redox states *Nature* **425** 698–701

[324] Boese D and Schoeller H 2001 Influence of nanomechanical properties on single-electron tunneling: a vibrating single-electron transistor *Europhys. Lett.* **54** 668

[325] van der Zant H S J *et al* 2006 Molecular three-terminal devices: fabrication and measurements *Faraday Discuss.* **131** 347–56

[326] Ron I *et al* 2010 Proteins as electronic materials: electron transport through solid-state protein monolayer junctions *J. Am. Chem. Soc.* **132** 4131–40

[327] Haick H and Cahen D 2008 Making contact: connecting molecules electrically to the macroscopic world *Prog. Surf. Sci.* **83** 217–61

[328] Jia C, Ma B, Xin N and Guo X 2015 Carbon electrode–molecule junctions: a reliable platform for molecular electronics *Acc. Chem. Res.* **48** 2565–75

[329] Lovrinčić R *et al* 2013 A new route to nondestructive top-contacts for molecular electronics on Si: Pb evaporated on organic monolayers *J. Phys. Chem. Lett.* **4** 426–30

[330] Yu X *et al* 2014 Fabrication of reproducible, integration-compatible hybrid molecular/Si electronics *Small* **10** 5151–60

[331] Noy G, Ophir A and Selzer Y 2010 Response of molecular junctions to surface plasmon polaritons *Angew. Chem., Int. Ed.* **49** 5734–6

[332] Shamai T and Selzer Y 2011 Spectroscopy of molecular junctions *Chem. Soc. Rev.* **40** 2293–305

[333] Vadai M *et al* 2013 Plasmon-induced conductance enhancement in single-molecule junctions *J. Phys. Chem. Lett.* **4** 2811–6

[334] Zelinskyy Y and May V 2015 Laser pulse induced transient currents in a molecular junction: effects of plasmon excitations of the leads *J. Chem. Phys.* **142** 224701

[335] Zhu W *et al* 2016 Quantum mechanical effects in plasmonic structures with subnanometre gaps *Nat. Commun.* **7** 11495

[336] Wang T and Nijhuis C A 2016 Molecular electronic plasmonics *Appl. Mater. Today* **3** 73–86

[337] Yu X *et al* 2015 Insights into solid-state electron transport through proteins from inelastic tunneling spectroscopy: the case of Azurin *ACS Nano* **9** 9955–63

[338] Arielly R, Vadai M, Kardash D, Noy G and Selzer Y 2014 Real-time detection of redox events in molecular junctions *J. Am. Chem. Soc.* **136** 2674–80

[339] Maruccio G *et al* 2005 Towards protein field-effect transistors: report and model of a prototype *Adv. Mater.* **17** 816–22

[340] Léger C, Jones A K, Albracht S P J and Armstrong F A 2002 Effect of a dispersion of interfacial electron transfer rates on steady state catalytic electron transport in [NiFe]-hydrogenase and other enzymes *J. Phys. Chem.* B **106** 13058–63

[341] Madden C *et al* 2012 Catalytic turnover of [FeFe]-hydrogenase based on single-molecule imaging *J. Am. Chem. Soc.* **134** 1577–82

[342] Parkin A, Cavazza C, Fontecilla-Camps J C and Armstrong F A 2006 Electrochemical investigations of the interconversions between catalytic and inhibited states of the [FeFe]-hydrogenase from desulfovibrio desulfuricans *J. Am. Chem. Soc.* **128** 16808–15

[343] Jones A, Sillery E, Albracht S P J and Armstrong F A 2002 Direct comparison of the electrocatalytic oxidation of hydrogen by an enzyme and a platinum catalyst *Chem. Commun.* 866–7

[344] Fleming B D, Johnson D L, Bond A M and Martin L L 2006 Recent progress in cytochrome P450 enzyme electrochemistry *Expert Opin. Drug Metab. Toxicol.* **2** 581–9

[345] Shukla A, Gillam E M, Mitchell D J and Bernhardt P V 2005 Direct electrochemistry of enzymes from the cytochrome P450 2C family *Electrochem. Commun.* **7** 437–42

[346] Kelly S M, Jess T J and Price N C 2005 How to study proteins by circular dichroism *Biochim. Biophys. Acta* **1751** 119–39

[347] Hu H-Y and Jiang L-L and Hong J-Y 2016 Study of protein amyloid-like aggregates by solid-state circular dichroism spectroscopy *Curr. Protein Pept. Sci.* **17** 1–4

[348] Naaman R, Beratan D N and Waldeck D 2011 *Electronic and Magnetic Properties of Chiral Molecules and Supramolecular Architectures* (Berlin: Springer)

[349] Billsten P, Wahlgren M, Arnebrant T, McGuire J and Elwing H 1995 Structural changes of T4 lysozyme upon adsorption to silica nanoparticles measured by circular dichroism *J. Colloid Interface Sci.* **175** 77–82

[350] Karlsson M and Carlsson U 2005 Protein adsorption orientation in the light of fluorescent probes: mapping of the interaction between site-directly labeled human carbonic anhydrase II and silica nanoparticles *Biophys. J.* **88** 3536–44

[351] Locuson C W, Gannett P M and Tracy T S 2006 Heteroactivator effects on the coupling and spin state equilibrium of CYP2C9 *Arch. Biochem. Biophys.* **449** 115–29

[352] Hutzler J M, Wienkers L C, Wahlstrom J L, Carlson T J and Tracy T S 2003 Activation of cytochrome P450 2C9-mediated metabolism: mechanistic evidence in support of kinetic observations *Arch. Biochem. Biophys.* **410** 16–24

[353] Antonini E and Brunori M 1971 *Hemoglobin and Myoglobin in Their Reactions with Ligands* (Amsterdam: North-Holland)

[354] Facci P, Alliata D, Andolfi L, Schnyder B and Kötz R 2002 Formation and characterization of protein monolayers on oxygen-exposing surfaces by multiple-step self-chemisorption *Surf. Sci.* **504** 282–92

[355] Facci P, Fontana M P, Dalcanale E, Costa M and Sacchelli T 2000 Molecular reorganization in Langmuir–Blodgett films of mesogenic Zn-porphyrin octaesters *Langmuir* **16** 7726–30

[356] Omura T and Sato R 1962 A new cytochrome in liver microsomes *J. Biol. Chem.* **237** PC1375–6

[357] Omura T and Sato R 1964 The carbon monoxide-binding pigment of liver microsomes I. Evidence for its hemoprotein nature *J. Biol. Chem.* **239** 2370–8

[358] Perlmann G E and Diringer R 1960 The structure of proteins *Annu. Rev. Biochem.* **29** 151–82

[359] Reid E, Cook G M W and Morré D J 2013 *Investigation of Membrane-Located Receptors* (Berlin: Springer)

[360] Mukhopadhyay S *et al* 2014 Nanoscale electron transport and photodynamics enhancement in lipid-depleted bacteriorhodopsin monomers *ACS Nano* **8** 7714–22

[361] Mukhopadhyay S, Gartner W, Cahen D, Pecht I and Sheves M 2016 Electron transport via a soluble photochromic photoreceptor *Phys. Chem. Chem. Phys.* **18** 25671–5

[362] Nicolini C *et al* 2001 P450scc engineering and nanostructuring for cholesterol sensing *Langmuir* **17** 3719–26

[363] Homola J, Yee S S and Gauglitz G 1999 Surface plasmon resonance sensors: review *Sensors Actuators* B **54** 3–15

[364] Sexton B A, Feltis B N and Davis T J 2008 Characterisation of gold surface plasmon resonance sensor substrates *Sensors Actuators* A **141** 471–5

[365] Millo D, Ranieri A, Koot W, Gooijer C and van der Zwan G 2006 Towards combined electrochemistry and surface-enhanced resonance raman of heme proteins: improvement of diffusion electrochemistry of cytochrome c at silver electrodes chemically modified with 4-mercaptopyridine *Anal. Chem.* **78** 5622–5

[366] Parson W W 2015 *Modern Optical Spectroscopy: with Exercises and Examples from Biophysics and Biochemistry* (Berlin: Springer)

[367] Kitagawa T and Hirota S 2006 Raman spectroscopy of proteins *Handbook of Vibrational Spectroscopy* (New York: Wiley)

[368] Siebert F and Hildebrandt P 2008 *Vibrational Spectroscopy in Life Science* (New York: Wiley)

[369] Andrew C R and Sanders-Loehr J 1996 Copper–Sulfur proteins: using Raman spectroscopy to predict coordination geometry *Acc. Chem. Res.* **29** 365–72

[370] Schulte A, Buchter S, Galkin O and Williams C 1995 Raman spectroscopic observation of a conformational change at the heme-protein linkage in myoglobin at high pressure *J. Am. Chem. Soc.* **117** 10149–50

[371] Delfino I, Bizzarri A R and Cannistraro S 2005 Single-molecule detection of yeast cytochrome c by surface-enhanced Raman spectroscopy *Biophys. Chem.* **113** 41–51

[372] Nack M, Radu I, Bamann C, Bamberg E and Heberle J 2009 The retinal structure of channelrhodopsin-2 assessed by resonance Raman spectroscopy *FEBS Lett.* **583** 3676–80

[373] Unno M, Kumauchi M, Sasaki J, Tokunaga F and Yamauchi S 2002 Resonance Raman spectroscopy and quantum chemical calculations reveal structural changes in the active site of photoactive yellow protein *Biochemistry* **41** 5668–74

[374] Gerscher S *et al* 1997 Chromophore–anion interactions in halorhodopsin from natronobacterium pharaonis probed by time-resolved resonance Raman spectroscopy *Biochemistry* **36** 11012–20

[375] Todorovic S, Jung C, Hildebrandt P and Murgida D H 2006 Conformational transitions and redox potential shifts

of cytochrome P450 induced by immobilization *J. Biol. Inorg. Chem.* **11** 119–27

[376] Bonifacio A *et al* 2008 Active-site structure, binding and redox activity of the heme–thiolate enzyme CYP2D6 immobilized on coated Ag electrodes: a surface-enhanced resonance Raman scattering study *J. Biol. Inorg. Chem.* **13** 85–96

[377] Wollenberg L A 2011 Immobilized cytochrome P450 2C9 (CYP2C9): applications for metabolite generation, monitoring protein-protein interactions, and improving *in vivo* predictions using enhanced *in vitro* models *PhD Thesis* West Virginia University (DAI-B 73/03, Dissertation Abstracts International)

[378] Peterlinz K A and Georgiadis R 1996 *In situ* kinetics of self-assembly by surface plasmon resonance spectroscopy *Langmuir* **12** 4731–40

[379] Drake P A and Bohn P W 1995 Anomalous diffusion. Surface plasmon resonance measurements as probes of nanometer-scale film-swelling dynamics for CH_3OH in poly(methyl methacrylate) *Anal. Chem.* **67** 1766–71

[380] Jordan C E, Frutos A G, Thiel A J and Corn R M 1997 Surface plasmon resonance imaging measurements of DNA hybridization adsorption and streptavidin/DNA multilayer formation at chemically modified gold surfaces *Anal. Chem.* **69** 4939–47

[381] Jin Y, Shao Y and Dong S 2003 Direct electrochemistry and surface plasmon resonance characterization of alternate layer-by-layer self-assembled DNA-myoglobin thin films on chemically modified gold surfaces *Langmuir* **19** 4771–7

[382] Saban S 2011 Development of an *in vitro* model system for studying the interaction of Equus caballus lgE with its high-affinity Fc receptor *PhD Thesis* The University of Sheffield

[383] Baba A, Knoll W and Advincula R 2006 Simultaneous *in situ* electrochemical, surface plasmon optical, and atomic force microscopy measurements: investigation of conjugated polymer electropolymerization *Rev. Sci. Instrum.* **77** 64101

[384] Baba A, Taranekar P, Ponnapati R R, Knoll W and Advincula R C 2010 Electrochemical surface plasmon resonance (EC-SPR) and waveguide enhanced glucose biosensing with N-alkylaminated polypyrrole/glucose oxidase multilayers *ACS Appl. Mater. Interfaces* **2** 2347–54

[385] Tao N J 1996 Probing potential-tuned resonant tunneling through redox molecules with scanning tunneling microscopy *Phys. Rev. Lett.* **76** 4066–9

[386] Chi Q *et al* 2010 Approach to interfacial and intramolecular electron transfer of the diheme protein cytochrome c4 assembled on Au(1 1 1) surfaces *J. Phys. Chem.* B **114** 5617–24

[387] Karlsson J-J, Nielsen M F, Thuesen M H and Ulstrup J 1997 Electrochemistry of cytochrome c4 from *Pseudomonas stutzeri J. Phys. Chem.* B **101** 2430–6

[388] Wang M, Bugarski S and Stimming U 2008 Topological and electron-transfer properties of glucose oxidase adsorbed on highly oriented pyrolytic graphite electrodes *J. Phys. Chem.* C **112** 5165–73

[389] Vaz-Domínguez C, Pita M, de Lacey A L, Shleev S and Cuesta A 2012 Combined ATR-SEIRAS and EC-STM study of the immobilization of laccase on chemically modified Au electrodes *J. Phys. Chem.* C **116** 16532–40

[390] Möller C, Allen M, Elings V, Engel A and Müller D J 1999 Tapping-mode atomic force microscopy produces faithful high-resolution images of protein surfaces *Biophys. J.* **77** 1150–8

[391] Nussio M R *et al* 2010 AFM study of the interaction of cytochrome P450 2C9 with phospholipid bilayers *Chem. Phys. Lipids* **163** 182–9

[392] Alessandrini A and Facci P 2011 Unraveling lipid/protein interaction in model lipid bilayers by atomic force microscopy *J. Mol. Recognit.* **24** 387–96

[393] Tran T D *et al* 2010 Electrochemical analysis of azurin thermodynamic and adsorption properties at monolayer-protected cluster film assemblies—evidence for a more homogeneous adsorption interface *J. Colloid Interface Sci.* **352** 50–8

[394] Bayburt T H and Sligar S G 2002 Single-molecule height measurements on microsomal cytochrome P450 in nanometer-scale phospholipid bilayer disks *Proc. Natl Acad. Sci. USA* **99** 6725–30

[395] Archakov A I and Ivanov Y D 2011 Application of AFM and optical biosensor for investigation of complexes formed in P450-containing monooxygenase systems *Biochim. Biophys. Acta* **1814** 102–10

[396] Wang H, Yang Y and Erie D A 2007 Characterization of protein–protein interactions using atomic force microscopy *Protein Interactions* ed P Schuck (New York, PA: Springer) pp 39–77

[397] Zhang X *et al* 2017 The dynamic conductance response and mechanics-modulated memristive behavior of the Azurin monolayer under cyclic loads *Phys. Chem. Chem. Phys.* **19** 6757–67

[398] Lyshevski S E 2007 *Nano and Molecular Electronics Handbook* (Boca Raton, FL: CRC Press)

[399] Albrecht T, Li W-W, Haehnel W, Hildebrandt P and Ulstrup J 2006 Voltammetry and *in situ* scanning tunneling microscopy of de novo designed heme protein monolayers on Au(1 1 1)-electrode surfaces *Bioelectrochemistry* **69** 193–200

[400] Leopold M C and Bowden E F 2002 Influence of gold substrate topography on the voltammetry of cytochrome c adsorbed on carboxylic acid terminated self-assembled monolayers *Langmuir* **18** 2239–45

[401] Zhang J *et al* 2012 Interfacial electrochemical electron transfer in biology—towards the level of the single molecule *Electronproton Coupling Biol. Energy Transduct.* **586** 526–35

[402] Beratan D N and Balabin I A 2008 Heme–copper oxidases use tunneling pathways *Proc. Natl Acad. Sci.* **105** 403–4

[403] Horsley J R, Yu J, Moore K E, Shapter J G and Abell A D 2014 Unraveling the interplay of backbone rigidity and electron rich side-chains on electron transfer in peptides: the realization of tunable molecular wires *J. Am. Chem. Soc.* **136** 12479–88

[404] Sepunaru L *et al* 2015 Electronic transport via homopeptides: the role of side chains and secondary structure *J. Am. Chem. Soc.* **137** 9617–26

[405] Yu J, Huang D M, Shapter J G and Abell A D 2012 Electrochemical and computational studies on intramolecular dissociative electron transfer in β-peptides *J. Phys. Chem.* C **116** 26608–17

[406] Beratan D N and Hopfield J J 1984 Calculation of tunneling matrix elements in rigid systems: mixed-valence dithiaspirocyclobutane molecules *J. Am. Chem. Soc.* **106** 1584–94

[407] Pirbadian S *et al* 2014 Shewanella oneidensis MR-1 nanowires are outer membrane and periplasmic extensions of the extracellular electron transport components *Proc. Natl Acad. Sci. USA* **111** 12883–8

[408] Jiang N *et al* 2013 Distance-independent charge recombination kinetics in cytochrome c-cytochrome c peroxidase complexes: compensating changes in the electronic coupling and reorganization energies *J. Phys. Chem.* B **117** 9129–41

[409] Payne T M, Yee E F, Dzikovski B and Crane B R 2016 Constraints on the radical cation center of cytochrome

c peroxidase for electron transfer from cytochrome c *Biochemistry* **55** 4807–22

[410] El-Naggar M Y *et al* 2010 Electrical transport along bacterial nanowires from Shewanella oneidensis MR-1 *Proc. Natl Acad. Sci.* **107** 18127–31

[411] Enderby J E and Barnes A C 1990 Liquid semiconductors *Rep. Prog. Phys.* **53** 85

[412] Ding M *et al* 2016 Nanoelectronic investigation reveals the electrochemical basis of electrical conductivity in shewanella and geobacter *ACS Nano* **10** 9919–26

[413] Malvankar N S *et al* 2011 Tunable metallic-like conductivity in microbial nanowire networks *Nat. Nano* **6** 573–9

[414] Clarke T A *et al* 2011 Structure of a bacterial cell surface decaheme electron conduit *Proc. Natl Acad. Sci.* **108** 9384–9

[415] Malvankar N S *et al* 2015 Structural basis for metallic-like conductivity in microbial nanowires *mBio* **6** e00084

[416] Xiao K *et al* 2016 Low energy atomic models suggesting a pilus structure that could account for electrical conductivity of geobacter sulfurreducens pili *Sci. Rep.* **6** 23385

[417] Lee C and Mertz B 2016 Theoretical evidence for multiple charge transfer pathways in bacteriorhodopsin *J. Chem. Theory Comput.* **12** 1639–46

[418] Li R *et al* 2010 Bidirectional mediation of TiO_2 nanowires field effect transistor by dipole moment from purple membrane *Nanoscale* **2** 1474–9

[419] Hansen A G *et al* 2003 Adsorption and interfacial electron transfer of saccharomyces cerevisiae yeast cytochrome c monolayers on Au(1 1 1) electrodes *Langmuir* **19** 3419–27

[420] Heering H A, Wiertz F G M, Dekker C and de Vries S 2004 Direct immobilization of native yeast Iso-1 cytochrome c on bare gold: fast electron relay to redox enzymes and zeptomole protein-film voltammetry *J. Am. Chem. Soc.* **126** 11103–12

[421] Baymann F *et al* 2003 Voltammetry of a 'protein on a rope' *FEBS Lett.* **539** 91–4

[422] Davis J J, Bruce D, Canters G W, Crozier J and Hill H A O 2003 Genetic modulation of metalloprotein electron transfer at bare gold *Chem. Commun.* 576–7

[423] Davis J J *et al* 1998 Protein adsorption at a gold electrode studied by *in situ* scanning tunnelling microscopy *New J. Chem.* **22** 1119–23

[424] Kazlauskaite J, Westlake A C G, Wong L-L and Hill H A O 1996 Direct electrochemistry of cytochrome P450cam *Chem. Commun.* 2189–90

[425] Fantuzzi A, Fairhead M and Gilardi G 2004 Direct electrochemistry of immobilized human cytochrome P450 2E1 *J. Am. Chem. Soc.* **126** 5040–1

[426] Lo K K-W, Wong L-L and Hill H A O 1999 Surface-modified mutants of cytochrome P450cam: enzymatic properties and electrochemistry *FEBS Lett.* **451** 342–6

[427] Armstrong F A, Hill H A O and Walton N J 1988 Direct electrochemistry of redox proteins *Acc. Chem. Res.* **21** 407–13

[428] Dolidze T D, Rondinini S, Vertova A, Waldeck D H and Khoshtariya D E 2007 Impact of self-assembly composition on the alternate interfacial electron transfer for electrostatically immobilized cytochrome c *Biopolymers* **87** 68–73

[429] Chi Q, Zhang J, Andersen J E T and Ulstrup J 2001 Ordered assembly and controlled electron transfer of the blue copper protein azurin at gold (1 1 1) single-crystal substrates *J. Phys. Chem.* B **105** 4669–79

[430] Ulman A 1995 *Characterization of Organic Thin Films* (Boston, MA: Manning Publications)

[431] Sagara T, Niwa K, Sone A, Hinnen C and Niki K 1990 Redox reaction mechanism of cytochrome c at modified gold electrodes *Langmuir* **6** 254–62

[432] Rusling J F and Nassar A E F 1993 Enhanced electron transfer for myoglobin in surfactant films on electrodes *J. Am. Chem. Soc.* **115** 11891–7

[433] Hahn C E W, Hill H A O, Ritchie M D and Sear J W 1990 The electrochemistry of proteins entrapped in nafion *J. Chem. Soc. Chem. Commun.* 125–6

[434] Munge B, Estavillo C, Schenkman J B and Rusling J F 2003 Optimization of electrochemical and peroxide-driven oxidation of styrene with ultrathin polyion films containing cytochrome P450cam and myoglobin *ChemBioChem* **4** 82–9

[435] Lee I, Lee J W, Warmack R J, Allison D P and Greenbaum E 1995 Molecular electronics of a single photosystem I reaction center: studies with scanning tunneling microscopy and spectroscopy *Proc. Natl Acad. Sci.* **92** 1965–9

[436] Mikayama T *et al* 2009 The electronic behavior of a photosynthetic reaction center monitored by conductive atomic force microscopy *J. Nanosci. Nanotechnol.* **9** 97–107

[437] Lee I, Lee J W and Greenbaum E 1997 Biomolecular electronics: vectorial arrays of photosynthetic reaction centers *Phys. Rev. Lett.* **79** 3294–7

[438] Gerster D *et al* 2012 Photocurrent of a single photosynthetic protein *Nat. Nano* **7** 673–6

[439] Carmeli I, Frolov L, Carmeli C and Richter S 2007 Photovoltaic activity of photosystem I-based self-assembled monolayer *J. Am. Chem. Soc.* **129** 12352–3

[440] Segal D, Nitzan A, Davis W B, Wasielewski M R and Ratner M A 2000 Electron transfer rates in bridged molecular systems 2. A steady-state analysis of coherent tunneling and thermal transitions *J. Phys. Chem.* B **104** 3817–29

[441] Albrecht T, Guckian A, Kuznetsov A M, Vos J G and Ulstrup J 2006 Mechanism of electrochemical charge transport in individual transition metal complexes *J. Am. Chem. Soc.* **128** 17132–8

[442] Skov L K, Pascher T, Winkler J R and Gray H B 1998 Rates of intramolecular electron transfer in Ru(bpy)2(im) (His83)-modified azurin increase below 220 K *J. Am. Chem. Soc.* **120** 1102–3

[443] Wang H *et al* 2009 Unusual temperature dependence of photosynthetic electron transfer due to protein dynamics *J. Phys. Chem.* B **113** 818–24

[444] Beebe J M, Kim B, Gadzuk J W, Daniel Frisbie C and Kushmerick J G 2006 Transition from direct tunneling to field emission in metal-molecule-metal junctions *Phys. Rev. Lett.* **97** 26801

[445] Xie Z, Bâldea I, Smith C E, Wu Y and Frisbie C D 2015 Experimental and theoretical analysis of nanotransport in oligophenylene dithiol junctions as a function of molecular length and contact work function *ACS Nano* **9** 8022–36

[446] Raichlin S 2017 Solid state electron transport via myoglobin protein and the role of substrate-protein coupling in such systems *PhD Thesis* Weizmann Institute of Science

[447] Sedghi G *et al* 2011 Long-range electron tunnelling in oligo-porphyrin molecular wires *Nat. Nano* **6** 517–23

[448] Bostick C D *et al* 2016 Immobilized cytochrome P450 for monitoring of P450-P450 interactions and metabolism *Drug Metab. Dispos. Biol. Fate Chem.* **44** 741–9

[449] Frenkel J 1938 On pre-breakdown phenomena in insulators and electronic semi-conductors *Phys. Rev.* **54** 647–8

[450] Hummel M A, Gannett P M, Aguilar J and Tracy T S 2008 Substrate proton to heme distances in CYP2C9 allelic variants and alterations by the heterotropic activator, dapsone *Arch. Biochem. Biophys.* **475** 175–83

[451] Wang W, Lee T, Kretzschmar I and Reed M A 2004 Inelastic electron tunneling spectroscopy of an alkanedithiol self-assembled monolayer *Nano Lett.* **4** 643–6

[452] Binnig G, Garcia N and Rohrer H 1985 Conductivity sensitivity of inelastic scanning tunneling microscopy *Phys. Rev.* B **32** 1336–8

[453] Ho W 2002 Single-molecule chemistry *J. Chem. Phys.* **117** 11033–61

[454] Hansma P K and Coleman R V 1974 Spectroscopy of biological compounds with inelastic electron tunneling *Science* **184** 1369

[455] Hillebrecht J R *et al* 2005 Optimization of protein-based volumetric optical memories and associative processors by using directed evolution *NanoBiotechnology* **1** 141–51

[456] Hayashi S, Tajkhorshid E and Schulten K 2003 Molecular dynamics simulation of bacteriorhodopsin's photoisomerization using *ab initio* forces for the excited chromophore *Biophys. J.* **85** 1440–9

[457] Xu J, Bhattacharya P, Marcy D L, Stuart J A and Birge R R 2001 Photoconduction in bacteriorhodopsin/GaAs heterostructures *Electron. Lett.* **37** 648–9

[458] Gillespie N B *et al* 2005 Characterization and photochemistry of 13-desmethyl bacteriorhodopsin *J. Phys. Chem.* B **109** 16142–52

[459] He T, Friedman N, Cahen D and Sheves M 2005 Bacteriorhodopsin monolayers for optoelectronics: orientation and photoelectric response on solid supports *Adv. Mater.* **17** 1023–7

[460] Lee I *et al* 2006 Photoinduced surface potential change of bacteriorhodopsin mutant D96N measured by scanning surface potential microscopy *J. Phys. Chem.* B **110** 10982–90

[461] Shin J, Bhattacharya P, Yuan H-C, Ma Z and Váró G 2007 Low-power bacteriorhodopsin-silicon n-channel metal-oxide field-effect transistor photoreceiver *Opt. Lett.* **32** 500–2

[462] Xu J *et al* 2003 Direct measurement of the photoelectric response time of bacteriorhodopsin via electro-optic sampling *Biophys. J.* **85** 1128–34

[463] Koyama K, Yamaguchi N and Miyasaka T 1994 Antibody-mediated bacteriorhodopsin orientation for molecular device architectures *Science* **265** 762–5

[464] Koyama K, Yamaguchi N and Miyasaka T 1995 Molecular organization of bacterio-rhodopsin films in optoelectronic devices *Adv. Mater.* **7** 590–4

[465] Jin Y D, Friedman N, Sheves M and Cahen D 2007 Bacteriorhodopsin-monolayer-based planar metal–insulator–metal junctions via biomimetic vesicle fusion: preparation, characterization, and bio-optoelectronic characteristics *Adv. Funct. Mater.* **17** 1417–28

[466] Jin Y D *et al* 2008 Bacteriorhodopsin as an electronic conduction medium for biomolecular electronics *Chem. Soc. Rev.* **37** 2422–32

[467] Berthoumieu O *et al* 2012 Molecular scale conductance photoswitching in engineered bacteriorhodopsin *Nano Lett.* **12** 899–903

[468] Patil A V, Premaraban T, Berthoumieu O, Watts A and Davis J J 2012 Engineered bacteriorhodopsin: a molecular scale potential switch *Chem. Eur. J.* **18** 5632–6

[469] Patil A V, Premaruban T, Berthoumieu O, Watts A and Davis J J 2012 Enhanced photocurrent in engineered bacteriorhodopsin monolayer *J. Phys. Chem.* B **116** 683–9

[470] Salomon A *et al* 2007 What is the barrier for tunneling through alkyl monolayers? Results from n- and p-Si–alkyl/ Hg junctions *Adv. Mater.* **19** 445–50

[471] Lee I, Lee J W, Stubna A and Greenbaum E 2000 Measurement of electrostatic potentials above oriented single photosynthetic reaction centers *J. Phys. Chem.* B **104** 2439–43

[472] Feifel S C, Lokstein H, Hejazi M, Zouni A and Lisdat F 2015 Unidirectional photocurrent of photosystem i on π-system-modified graphene electrodes: nanobionic approaches for the construction of photobiohybrid systems *Langmuir* **31** 10590–8

[473] Korpany K V *et al* 2012 Conductance switching in the photoswitchable protein dronpa *J. Am. Chem. Soc.* **134** 16119–22

[474] Lee T, Kim S-U, Min J and Choi J-W 2010 Multilevel biomemory device consisting of recombinant azurin/ cytochrome c *Adv. Mater.* **22** 510–4

[475] Gould J L 1984 Magnetic field sensitivity in animals *Annu. Rev. Physiol.* **46** 585–98

[476] Ritz T, Adem S and Schulten K 2000 Model for photoreceptor-based magnetoreception in birds *Biophys. J.* **78** 707–18

[477] Xie Z *et al* 2011 Spin specific electron conduction through DNA oligomers *Nano Lett.* **11** 4652–5

[478] Naaman R and Waldeck D H 2012 Chiral-induced spin selectivity effect *J. Phys. Chem. Lett.* **3** 2178–87

[479] Medina E, Lopéz F, Ratner M A and Mujica V 2012 Chiral molecular films as electron polarizers and polarization modulators *Europhys. Lett.* **99** 17006

[480] Mondal P C, Fontanesi C, Waldeck D H and Naaman R 2016 Spin-dependent transport through chiral molecules studied by spin-dependent electrochemistry *Acc. Chem. Res.* **49** 2560–8

[481] Göhler B *et al* 2011 Spin selectivity in electron transmission through self-assembled monolayers of double-stranded DNA *Science* **331** 894

[482] Gutierrez R, Díaz E, Naaman R and Cuniberti G 2012 Spin-selective transport through helical molecular systems *Phys. Rev.* B **85** 81404

[483] Kumar A *et al* 2017 Chirality-induced spin polarization places symmetry constraints on biomolecular interactions *Proc. Natl Acad. Sci.* **114** 2474–8

[484] Naaman R and Waldeck D H 2015 Spintronics and chirality: spin selectivity in electron transport through chiral molecules *Annu. Rev. Phys. Chem.* **66** 263–81

[485] Carmeli I, Kumar K S, Heifler O, Carmeli C and Naaman R 2014 Spin selectivity in electron transfer in photosystem I *Angew. Chem., Int. Ed.* **53** 8953–8

[486] Mishra D *et al* 2013 Spin-dependent electron transmission through bacteriorhodopsin embedded in purple membrane *Proc. Natl Acad. Sci.* **110** 14872–6

[487] Einati H, Mishra D, Friedman N, Sheves M and Naaman R 2015 Light-controlled spin filtering in bacteriorhodopsin *Nano Lett.* **15** 1052–6

[488] Roy P *et al* 2016 Spin-controlled photoluminescence in hybrid nanoparticles purple membrane system *ACS Nano* **10** 4525–31

[489] Zhang B, Song W, Pang P, Ynan Zhao Y, Zhang P, Csabai I, Vattay G and Lindsay S 2017 Observation of giant conductance fluctuations in a protein *Nano Futures* **1** 035002